Large Scale Testing and Modelling of Reinforced Concrete Flat Plate Systems in Seismic Areas

by

Dritan Topuzi

A thesis
presented to the University of Waterloo
in fulfillment of the
thesis requirement for the degree of
Doctor of Philosophy
in
Civil Engineering

Waterloo, Ontario, Canada, 2015

I hereby declare that I am the sole author of this thesis. This is a true copy of the thesis, including any required final revisions, as accepted by my examiners.

I understand that my thesis may be made electronically available to the public.

Abstract

The focus of this research is on developing new punching shear retrofit techniques for slab-column connections to improve the seismic response of flat-plate systems. Previous tests have shown the effectiveness of using shear reinforcement to enhance the shear strength and ductility of individual slab-column connections. However, while ductility reduces the earthquake impact on structures, increased stiffness attracts higher forces. Herein, a new type of punching shear retrofit element, shear bolts with flexible washers, is introduced. The flexible washers allow for shear crack opening during the lateral displacements, while at the same time providing control of the crack width by using the appropriate washer thickness and/or stiffness. A set of six slab-column connections retrofitted with this new type of shear reinforcement was tested. The results show that this technique improves the lateral load-deformation response of the connections, increasing the ductility without a commensurate increase in stiffness. Lower stiffness results in lower shear forces attracted by the column and continuous opening and closing of cracks results in higher energy dissipation through friction within the crack interfaces.

The effect of this type of shear reinforcement on the response of an assembled structure is also important. This study investigates such behaviour analytically, using various connection hysteretic responses to check how energy dissipation within individual connections affects the overall energy dissipation of a flat-plate system. Different lateral load supporting systems were investigated to determine the hysteretic response needed at slab-column connections to avoid sudden collapse.

This research shows how to achieve the desired characteristics of a flat plate structure subjected to an earthquake - sufficient strength and stiffness to withstand moderate intensity shaking, and sufficient ductility to act in parallel with a more rigid structural system under strong base motions. Such design of slab-column connections is in agreement with the philosophy of "capacity design", where the designer "tells the structure what it should do in the event of a major earthquake". The presented system was designed for slab retrofit. However, it can be anticipated that similar concepts can be used in the construction of new slabs in seismic zones.

Acknowledgements

I am grateful to Dr. Marianna Polak and Dr. Sriram Narasimhan for their encouragement and guidance throughout the development of this research and the expertise shared with me on this subject.

I am also very grateful for the inspiration given to me by the late Dr. Donald Grierson and his insight and extended experience shared at the beginning of this program.

The presented research was funded by a grant from the Natural Sciences and Engineering Research Council (NSERC) of Canada. The ready mixed concrete was donated by Hogg Fuel and Supply Ltd. in Kitchener, ON.

This research involved experimental work in the Structural Laboratory of Civil and Environmental Engineering, University of Waterloo, where I would like to thank Doug Hirst, Richard Morrison, and Rob Sluban. Without their help, my experiments could not have been completed. For helping me in the laboratory, I also want to thank Joseph Stoner, Jae Kang, Serhan Kirlangic, Paulina Arczewska, Yen Wu, and Doreen Zauft.

The analytical component of this work was made possible by the facilities of the Shared Hierarchical Academic Research Computing Network (SHARCNET) and Compute/Calcul Canada. Without the parallel processing capabilities of SHARCNET, the numerical analyses of this component would have not been possible.

I owe my deepest gratitude to my wife Marsilda and my daughter Iris, for their deep understanding of my extended working and studying hours and for being my primary motivation.

Finally, I would like to thank Christian Witt, the former president of Schoeck Canada Inc. and supervisor in my job, for his encouragement and support in completing this program.

Dedication

To my Family

Table of Contents

List of Tables

List of Figures

Chapter 1

Introduction

1.1 Reinforced Concrete Flat Plate Systems

Reinforced concrete flat plate structures are widely used as structural systems. They consist of a flat slab and columns with no beams to support the slab. Three common types of slabs are shown in Fig. 1.1. The system shown in Fig. 1.1(c), known as a flat plate system, will be the focus of this research.

The flat plate system is popular in construction (Fig. 1.2) because it offers low storey height, ease of construction, better architectural appearance, and low construction costs. However, when exposed to large vertical forces or horizontal deformations, especially during an earthquake, this type of structure is vulnerable to punching shear failure at the slab-column connections. Cracks occur inside the slab, in the vicinity of the column perimeter, and may propagate at an angle of 20 to 45 degrees leading to punching failure of the joint, as shown in Fig. 1.3. This type of failure is usually brittle, particularly if no shear reinforcement is used in the slab around the column. Brittle failures are sudden and catastrophic for the safety of building occupants. In some cases, the failure of a joint may cause the failure of the adjacent joints, triggering a progressive collapse of part or even the entire building.

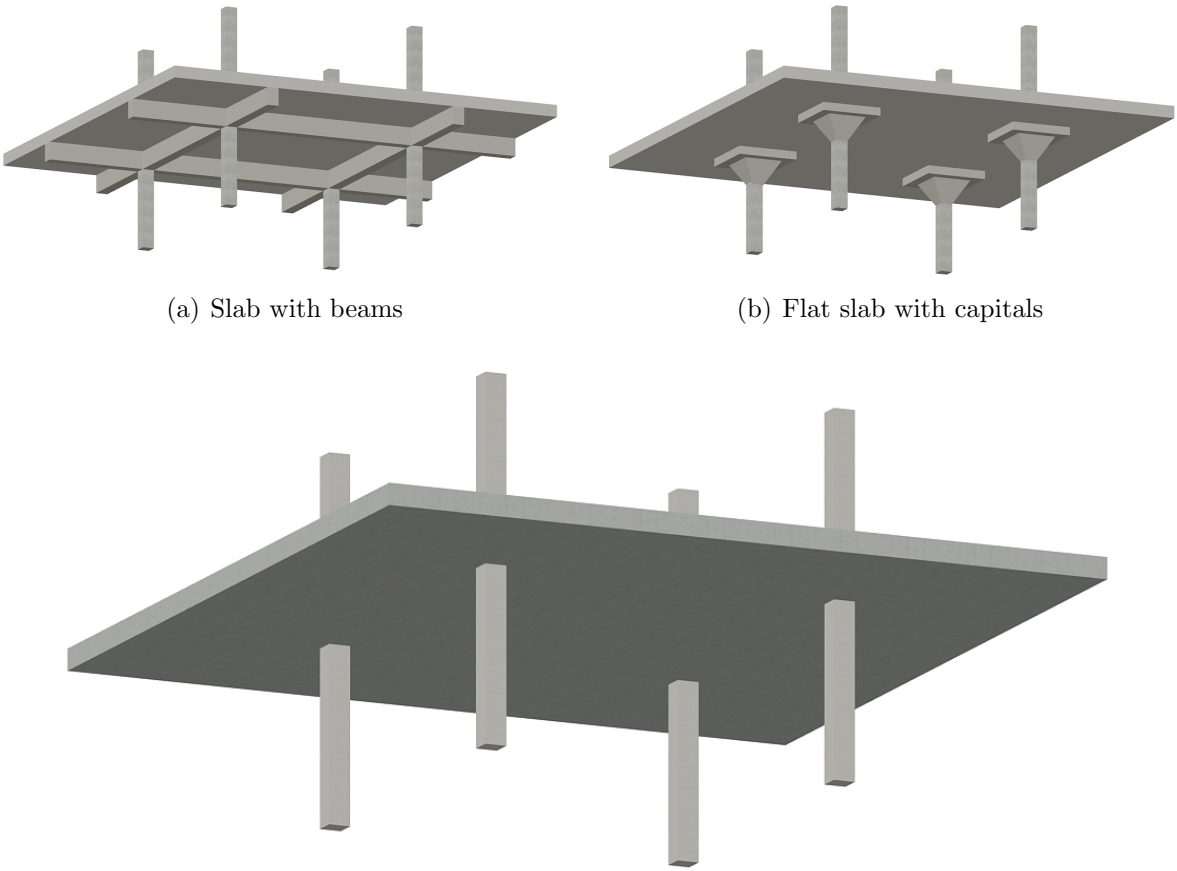

(a) Slab with beams

(b) Flat slab with capitals

(c) Flat plate

Figure 1.1: Various types of slabs

(a)

(b)

Figure 1.2: Flat Slab Buildings (Gateway Project II, Hong Kong, adapted from City University of Hong Kong website)

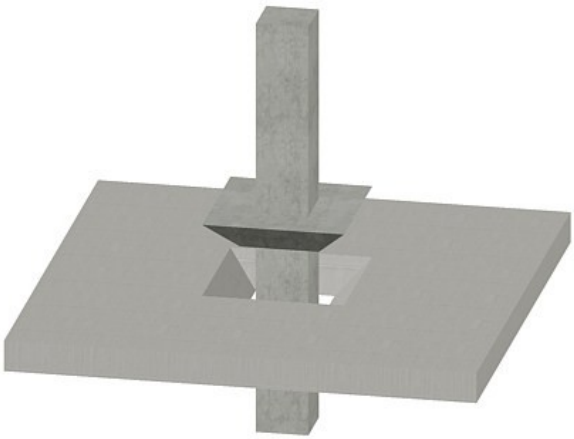

(a) 3D view

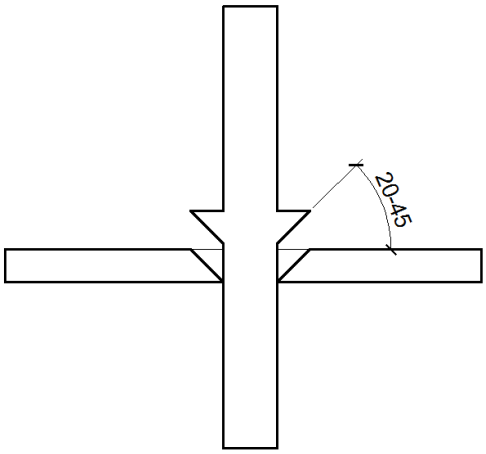

(b) section

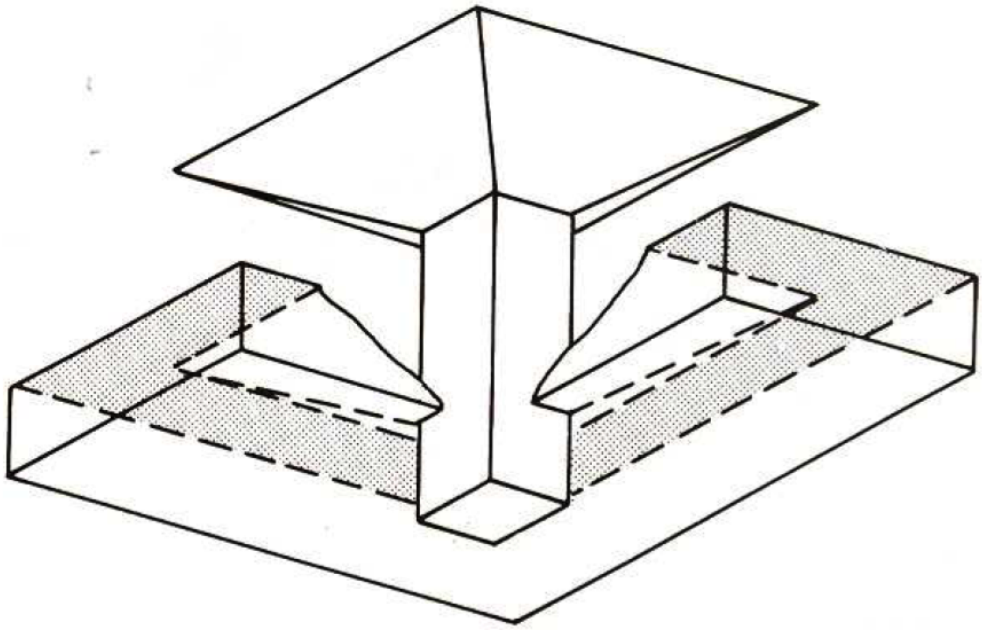

(c) Punching Cone [35]

Figure 1.3: Punching Failure

Punching failures in slab-column connections can be mitigated in the following ways:

1. By increasing the area of concrete resisting shear stresses. This can be achieved by increasing the thickness of the slab, providing a drop panel or capital (Fig. 1.1(b)), or increasing the dimensions of the column.

2. Providing concrete of higher strength.

3. Providing additional shear strength by using shear reinforcement within the slab around the column perimeter.

The first two methods are effective in increasing punching strength, but not ductility [39]. Adding shear reinforcement increases both strength and ductility, and it is also the most practical way of retrofitting existing slab-column connections. Previous research carried out on shear retrofitting of slab column connections is discussed in Section 2.2.

1.2 Cases of Punching Shear Failures

On 25 January 1971, about two-thirds of a 16-storey building collapsed while under construction at 2000 Commonwealth Ave., Boston, MA, USA. Punching shear was determined as the trigger to progressive collapse. Based on interviewed eyewitnesses, the failure took place in three phases. It started with the punching shear failure in the roof at one column, it proceeded with the collapse of the roof slab, and, finally, the progressive collapse of most of the structure. Fortunately, the collapse occurred slowly and most of the workers left the building; however four of them died [26].

On 2 March 1973, the Skyline Plaza in Bailey's Crossroads, Virginia, USA, collapsed while under construction (Fig. 1.4). It was a partial progressive collapse, starting from the 24th floor, due to premature removal of shoring and insufficient concrete strength of the flat slab. The collapse extended vertically all the way to the ground, leaving the structure with a gap between two separate towers. Fourteen workers were killed [26].

Two Canadian school buildings with 150 mm thick flat plate floors and 300 mm circular columns experienced abnormal floor deflections. A typical crack pattern on the

top of the slabs at each column emerged as a circle slightly larger in diameter than the column and four radial cracks along the diagonals of the slab panels. Fortunately, these shear failures were quickly repaired, without causing building collapse [17].

Figure 1.4: Skyline Plaza collapse, Fairfax County, VA, USA, 1973. (Courtesy of NIST)

1.3 Reinforced Concrete Flat Plate Systems in Seismic Areas

When subjected to lateral loading associated with earthquakes, the inter-story drifts induced in the building make the slab-column connection rotate, thereby increasing the moment demands on the connections and further increasing the shear stresses in the slab around the column. Additionally, the cyclic displacements deteriorate the strength and stiffness of the connection, making flat-plate structures prone to punching failure under earthquake loading. In the Mexico City earthquake in 1985, structures having waffle slabs proved to be the most vulnerable to failure of all types of structures. The rate of damage in waffle slab buildings was almost twice compared to common frame buildings with floor systems consisting of concrete beams and a monolithic slab [52], [41].

To avoid failure, the slab-column connections need adequate strength and ductility to be able to undergo plastic deformations. Furthermore, the connection needs to preserve post-failure resistance following an earthquake, to support vertical service loads and avoid progressive collapse of the entire structure. Shear studs and shear bolts have been proven to increase the ductility of connections and consequently improve the structural response of flat-plate systems under seismic forces.

1.4 Objective of this Research

The focus of this research is on developing a new technique of punching shear retrofit of reinforced concrete flat plate-column systems for improved response in seismic areas. The response of structures in seismic areas may be improved by increasing their strength and/or ductility. The necessary strength guarantees the safety of structures, but it would not be economical to design all buildings to stay in the elastic range under earthquake loading. This is why ductility is an important property for the performance of structures in seismic areas, allowing structural members to form hinges and deform plastically. The ability of structures to sustain large deformations allows people to be evacuated during

or immediately after an earthquake. While ductility reduces the earthquake impact on structures, increased stiffness attracts higher forces.

The development of a shear retrofit technique for the design of slab-column joints with increased ductility and flexibility, without a commensurate increase in strength, is the objective of this research. A combination of experimental and analytical results is considered for this investigation.

1.4.1 Experimental Research

Various punching shear retrofitting techniques have been recently developed which increase the strength and the ductility of the slab-column connection, but also its stiffness, as a consequence. The main objective of the experimental component of this research is focused on finding better alternatives for shear reinforcement retrofitting of slab-column connections for increased ductility, without considerably increasing strength and stiffness. The effect of the proposed retrofit technique on the punching crack interface behaviour and on the response of slab-column connections was tested. Six full-scale slab-column joints were tested, subjected to a constant vertical load and a cyclic displacement-controlled lateral loading (Fig. 1.5).

1.4.2 Analytical Research

This test program and earlier similar experimental research have shown the effectiveness of using shear reinforcement, and in particular shear bolts, to retrofit the shear capacity and ductility of individual slab-column connections [7]. However, quantifying the effect of these types of reinforcement on the behaviour of a complete structure is important in order to understand and advance this technology. As it is not practical to test a full scale structure in the lab, the objective of this study is the investigation of system behaviour using a computer-based model, which incorporates the joint behaviour (determined experimentally and/or analytically) into the evaluation of the seismic response of flat plate frames.

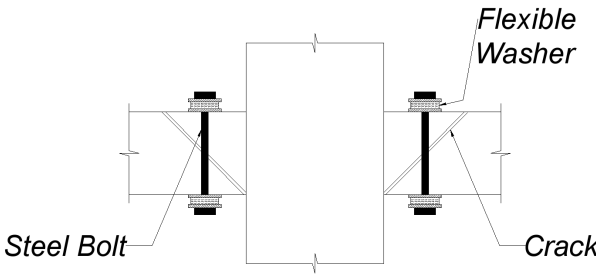

(a) Shear Reinforcement

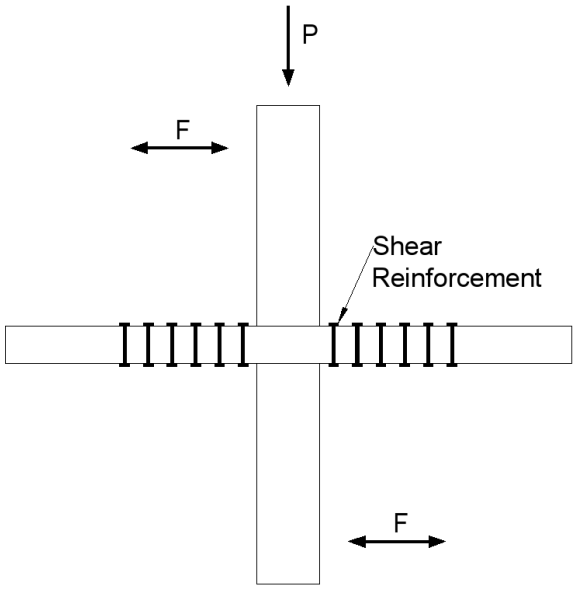

(b) Specimen

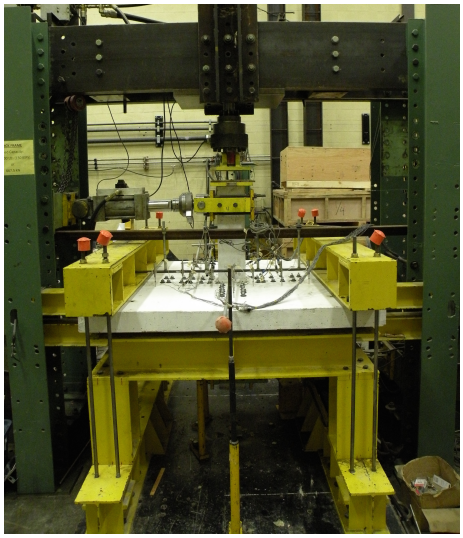

(c) Testing Frame

Figure 1.5: Experimental Research Components

Fig. 1.6 shows the sequence of the analytical research. The effect of the proposed shear reinforcement on the crack interface behaviour is investigated first. This response is then incorporated into the slab-column joint model, to investigate the effect on the lateral response of the joint. Modelling of frames, as assemblages of these joints, enables then the investigation of the performance of flat plate systems, under seismic forces.

1.5 Contributions of this Research

This research involved an experimental investigation of new shear reinforcement retrofitting techniques, which increase the ductility of slab-column connections, without considerably increasing strength and stiffness. Such connections improve the performance of flat plate structures subjected to earthquake loading, allowing for a ductile behaviour without attracting higher seismic forces. This research is the first of its kind to introduce controlled-anchorage shear reinforcement, for applications involving flat plate systems in seismic areas.

Models were developed to prove the effectiveness of such shear reinforcement at a micro-level, focused at the crack interface response, and at a macro-level, focused on the performance of frames, as assemblage of these joints. These models involved the integration of other original or modified models, adjusted for the slab-column joints and flat-plate systems. The associated computer code is linked to the finite element open source platform OpenSees [38] (Open System for Earthquake Engineering Simulation) widely used in structural engineering research. Thereafter, it is possible to analyse complex structures, due to the extensive library of relevant structural and loading features included in OpenSees. The computer code, written in C++, may be integrated into the original code of OpenSees, or linked as Dynamic Link Library (DLL).

A combination of computational and experimental components enhances the practical value of this research in the analysis and retrofit of reinforced concrete flat plate building systems. Tests showed the effectiveness of controlled-anchorage shear reinforcement in improving the ductility of joints, while the large scale models showed the effectiveness

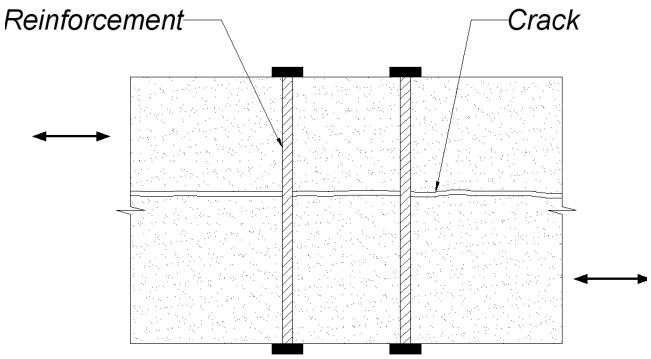

(a) Crack Model

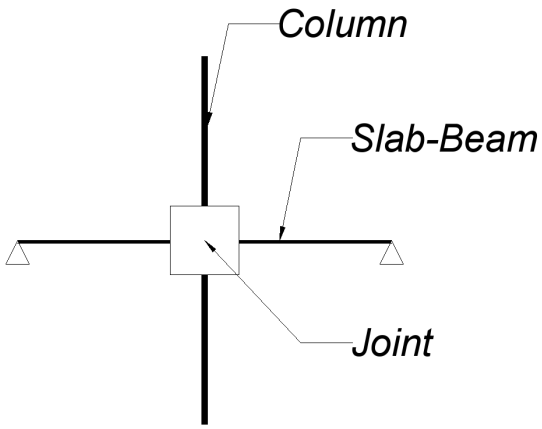

(b) Joint Model

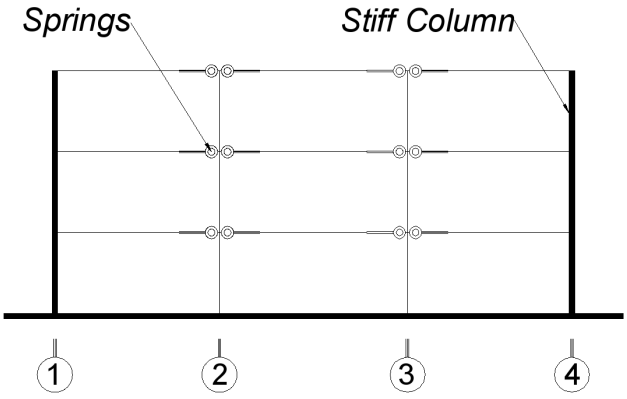

(c) Frame Model

Figure 1.6: Analytical Research Components

of such reinforcement on the seismic response of flat plate structures, testing of which is otherwise not feasible.

1.6 Organization of the Thesis

Chapter 2 reviews the available literature on previous research done on experimental and/or analytical/numerical work on isolated slab-column connections and full scale reinforced concrete flat plate systems.

Chapter 3 presents the experimental work conducted during the course of this research, describes the test setup and reports the collected results.

Chapter 4 presents analytical modelling and parameter analyses of the crack interface behaviour and slab-column joints.

Chapter 5 presents a parameter investigation of flat plate systems as assemblage of different slab-column joints, subjected to various types of loadings.

Chapter 6 presents a discussion of the experimental and analytical results and the main conclusions, along with suggestions for future research on the topic.

Chapter 2

Literature Review

This chapter describes literature on previous work related to flat slabs. In Section 2.1 the research on modelling of flat plate systems is presented. In Section 2.2 the experimental research on punching shear retrofitting techniques is introduced, and in Section 2.2.3 the relevant previous research undertaken at the University of Waterloo is introduced.

2.1 Analytical Models

Large scale modelling of slab-column joints and flat plate systems enables the analysis of such structures using practical CPU time. This, however, comes with lower accuracy compared to more detailed finite element models, due to more conservative approximations accepted in modelling. Proper calibration of large-scale models, based on test results and detailed modelling, is necessary for a reasonable accuracy. This section reviews typical analytical models, used in the analysis and design of flat plate systems, and other models considered in the analytical part of this research.

2.1.1 The Direct Design Method

The calculation of slab moments in the Direct Design Method is based on the *statical moment*, M_0, calculated panel by panel [1, 35]:

$$M_0 = \frac{wl_2 l_n^2}{8} \tag{2.1}$$

The statical moment is then divided between positive and negative moments, which are further divided between middle strips and column strips. This method is subjected to restrictions related to structural regularity [43].

2.1.2 The Equivalent Frame Method

In this approach, the beam stiffness is computed in the conventional manner as a beam of height equal to the slab height and width equal to the original width of the slab strip bounded laterally by the centrelines of the panels on each side of the centreline of columns. The columns are considered to be attached to the continuous slab-beam by torsional members which are transverse to the plane frame. Torsional deformation of these supporting members reduces the effective flexural stiffness of the column at the support. This effect is accounted for by using what is known as *equivalent column*, with stiffness less than that of the actual column [35].

$$\frac{1}{K_{ec}} = \frac{1}{\Sigma K_c} + \frac{1}{K_t} \tag{2.2}$$

where: K_{ec} =flexural stiffness of equivalent column, K_c = flexural stiffness of actual column, and K_t = torsional stiffness of edge beam; all expressed in terms of moment per unit rotation.

The Effective Slab Width

In this approach, the slab is modelled as an equivalent beam with width $\alpha_i l_2$, where l_2 is the original width of the slab strip bounded laterally by the centrelines of the panels on each side of the centreline of columns. The effective slab-width factor α_i is computed by elastic plate theory such that a beam having depth equal to the slab depth and width equal to $\alpha_i l_2$ subjected to a uniform rotation angle θ would allow the column to have the same amount of rotation as in the case of the original slab-column connection [35].

2.1.3 Yield-Line Analysis

In a slab subjected to high loads, the reinforcement will yield first in regions of high moments. These portions will then act as plastic hinges, able to sustain the plastic moment while deforming plastically. Any further increase of loading will rotate the plastic hinge, and the moments will be redistributed to adjacent sections of the slab, causing them to yield. Eventually, a mechanism will form, in which the slab can deform plastically without an increase in the applied load. This method uses rigid plastic theory to compute the failure loads corresponding to given plastic moment resistances in various parts of the slab. It determines the capacity of trial designs, rather than designing the slab. As an upper bound method, it will predict a collapse load greater than the true load if an incorrect mechanism has been selected [35, 43].

2.1.4 The Strip Method

This method gives a lower-bound equilibrium solution to the moments in a slab. As such it provides a safe estimate of the capacity of the slab in flexure [35]. In contrast to the yield-line analysis, the strip method is a design method, by which the slab thickness and reinforcement can be determined.

2.1.5 Shortcomings of Commonly Used Slab Models

However, none of the aforementioned methods consider the non-linear behaviour of the slab-column connection and its strength and stiffness degradation under cyclic loading. Recent research has been carried out on this topic, aiming to capture the non-linear behaviour of flat-plate systems. Two of these models are discussed in the following sections.

2.1.6 Nonlinear Model by Kang et al. [28]

Kang et al. (2009) proposed a nonlinear model as shown in Fig. 2.1. A fibre model was used for the column and an effective slab width model was used for the effective slab-beam framing between the columns. The rigid-plastic torsional spring models the moment transfer at the slab-column connection, within the slab transfer width of $c_2 + 3d$, where c_2 is the width of the column and d is the thickness of the slab. The column strip plastic hinges model slab moments on either side of the column.

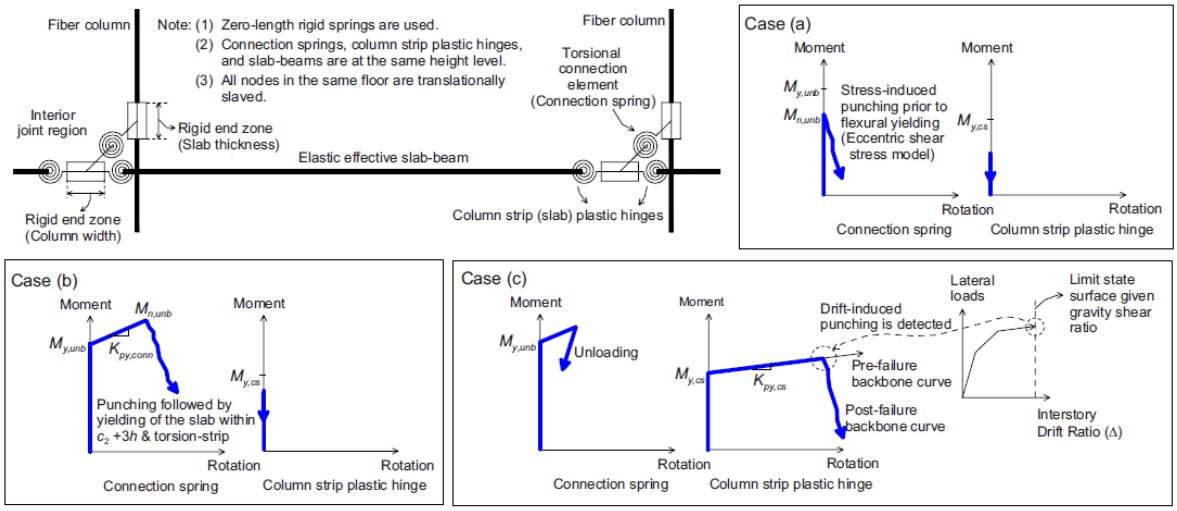

Figure 2.1: Nonlinear model developed by Kang et al. [28]

Flexural yielding occurs only if the moment capacity of the column strip plastic hinge is reached, or if the unbalanced moment capacity of the torsional spring is reached. Punching failure is modelled by the torsional spring and can occur if the shear stress on the slab critical section reaches a critical value or if the limit state [16] associated with interstory drift versus gravity shear stress ratio on the critical section is reached.
Three types of failure may happen in this analytical model:

- Punching failure prior to yielding of slab reinforcement.
- Punching failure after yielding of slab reinforcement within the transfer width.
- Punching failure after yielding of slab reinforcement within the column strip.

2.1.7 Nonlinear Model by Tian et al. [58]

Tian et al. (2009) developed a nonlinear model of a slab-column connection using elastic-plastic springs. Yielding of these springs is determined based on the strength of the connection (Fig. 2.2) in shear, flexure, and torsion, as following:

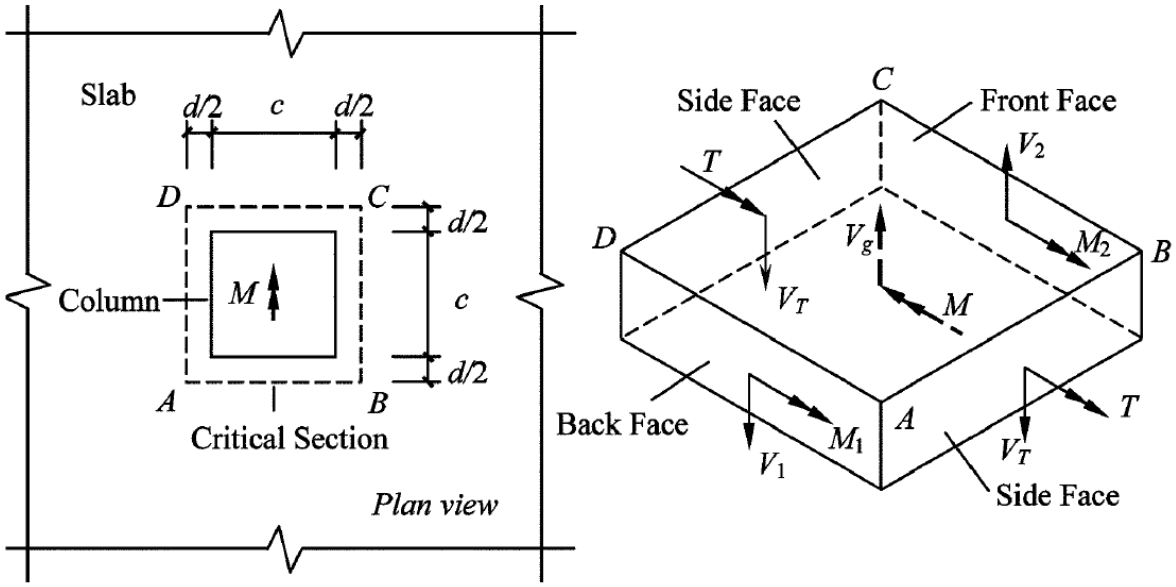

Figure 2.2: Internal forces acting on the critical section

Connection shear strength

The connection shear strength is defined as:

$$V_n = 0.65\xi A_c(\rho f_y \sqrt{f'_c})^{1/2} \text{ (in SI units)} \tag{2.3}$$

where: $A_c = 4(c+d)d$ and $\xi = \sqrt{\frac{d}{c}}$

Unbalanced moment resisted by flexure at the bending faces

The flexural strength at the back and front faces of the critical section is determined as: [58]

$$M_{n,1} = A_{s,1} f_{y,1} d_1 \frac{c+d}{s_1}(1 - 0.59\frac{A_{s,1} f_{y,1}}{s_1 d_1 f'_c}) \tag{2.4a}$$

$$M_{n,2} = A_{s,2} f_{y,2} d_2 \frac{c+d}{s_2} (1 - 0.59 \frac{A_{s,2} f_{y,2}}{s_2 d_2 f_c^{'}}) \tag{2.4b}$$

where $f_c^{'}$ is the concrete compressive strength; $A_{s,1}$, $f_{y,1}$, d_1, and s_1 denote the bar area, yield strength, effective depth, and spacing of top bars located in a width of c + d centered on the column, respectively, and $A_{s,2}$, $f_{y,2}$, d_2, and s_2 are defined similarly but for the bottom reinforcement. For connections with bottom reinforcement terminated at the column, $M_{n,2}$ is limited to the flexural cracking moment evaluated for a width of slab equal to c + d.

Unbalanced moment resisted by shear at bending faces

The maximum shear values that can be resisted at the side faces may be defined as:

$$V_{n,1} = 0.25 V_n \tag{2.5a}$$

$$V_{n,2} = 0.25 V_n^{'} \tag{2.5b}$$

where: V_n is the shear capacity of a connection subjected to gravity load only and $V_n^{'}$ is the shear capacity if an upward vertical load acts on the slab, causing tension in the slab bottom surface close to the column. V_n is determined by Equation 2.3. For $V_n^{'}$, bottom reinforcement properties must be used.

The rotational strength of the connection from shear $V_{n,1}$ and $V_{n,2}$ is defined as a moment about the critical section centroid as:

$$M_{vn,1} = V_{n,1} (\frac{c+d}{2}) \tag{2.6a}$$

$$M_{vn,2} = V_{n,2} (\frac{c+d}{2}) \tag{2.6b}$$

The unbalanced moment resisted by flexure and shear at a plastic hinge may be combined as a sum of both moments:

$$M_{n,1}^{*} = M_{n,1} + M_{vn,1} \tag{2.7a}$$

$$M^*_{n,2} = M_{n,2} + M_{vn,2} \tag{2.7b}$$

Unbalanced moment resisted by torsion at side faces

Kanoh and Yoshizaki [29] conducted a series of tests to determine the torsional strength for a slab-column connection, without the presence of gravity shear, as shown in Fig. 2.3. Tian et al. incorporated this research into their model. For simplicity, T_0 was defined as a function of critical section geometry and concrete strength:

$$T_0 = \nu_T (c + d) d_0^2 \tag{2.8}$$

where: ν_T is the nominal torsional shear strength, defined as $\nu_T = 2.1\sqrt{f'_c}$ (MPa) based on test results and d_0 is the distance between top and bottom reinforcement layers.
In the presence of gravity shear, a reasonable interaction relationship is:

$$\frac{T_n}{T_0} + \frac{V_T}{V_{n,1}} = 1 \tag{2.9}$$

where: V_T is the shear force on the side faces of the critical section.

The torsional strength in the presence of gravity shear would then be:

$$T_n = (1 - \frac{V_g - V_{n,1} + V_{n,2}}{2V_{n,1}}) \tag{2.10}$$

This model will be considered in this research in determining failure of the connection and the effect of the third direction on a two-dimensional frame, by considering the torsional strength described above.

2.1.8 Beam-Column Joint Model by Lowes et al. [34]

Lowes et al. developed a 2D model of the beam-column joint, which will serve as a basis of the slab-column connection model to be developed in this research. The element is shown in Fig. 4.10. It includes eight bar-slip components which are intended to simulate

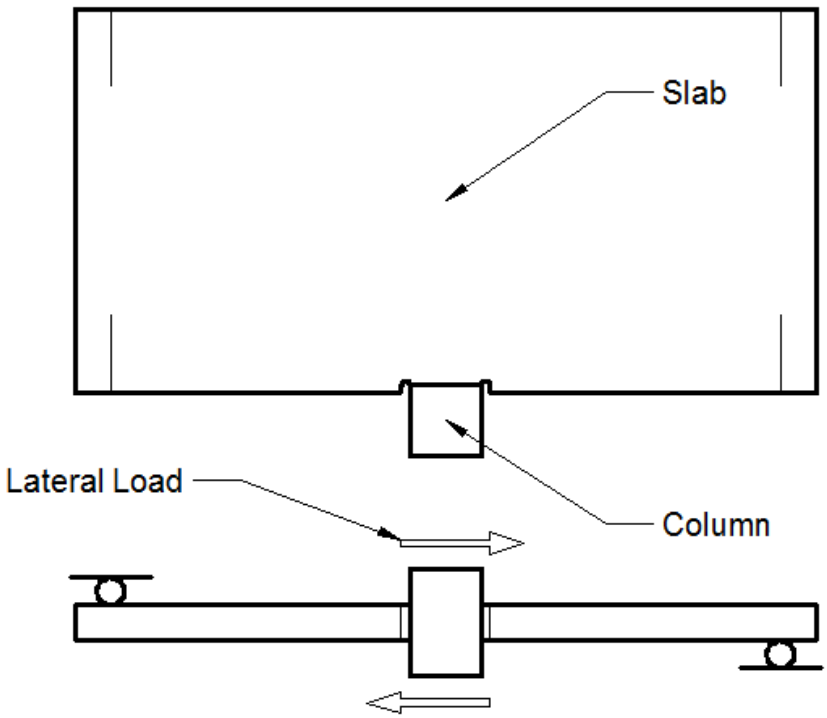

Figure 2.3: Test Scheme for the Determination of T_0 [29]

stiffness and strength loss associated with bond-strength deterioration for beam and column longitudinal reinforcement embedded in the joint core, one shear-panel component which is intended to simulate strength and stiffness loss associated with shear failure of the joint core, and four interface-shear components which are intended to simulate loss of shear-transfer capacity at the joint-beam and joint-column interface. This model and its use in this research are further discussed in section 4.2.2.2.

2.1.9 Crack Interface Behaviour [61, 62]

Walraven developed an aggregate interlock model to determine the shear stress-slip along a crack interface. While the aggregates slip and crush the matrix, the springs representing the reinforcement crossing the crack restrain the opening of cracks, as shown in Fig. 2.4. In this research, this model is used to model the behaviour along the punching crack interface, as further described and implemented in Chapter 4.

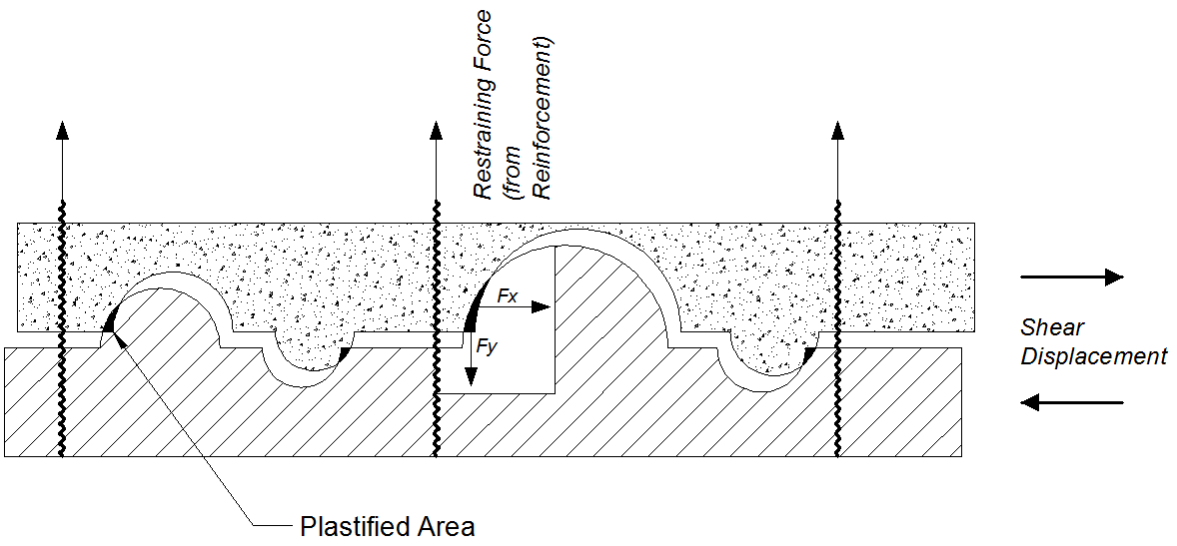

Figure 2.4: Walraven Model [61, 62]

2.2 Experimental Research on Slab Shear Reinforcing Techniques

Shear reinforcement is an efficient method of preventing punching shear failure of slab-column joints, by preventing the propagation of punching shear cracks. In general shear reinforcing consists of a properly anchored bar crossing the crack. The selection of the type of shear reinforcement depends on several factors, including availability, cost and whether it is for a new construction or for the retrofit of an existing slab.

2.2.1 Shear Reinforcement Used in New Construction

In new construction, shear reinforcement is embedded into the concrete before the slab is cast. The three main groups are: (1) structural steel sections (2) bent bars and stirrups and (3) headed bars including shear studs (Fig. 2.5).

Research on shear reinforcement in slabs was initiated by Graf in 1933 [22] and Wheeler in 1936 [63]. However, most of the tests and practical design provisions came later in the 1970s and 1980s, with the contributions of Hawkins in 1974 [23], Hawkins

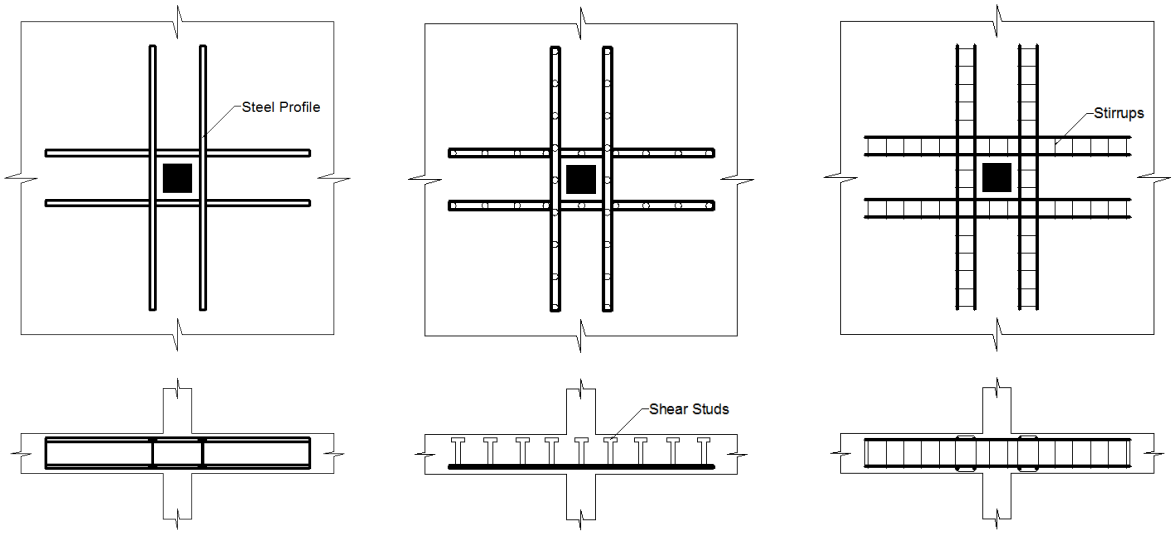

(a) Profiles (b) Shear Studs (c) Stirrups

Figure 2.5: Types of Shear Reinforcement

and Corley in 1974 [25], Langhor et al. in 1976 [32], Dilger et al. in 1978 [11], Seible et al. in 1980 [54], Dilger and Ghali in 1981 [10], Andra in 1981 [4], Pillai et al. in 1982 [49], Regan in 1985 [51] and Mokhtar et al. in 1985 [42].

Hawkins and Corley [25] tested the effect of I-shape profiles in edge slab-column connections, concluding that the I-shape steel increases shear and rotation capacity of the connection. However, these sections cause a congestion of reinforcement in the connection, making this type of punching shear reinforcement not practical except for thick slabs and large columns.

Dilger and Ghali [10] tested shear studs welded to a bottom steel strip. Tests showed that the shear capacity and ductility of the connection were increased. The stud heads provide anchorage to concrete allowing the studs to yield, and allowing very good performance under both static and dynamic loading conditions.

Megally and Ghali [40] tested five interior slab-column connections, four of which were strengthened by shear capital, drop panel, stirrups, and shear studs, respectively. They concluded that a shear capital and a drop panel increase the punching shear capacity, but not the ductility of the connection. Stirrups increase strength, but not ductility, due

to poor anchorage. Shear studs substantially increased both strength and ductility of the connection.

2.2.2 Shear Reinforcement Used in Retrofitting Existing Structures

Existing slabs may need to be retrofitted for several reasons, such as to satisfy current codes or because they are subject to higher service loads than those used for the original design. The structural integrity of already damaged joints may also be restored by proper retrofitting. Research on retrofitting techniques was initiated by Ghali et al. (1974). Strengthening was provided by prestressing the slab around the column through tensile bolts placed in holes near the column. Tests showed that prestressing prevented or delayed the rotation and widening of the cracks necessary to create the failure surface. Later research was done by Ramos et al. (2000) who introduced shear heads consisting of steel I-beams around the column, and Ebead and Marzouk (2002) who used a similar approach using an integration of external steel plates and steel bolts bonded to the slab surface. Both these techniques improve the behaviour of the connection, changing the failure type from brittle to flexural, but they are elaborate and change the aesthetics of the slab.

In 2013 Fernandez et al. [53] tested 20 slabs with dimensions 1,500mm x 1500mm x 125mm with various integrity reinforcement layouts to check the post-punching behaviour of flat slabs. This research concluded that the post punching strength of the slab-column connection can be increased by suitably anchored integrity or flexural reinforcement (Fig. 2.6).

Additional research on this issue has been carried out at the University of Waterloo, as further detailed in Section 2.2.3.

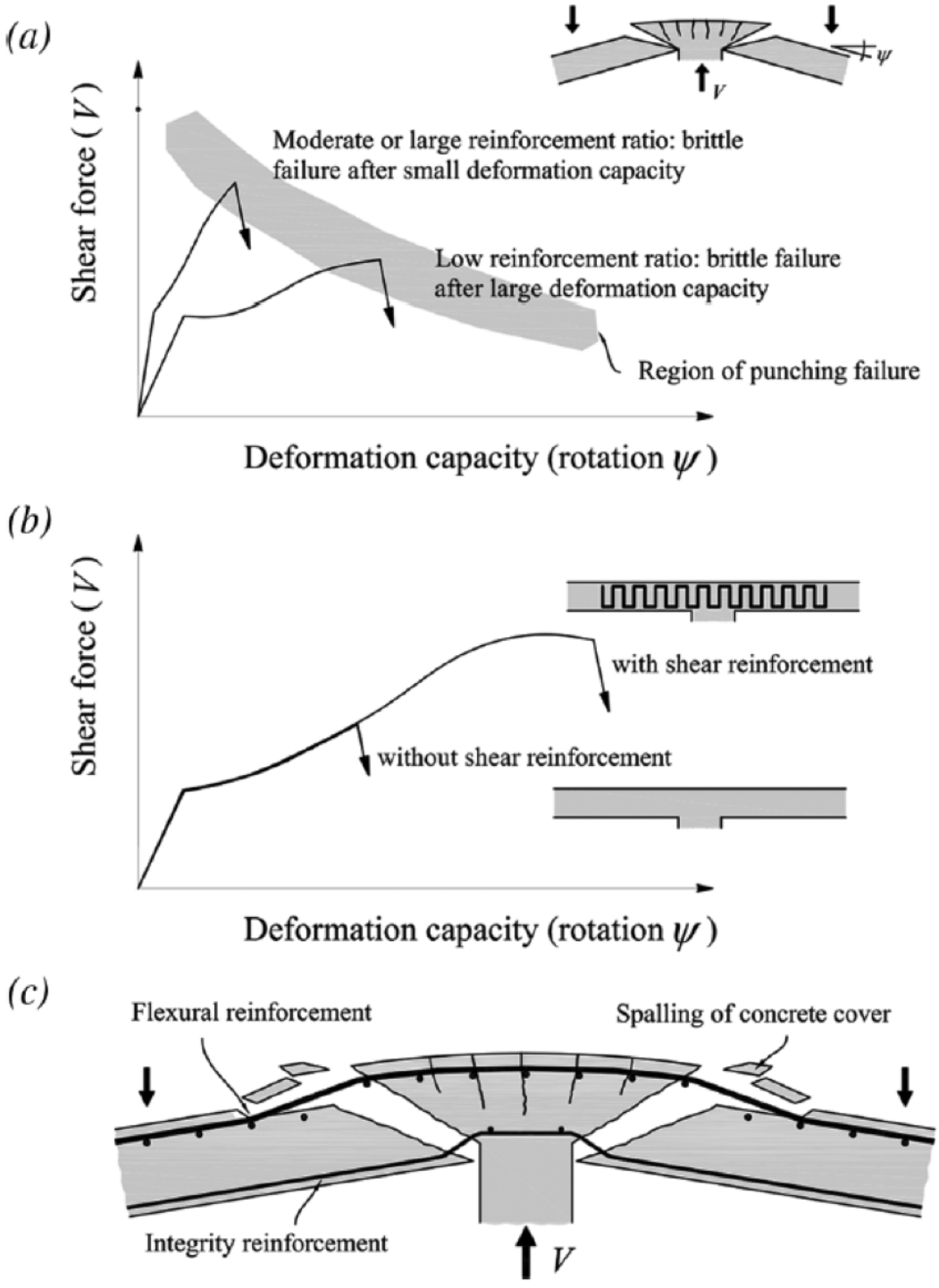

Figure 2.6: Behaviour of flat slab failing in punching shear: (a) brittle and ductile failures depending on amount of flexural reinforcement; (b) brittle and ductile failures for members without and with shear reinforcement; and (c) activation of flexural and integrity reinforcement after punching shear failure. [53]

2.2.3 Previous Research Work on Punching Shear at the University of Waterloo

Several test programs related to punching shear of reinforced concrete slab-column connections have been carried out at the University of Waterloo, involving both edge and interior connections, with and without openings near the column, and with and without shear reinforcement. The specimens were subjected to different combinations of vertical and lateral static cyclic loads. The shear reinforcement developed at the University of Waterloo is called *shear bolt* and consists of a headed rod threaded at the other end for anchoring using a washer and nut, as shown in Fig. 2.7. The bolts are installed in holes drilled in slabs around the column perimeter.

In 2003, El-Salakawy et al. [14] published the results of tests on four edge slab-column specimens strengthened by shear bolts, concluding that shear bolts can increase the capacity and ductility of slab-column edge connections. The failure mode of the specimens also changed from brittle punching shear mode to a more favourable flexural mode.

Adetifa and Polak (2005) [2] tested six interior slab column connections reinforced with shear bolts subjected to vertical loading only. All of the slabs were simply supported on four sides on the bottom surface. They concluded that the slab-column connections strengthened with four rows of shear bolts increased ultimate punching shear load by 42.3% and displacement ductility by 229%, compared to the specimens without shear bolts.

As a continuation of this work, Bu [6] tested several slab-column connections reinforced with shear bolts and compared them with unreinforced connections. The effect of openings in the slab close to the column was also analysed and tested. Steel shear bolts were shown to be an effective method for retrofitting slabs in seismic zones, changing the failure mode from brittle punching to ductile flexural. The reinforced slab-column connection showed higher ductility and the capability of undergoing more large drift cycles than unreinforced connections. The lateral load-deformation response is shown in Fig. 2.8; Joints SW1 and SW5 are not reinforced with shear bolts while SW2, SW3 and SW4

are reinforced with steel shear bolts with various numbers of rows.

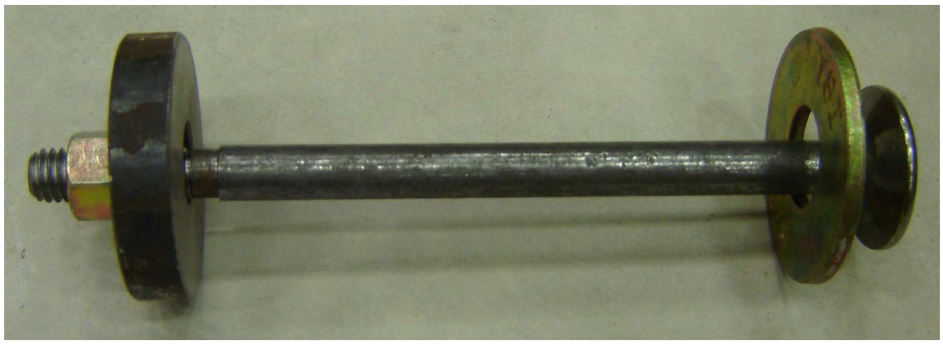

Figure 2.7: Steel Shear Bolt

In 2008, Lawler [33] tested slab-column connections reinforced with shear bolts made of glass fibre-reinforced polymer (GFRP). He concluded that FRP can be an effective reinforcement material for the retrofit of slab-column connections against punching shear failure in both static and seismic loadings.

In comparison to the slab-column connections reinforced with steel bolts tested by Bu, the FRP connections showed lower strength, but also less pinching, resulting in higher energy dissipation. This happened because the GFRP bolts were not perfectly tightened against the slab surface. This allowed for opening of cracks within the slab and the friction between the crack faces under cyclic loading dissipated more energy. The opening of cracks was also the reason of lower strength than in the connections reinforced with steel bolts.

The results of the last series of tests and the effect the internal crack friction has on the energy dissipation of the connection will be utilized in this research in the development of seismic shear strengthening techniques.

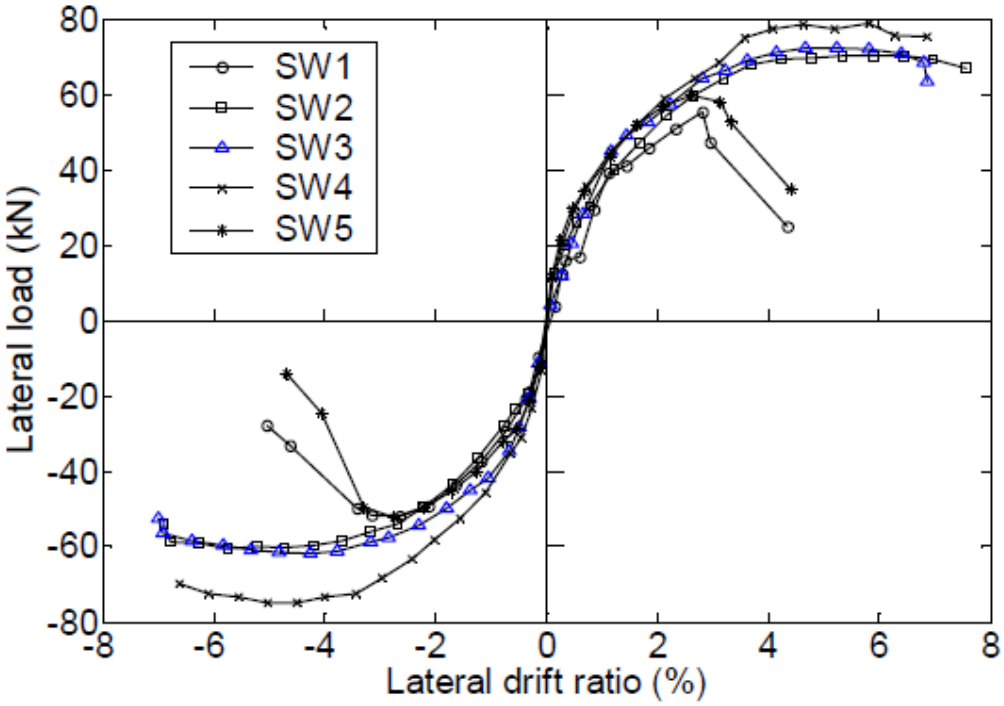

Figure 2.8: Backbone curves of horizontal load - drift ratio at top column end (Bu [6])

2.3 Experimental Research on Reinforced Concrete Flat Plate Systems

In 2008 Fick [18] tested a full scale flat plate frame, subjected to vertical loading and cyclic lateral displacements. The frame had three floors and 1x2 bays, with a a total of six columns. The dimensions and test setup are shown in Fig. 2.9. The following was concluded from this research:

1. Using and effective width factor of 1/3 of panel width resulted in a conservative estimate of stiffness for story drift ratios not exceeding 0.2%.

2. The limiting drift condition of the full-scale flat-plate structure falls within the bounds of test data from small-scale isolated slab-column tests.

3. A lower bound to the limiting story drift ratio (SDR) for slab-column connections

can be estimated with the following Equation:

$$SDR(\%) = 4(1 - 2\gamma) \tag{2.11}$$

where:

γ=gravity shear ratio, $\frac{V_g}{V_0} \leq 0.5$

V_g=gravity shear carried by the slab-column connection

V_0=nominal shear capacity of the slab-column connection, defined by the ACI Code

The test results of this experimental work are used in validating the frame model in section 5.2.

A considerable amount of experimental research is available on shear reinforcing of slab-column connections for new construction as well as for the retrofit of existing structures. The seismic performance of such connections, and flat plate systems in general, however, needs further investigation.

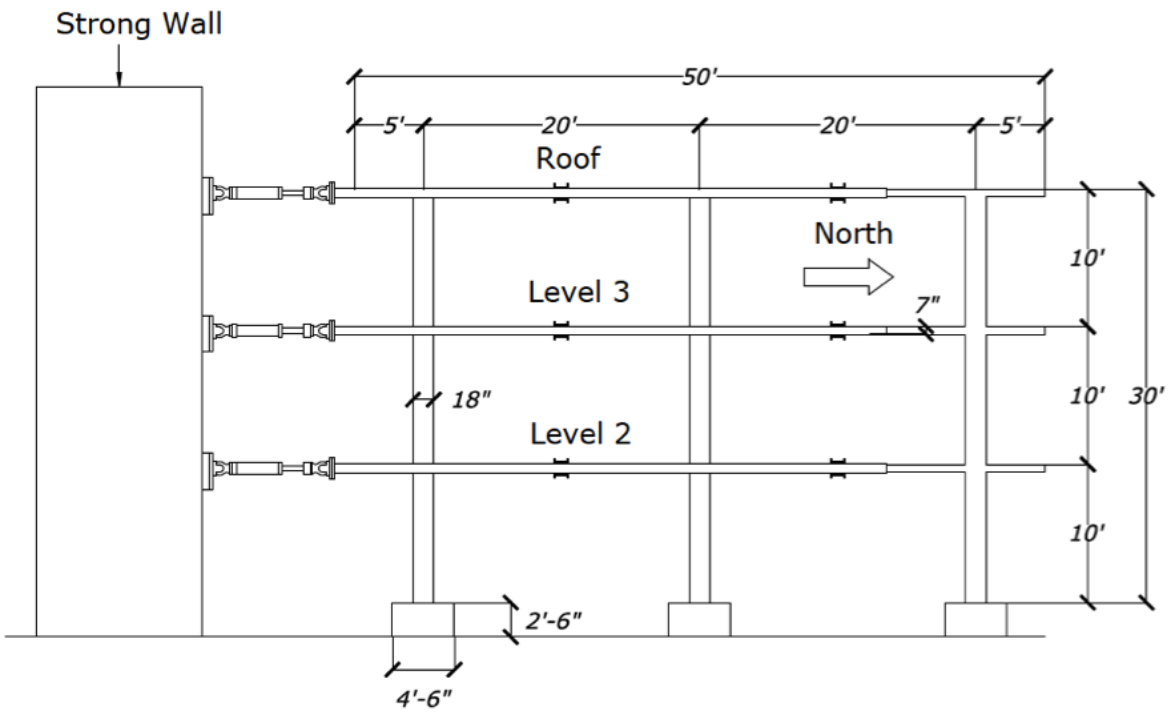

(a) Test Setup

(b) Frame Picture

Figure 2.9: Frame Tested by Fick *et al.* [18]

Chapter 3

Experiments on Slab-Column Connections

3.1 Introduction

This chapter describes the experimental part of the research, focused on the investigation of the behaviour of reinforced concrete slab-column connections retrofitted with different types of shear reinforcement while subjected to a combination of constant gravity loading and increasing cyclic lateral drift. The testing program consists of six specimens, five of which were shear retrofitted with a combination of steel bolts and flexible washers.

Based on experimental evidence, the installation of shear reinforcement introduces a high level of pinching in the lateral load-displacement response, as a result of increased strength and stiffness at the slab-column connection [6]. Stiff steel bolts keep the connection within a relatively elastic range, limiting the amount of plastic deformations. A shear reinforcement that would allow larger, but limited opening of cracks, without hindering the punching strength of the connection, would allow for remaining plastic deformations at the connection; decreasing pinching without allowing for a brittle punching failure. Such phenomenon has been observed from previous tests at the University of Waterloo [33], where slab-column connections were retrofitted in punching shear with GFRP bolts that were not completely tightened. This allowed slight opening of shear cracks,

resulting in lower pinching and ductile lateral load-deformation response.

Herein, a new type of punching shear retrofit elements, shear bolts with flexible washers, are introduced. The flexible washers allow for shear crack opening during the lateral displacements, while at the same time provide control of the crack width by using the appropriate washer thickness and/or stiffness. This study focuses on how such type of shear reinforcement can improve punching shear capacity of flat slabs, while introducing lower pinching to the lateral load-deformation response of slab-column connections. Such connection response would enable a more efficient capacity design of flat plate systems by distributing strength and stiffness more appropriately. Washers of different levels of flexibility were used with the bolts to test different levels of opening of punching shear cracks.

The results show that this type of shear reinforcement improves the lateral load-deformation response of the connections, increasing the ductility without a commensurate increase in strength. Lower strength also results in lower shear forces attracted by the column and continuous opening and closing of cracks results in higher energy dissipation through friction within the crack interfaces. The system was designed for slab retrofit, however it can be anticipated that similar concepts can be used in construction of new slabs in seismic zones.

A pilot test was conducted first in 2009, as part of an undergraduate research program [3], using Nitinol as shear reinforcement as described in Section 3.2. Subsequently, six specimens were tested, reinforced with a combination of steel bolts and flexible washers, as discussed in Section 3.3.

3.2 Pilot Test: Slab Shear Retrofitted with Nitinol

3.2.1 Introduction

This Section introduces the experimental work on a flat slab-column joint retrofitted with a combination of typical steel bolts and Nitinol restrainers as shear reinforcement.

The test of the Nitinol restrainer (Section 3.2.2) was part of this research program, while the test of the slab-column joint (Section 3.2.4) was part of an undergraduate research project [3], carried out under the supervision of this research program.

3.2.2 Application of nitinol in structural engineering

Nitinol (NiTi) is a shape memory alloy made of nickel and titanium. It can experience large deformations (up to 8% strain) and return to the undeformed shape by heating (known as the shape memory effect) or by removal of stress (known as the super-elastic effect).

Nitinol experiences phase transformation between its two states of austenite and martensite, introducing energy dissipation. Martensite is stable at low temperature and high stress, while austenite is stable at high temperatures and low stress. The behaviour of nitinol as a function of stress, strain, and temperature is shown in Fig. 3.1. At low temperatures, nitinol exhibits the shape memory effect; deformations are recovered by heating. At higher temperatures, it exhibits the super-elastic effect; deformations are completely recovered by unloading. At yet higher temperatures, it exhibits elasto-plastic behaviour with higher strength.

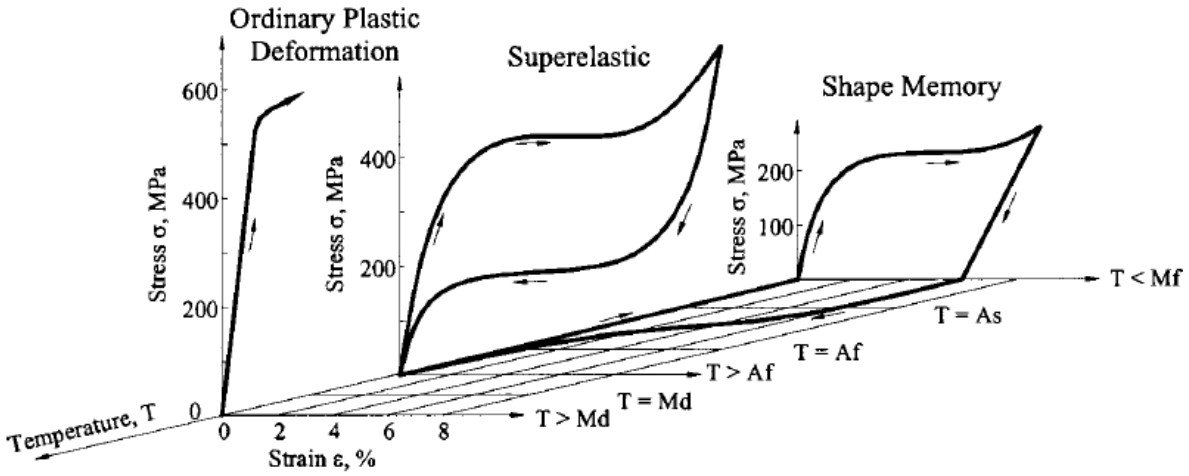

Figure 3.1: Stress-strain-temperature behaviour of NiTi [9]

Super-elastic nitinol possesses properties that make it efficient for applications in seismic resistant design and retrofit of structures. These properties include: hysteretic damping; large elastic strain range resulting in recentering capabilities; excellent fatigue properties; strain hardening at large strains; and a large stress plateau, providing force transmission limitations [9].

A successful application is the rehabilitation of the Basilica San Francesco in Assisi, Italy, which was severely damaged by an earthquake in 1997. Super-elastic nitinol wires were used to connect the tympanum to the roof [37].

3.2.3 The Nitinol Restrainer Test

3.2.3.1 Test set-up

The purpose of this test was to check the efficiency of a connection reinforced with Nitinol and the mechanical properties of the nitinol wires constituting the retrofit. Seven wires of diameter 0.08" (2mm) were combined as shown in Figs. 3.2(a) and 3.2(b). The wires pass through the sleeve which is threaded into the socket. A plug is placed among the wires in order to cause friction between the wires and the socket, once the sleeve is threaded into the socket. This friction must resist tension forces in the nitinol wires. The restrainer was tested in cyclic tension as shown in Fig. 3.2(c). Measurement of deformations was done in two ways: the total elongation of the restrainer was measured using the distance between the actuators, while the elongation of the wires was measured by four strain gauges. Different results were expected from these measurements due to slippage of wires from the connections.

The restrainer was subjected to a cyclic displacement controlled loading as following: First it was strained until 1%, considering the distance between the actuators, after which it was unloaded. This process of loading-unloading was repeated for strains of 2%, 3%, 4%, 5% and 6%. Then the restrainer was loaded until failure.

(a) Assembled nitinol restrainer

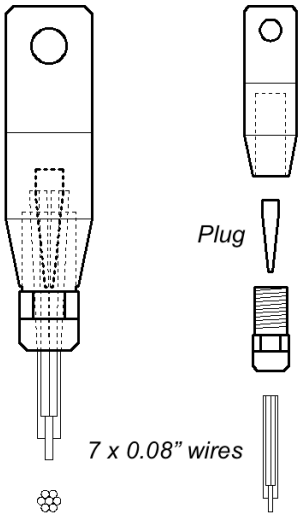

(b) Restrainer components

(c) Test set-up

Figure 3.2: Tensile Test of the Nitinol Restrainer

3.2.3.2 Results and Discussion

The recorded load-strain response is shown in Fig. 3.3. The grips did not allow wires to completely slip out, but high slippage was observed. This can also be seen from the load-strain response graph, where there is residual strain after each cycle within the elastic range of loading and compression forces at the end of the unloading cycle. The non-linearity of the response within low strain range and the high strain at the end of the yielding plateau are related to slipping of wires. The yielding plateau should have ended at a strain of around 6%.

Although slippage is a phenomenon that introduces energy dissipation because of friction, it needs to be minimized since it happens in one direction only. However, during the tests this factor was not controlled due to limitations in the connection design.

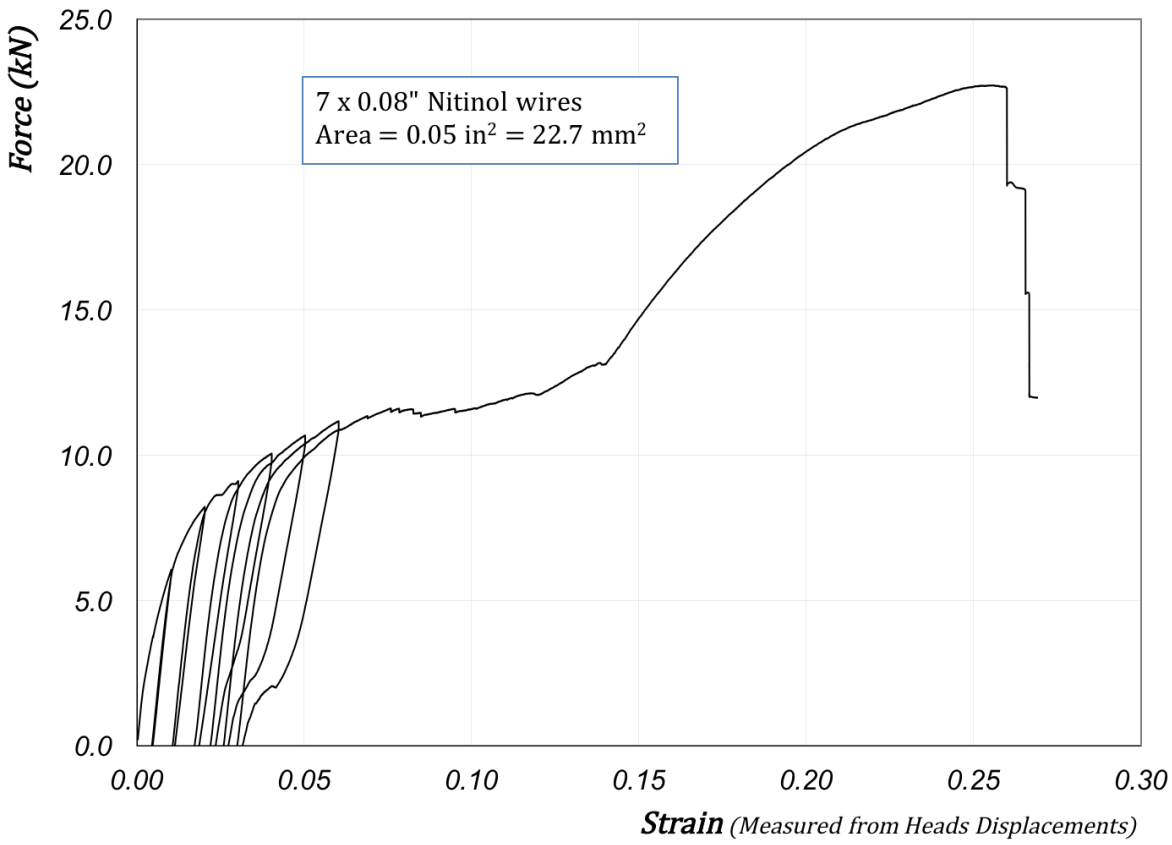

Figure 3.3: Force-strain relationship of the tested nitinol connection

3.2.4 The Slab-Column Connection Test

3.2.4.1 Test set-up

For comparison purposes, the slab was designed and tested similarly to the slab configuration reinforced with steel bolts only and tested by Bu [6] at the University of Waterloo in 2008. Eight out of the thirty two steel bolts in that slab were replaced by nitinol restrainers which were described in Section 3.2.3. Such configuration was decided based on the fact that from previous similar tests, only the first two rows of bolts experience deformations [6]. Out of the 16 bolts within the first two rows, half of the bolts were replaced by Nitinol considering their low stiffness compared to the steel ones. The plan configuration of shear reinforcement is shown in Fig. 3.4. The shear reinforcement is shown in Fig. 3.5. The rest of the test details are the same as described in [6] and

Section 3.3.

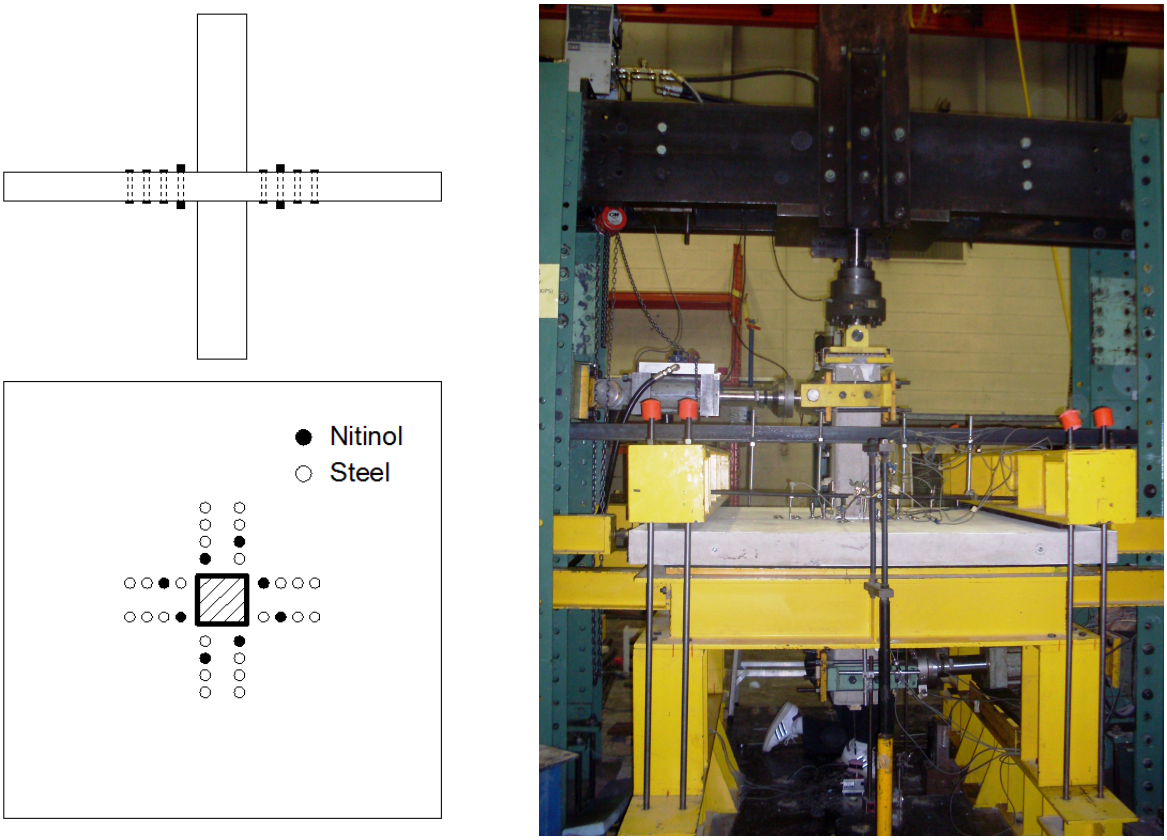

(a) Shear reinforcement configuration

(b) Test set-up

Figure 3.4: Slab-column connection specimen and test setup

The slab-column connection was subjected to a pseudo-dynamic displacement history, shown in Fig. 3.6, at the top of the columns. The measured lateral force applied at the top of the columns by the actuators was recorded at each step. The lateral force - displacement relation is shown in Fig. 3.7.

3.2.4.2 Results and Discussion

Comparing the slab-column connection reinforced with nitinol and steel bolts (CNiTi) to the slab connection with no shear reinforcement (C0) tested by Bu (Fig. 3.8(a)), it may be concluded that:

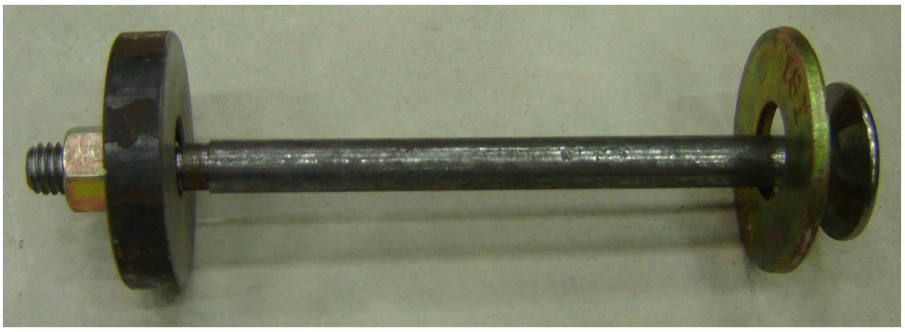

(a) Steel bolt

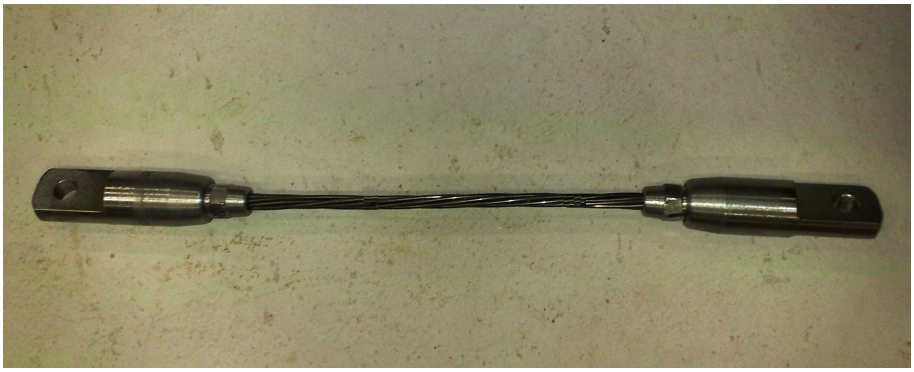

(b) Nitinol restrainer

(c) Shear reinforcement on the slab

Figure 3.5: Shear reinforcement used in the test

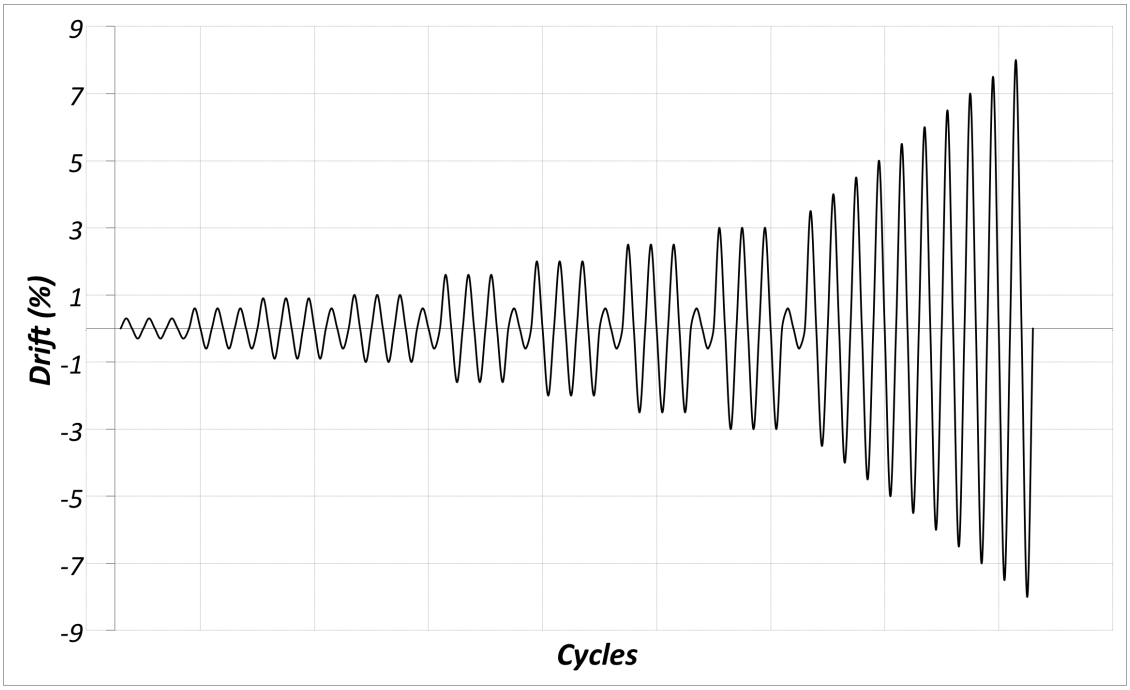

Figure 3.6: Applied Horizontal Displacement Path

- The CNiTi connection can experience larger lateral deformations (7% vs. 3% drift), while sustaining its load-carrying capacity, introducing a higher ductility in the joint response.
- The CNiTi connection shows less pinching than the C0 connection.
- The reinforcement of the CNiTi connection does not increase the stiffness, which would otherwise result in higher seismic forces.

Comparing the slab-column connection reinforced with nitinol and steel bolts (CNiTi) to the connection reinforced with steel bolts only (CS) tested by Bu (Fig 3.8(b)), it may be concluded that:

- The CNiTi connection shows a lower strength than the CS connection, resulting in lower seismic forces attracted by the slab-column joint.
- The CNiTi connection has less pinching than the CS connection.

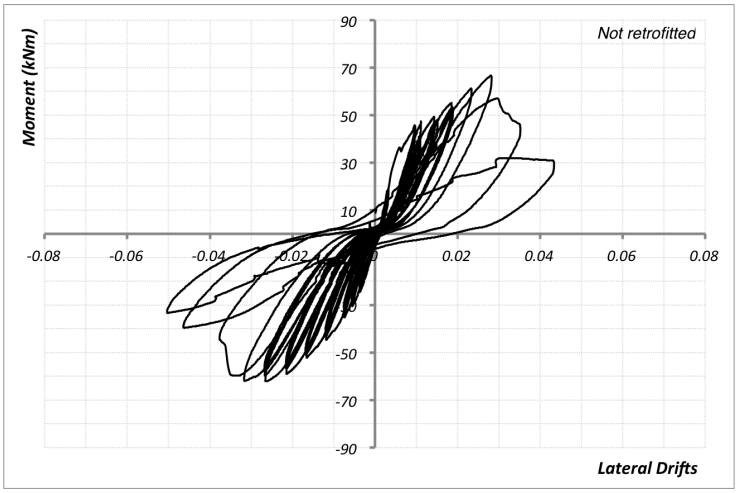

(a) C0 Connection

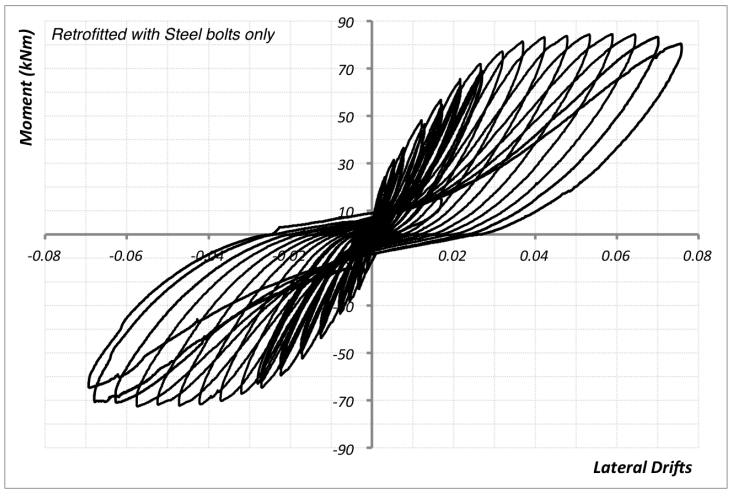

(b) CS Connection

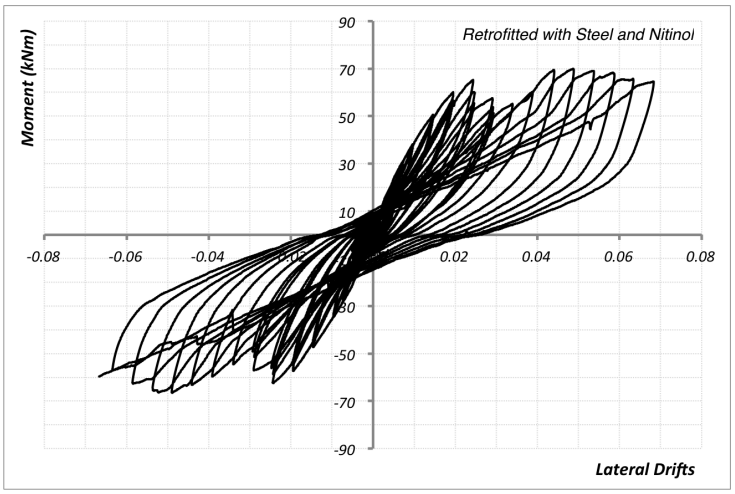

(c) CNiTi Connection

Figure 3.7: Moment-Drift Diagrams

- The CNiTi Connection undergoes the same lateral drift, preserving a high ductile behaviour.

From these comparisons it may be concluded that, as a result of lower stiffness, the CNiTi connection would attract lower seismic forces. The lateral force transferred to the columns would consequently be lower.

In this regard, the key feature of the connection design should be a 'soft connection', which allows for large displacements (rotations) without failing, even though it might have a lower strength than a steel reinforced connection. This would be achieved by allowing opening of cracks within a certain size during an earthquake event. In such a case, the lateral strength of the building may be concentrated on shear walls, while the slab-connections serve mostly for energy dissipation. One of the main challenges in the NiTi design, despite its obvious advantages, is that the level of slippage cannot be controlled. In addition, to take better advantage of Nitinol properties, the connection should be designed to undergo larger strains; possibly experiencing a full loop. Within the range of experienced strains on shear bolts, the benefits of Nitinol restrainers are not fully realized.

Building on these experiments, other experiments were carried out during this research, as further discussed in Section 3.3.

3.3 The Test Program

This study focuses on how anchorage-controlled shear reinforcement can improve the punching shear capacity, while introducing lower pinching to the lateral load-deformation response of slab-column connections. Such connection response would allow for more efficient capacity design of flat plate systems by distributing strength and stiffness more appropriately [47].

Six full-scale specimens were tested: SD01 being the control specimen, with no shear reinforcement, and SD02 to SD06 shear retrofitted with the configurations shown in Table

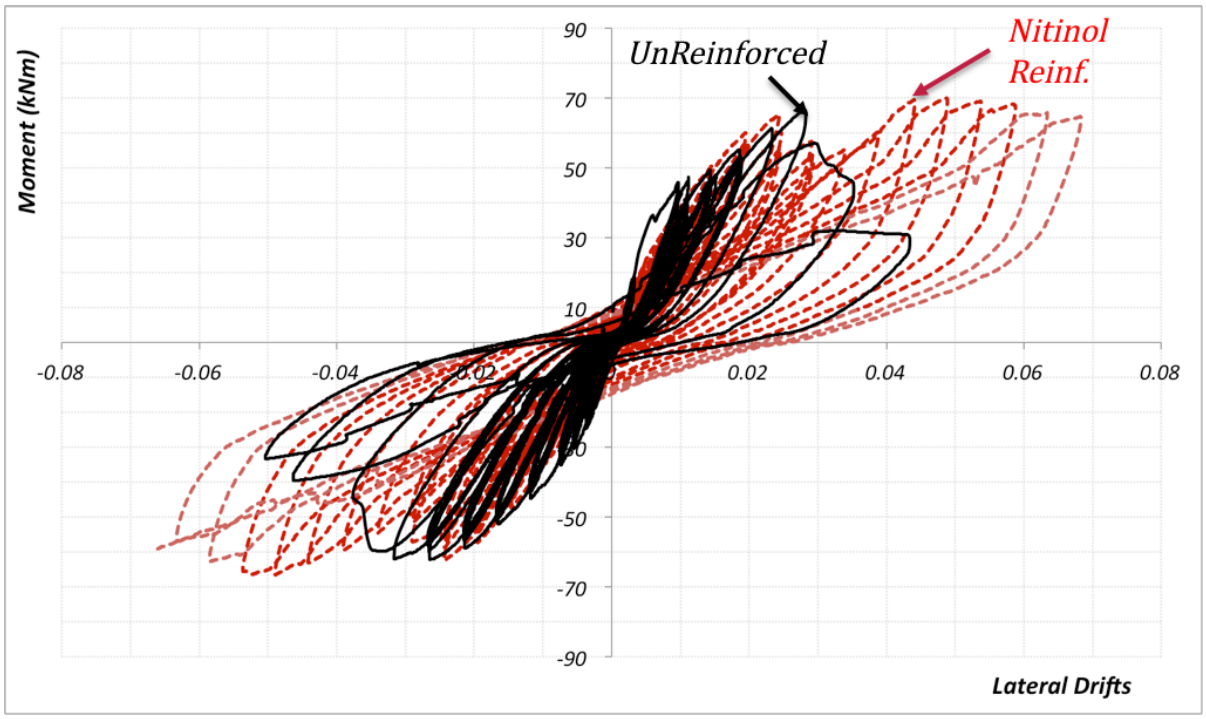

(a) C0 vs. CNiTi

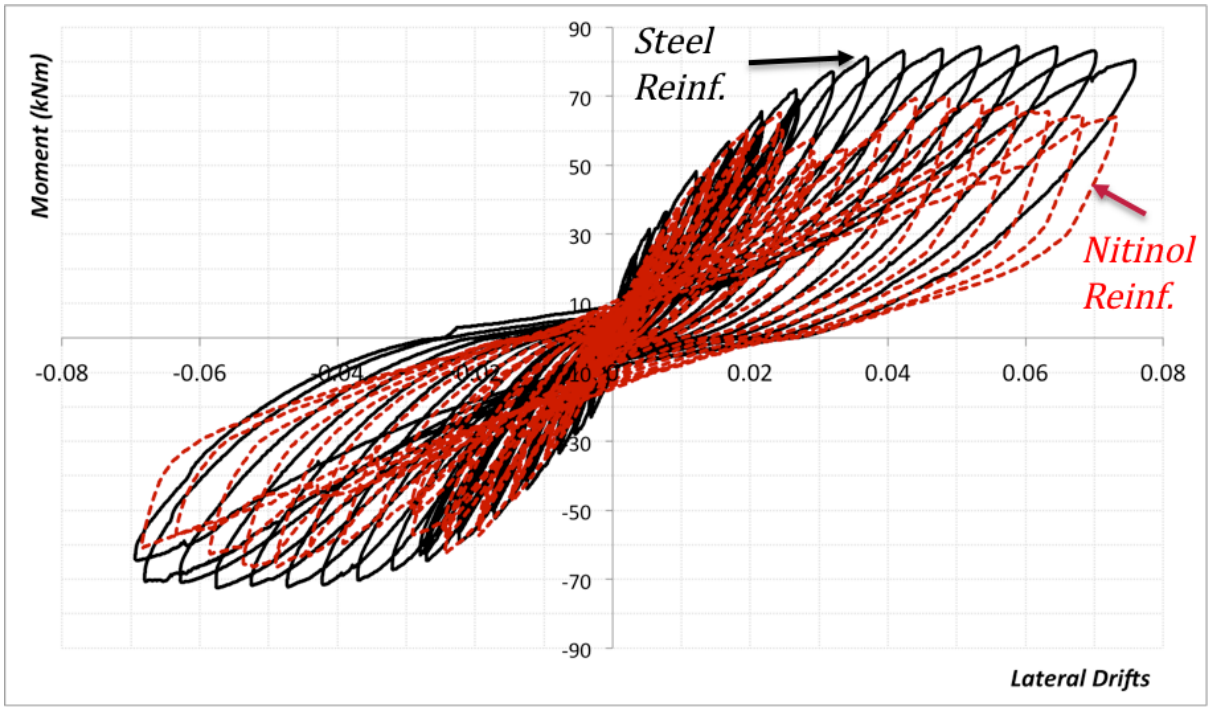

(b) CS vs. CNiTi

Figure 3.8: Comparison of Lateral Load-Deformation Responses

Table 3.1: Test specimens

Spec.	Dimensions (between supports) (m)	Vert. Load (kN)	Concrete Comp. Strength (MPa)	Concrete Tensile Strength (Split) (MPa)	Gravity Shear Ratio	Type of Shear Reinforcement
SD01	1.5 x 1.5 x 0.12	110	50	3.2	0.45	No Shear Reinforcement
SD02	1.5 x 1.5 x 0.12	110	50	3.2	0.45	SB + 1 × 3mm Neoprene Washer
SD03	1.5 x 1.5 x 0.12	110	41	3.0	0.50	SB + 1 × 3mm Nylon Washer
SD04	1.5 x 1.5 x 0.12	110	41	3.0	0.50	SB + 1 × 3mm Nylon Washer
SD05	1.5 x 1.5 x 0.12	110	50	3.2	0.45	SB + 2 × 3mm Nylon Washers
SD06	1.5 x 1.5 x 0.12	110	41	3.0	0.50	SB Only

3.1. The specimen design followed work done previously by Bu and Polak [6, 7]. All specimens were first subjected to a vertical load of V=110 kN, which was kept constant while the connection was subsequently subjected to lateral cyclic displacements, until failure, defined by a significant drop in the lateral strength. The magnitude of the vertical load was selected to the same as in the specimens tested by Bu [6], for comparison purposes. The test results would be affected by a different load; a higher load (higher gravity shear ratio) would result in a lower lateral deformability of the specimen.

The designed concrete strength of these specimens was 35 MPa, resulting in a gravity shear ratio $\frac{V}{V_n} = 0.54$, where: $V_n = 0.33\sqrt{f'_c}b_0 d = 203.8kN$ [1]; $b_0 = 4(c+d) = 1,160mm$ is the perimeter length of the critical section, and $d_{average} = 90mm$ is the effective thickness of the slab. The actual gravity shear ratios are shown in Table 3.1.

3.3.1 Specimen Dimensions

Since this research follows previous experimental work done at the University of Waterloo, the same specimen configuration has been considered with regard to dimensions and flexural reinforcement for comparison purposes. The shear reinforcement is the only difference from these specimens and the previous ones tested by Bu [6]. The specimens, shown in Fig. 3.9, may be regarded as taken from a prototype structure (Fig. 3.10) in which the flat slab spans 3.75m between columns [2]. All specimens have slab dimensions of 1,800 x 1,800 x 120 mm with top and bottom column stubs with a section of 200 x

200 mm and a length of 700 mm going through the centre of the slab. Figs. 3.12, 3.13, 3.14 and 3.16 show the preparation work for the specimens. Horizontal displacement controlled loads were applied at the column stubs, at a distance of 565 mm from the top and bottom faces of the slab. The specimens were simply supported at a 1,500 x 1,500 mm perimeter on the bottom face of the slab.

The dimensions of the slab were chosen to represent the portion of a full-scale slab located between the contraflexure lines for the case of gravity loads. Thick neoprene pads were provided on top and bottom of the slab to allow for rotations along the contraflexure lines. The neoprene pads were 25 mm thick and 50 mm wide, and installed along the lines of support, as shown in Fig. 3.9(a).

Due to the test setup used in this case, the orientation of the specimen relative to the applied gravity loading, is the opposite of a real case scenario in buildings. The top area of the slab specimen around the column was subjected to compression, while the bottom area was subjected to tension. The gravity load was applied, through the top column from the vertical actuator.

3.3.2 Flexural Reinforcement

On the bottom of the slab, the tension flexural reinforcement ratio was 1.05% for the outer bars (10M at 100 mm) and 1.3% for the inner bars (10M at 90 mm), to ensure the same flexural capacities in both orthogonal directions. On the top face of the slab the reinforcement ratio was 0.58% (10M at 200 mm) in both directions.

The reinforcement of the columns consisted of 8-25M bars (three bars on each face) with 10M at 100 mm closed ties. The columns were designed to transfer shear force and cyclic moment to the slab, while experiencing negligible deformations.

The configuration of the reinforcement is shown in Fig. 3.11.

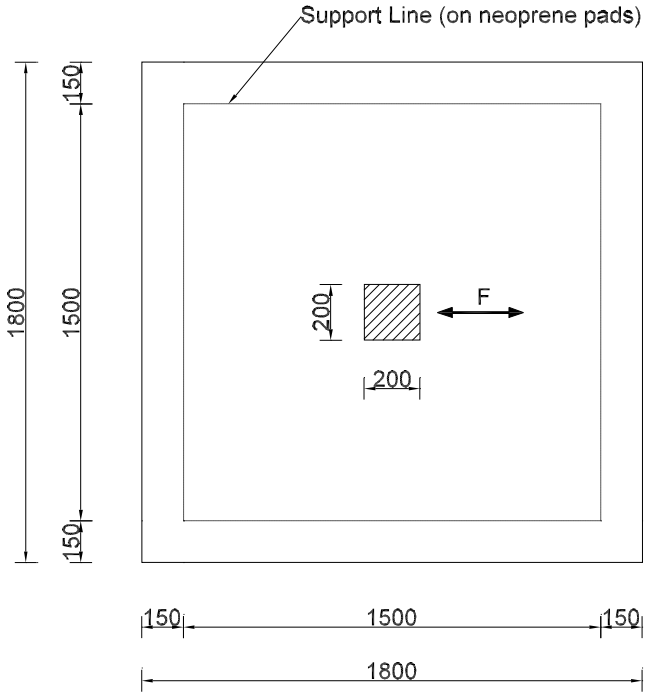

(a) Plan View

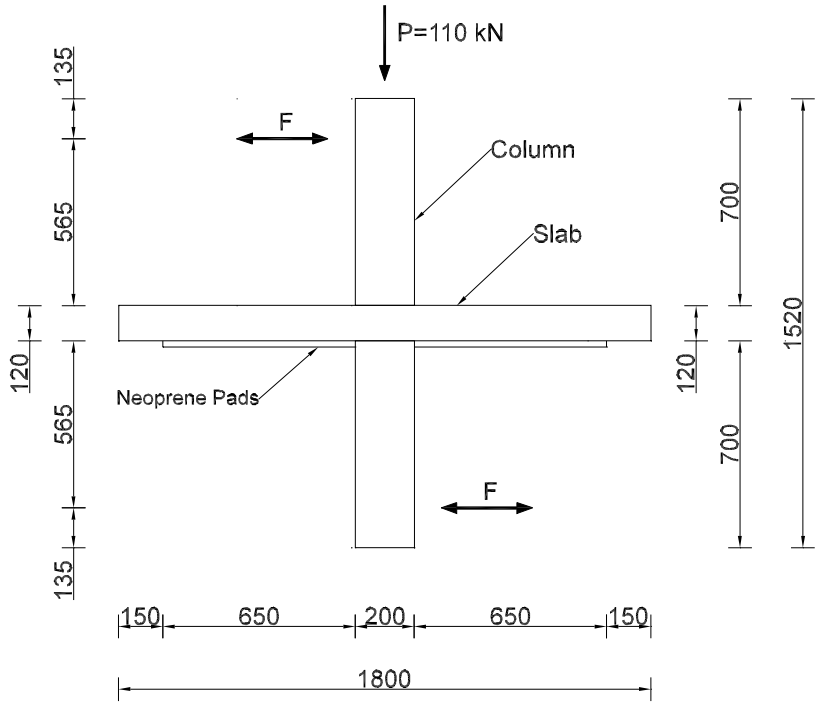

(b) Elevation View

Figure 3.9: Specimen dimensions, loading, and support conditions

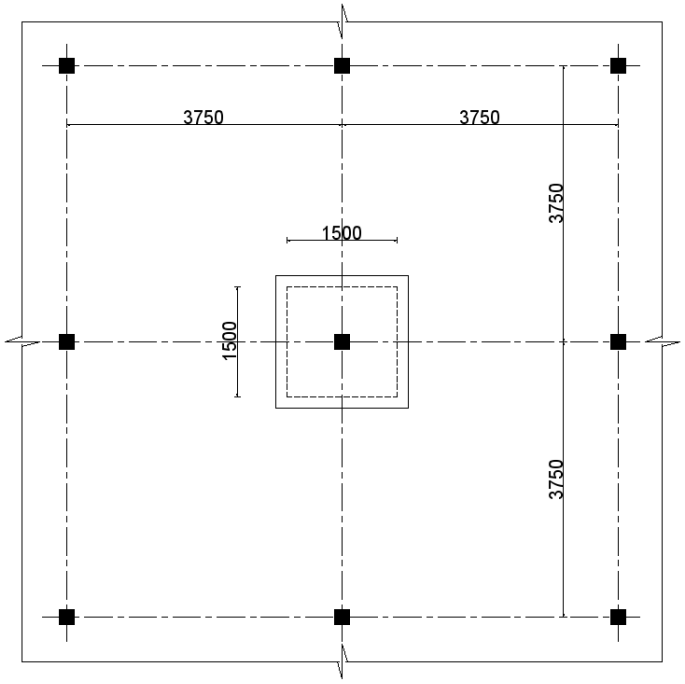

(a) Plan View of the Prototype Structure

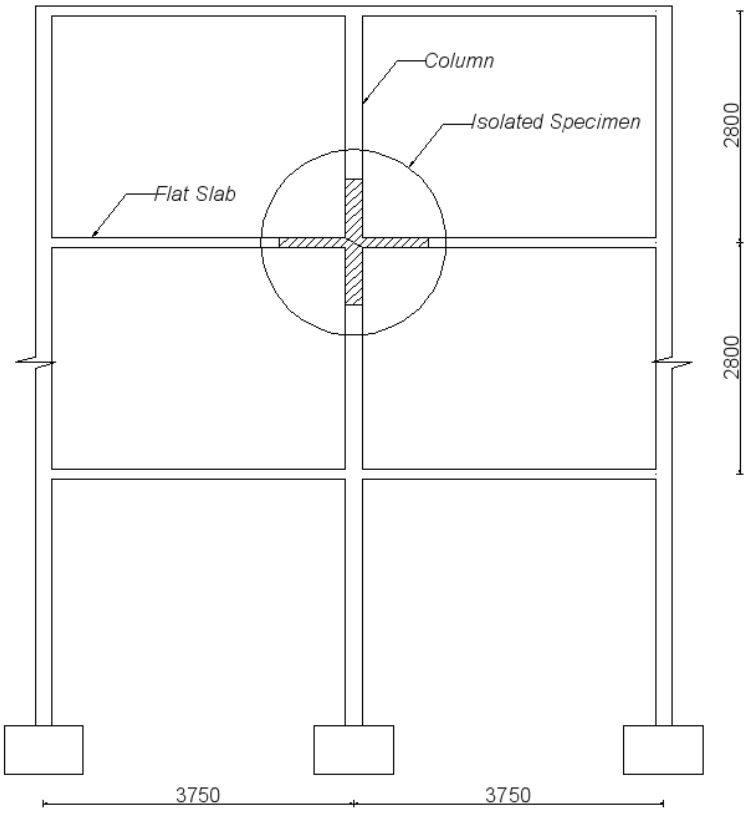

(b) Elevation View of the Prototype Structure

Figure 3.10: The Prototype Structure

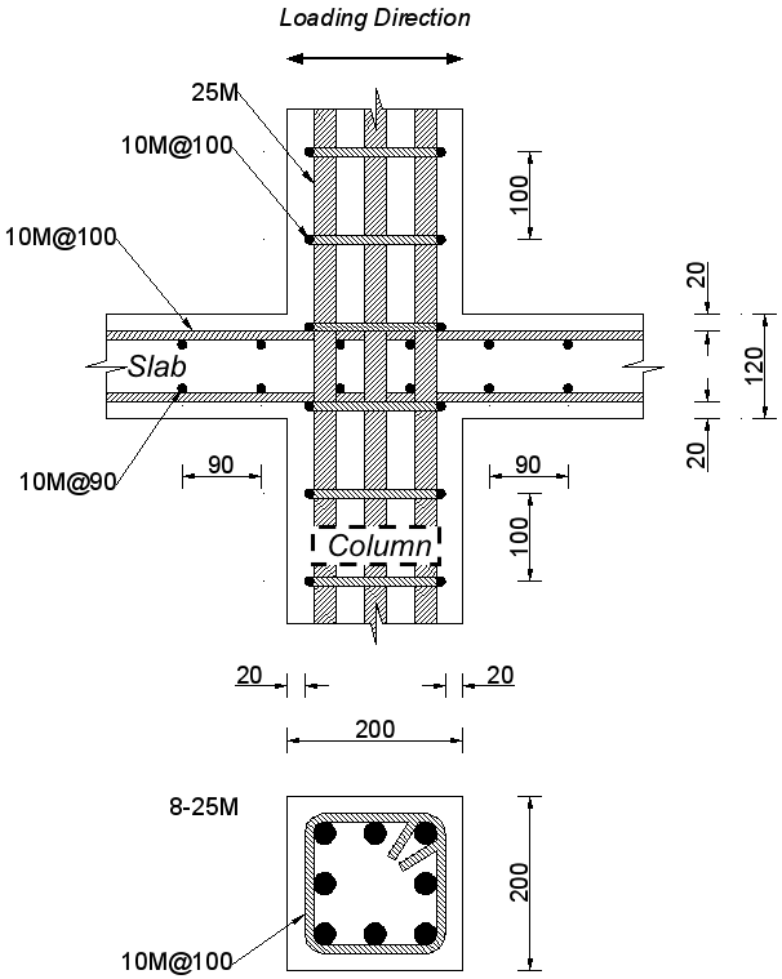

Figure 3.11: Slab and column reinforcement details

3.3.3 Transverse Shear Reinforcement

Shear bolts were installed into drilled holes on the existing slab structure. Each shear bolt assembly was made of a threaded steel rod with thick hardened steel washers and nuts on each end. Additional flexible washers were added between the steel washers, as shown in Fig. 3.15(a) and 3.15(b).

The following shear bolts setup was used for the tested specimens:

- Specimen SD01 had no shear reinforcement.
- Specimen SD02 had a single neoprene washer of 3mm (1/8 in.) thickness, one one side of the slab.

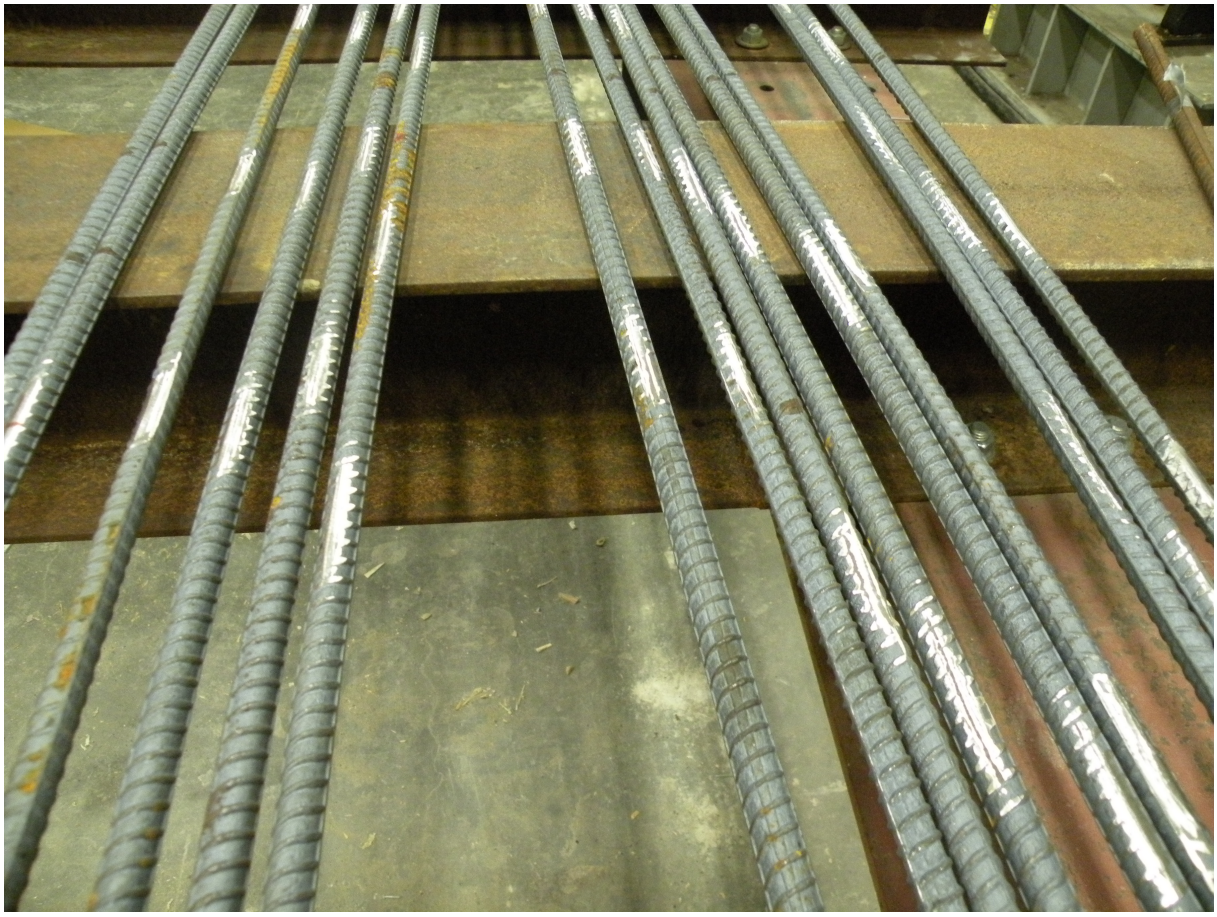

Figure 3.12: Strain Gauging of Flexural Reinforcement

- Specimens SD03 and SD04 had a single nylon washer of 3mm (1/8 in.) thickness, on one side of the slabs. This test was repeated to check for consistency, since this type of reinforcement was expected to provide the best results, based on the expectations that two nylon washers would introduce high degradation and the neoprene washer would provide negligible stiffness (a certain stiffness is necessary for serviceability loading).

- Specimen SD05 had two nylon washers of 3mm (1/8 in.) thickness, one on each side of the slab.

- Specimen SD06 had no flexible washers; steel bolts only.

Washers were chosen based on the expected amount of cracks opening in the slab.

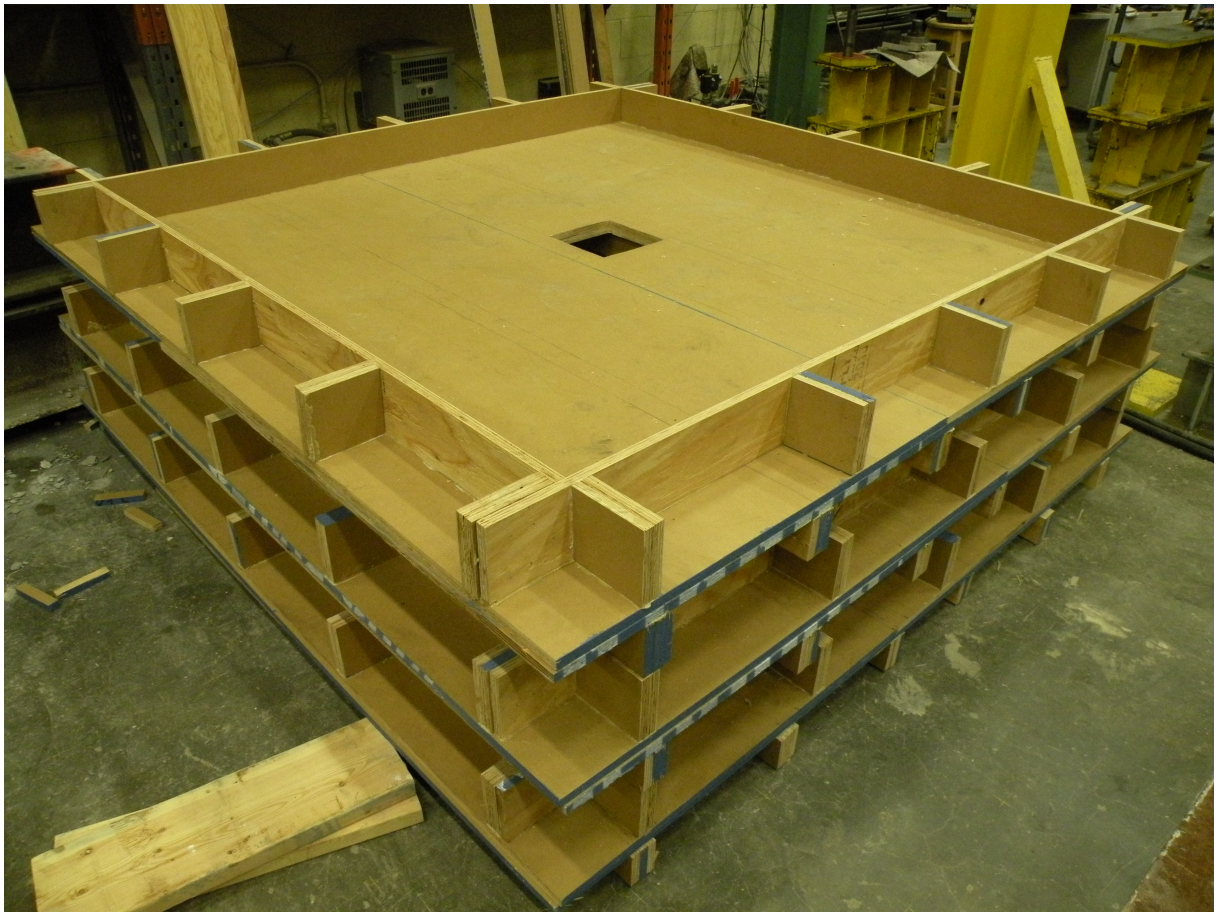

Figure 3.13: Specimen Formwork

Flexible materials were considered, which would attract practically all the deformation occurring within the bolt assembly. Their thickness was determined such that the opening of cracks would be limited by the amount of their squeezing. A peak compressive force, equal to the yielding of the steel bolts, was considered for these calculations. This was based on previous experiments where the bolts close to the column yielded.

The threaded bolts were of a nominal diameter of 9.5 mm (3/8 in.) and the holes in the concrete were drilled using a 12.7 mm (1/2 in.) drill bit. The diameter and mechanical properties of the bolts were chosen to be similar to the shear bolts used by Bu [6] for comparison purposes. SAE J429 Grade 2 bolts were selected with a specified yield strength of 393 MPa and tensile strength of 510 MPa. The material properties of the bolts are shown in Table 3.2. Six rows of bolts were installed on each of the five

Figure 3.14: Specimens Ready for Casting

retrofitted specimens and no bolts on the first specimen. The plan configuration of shear bolts, applicable to all specimens SD02 to SD06, is shown in Fig. 3.15(c).

3.3.4 Material Properties

The specimens were cast using ready-mixed concrete with a 35 MPa specified strength and max. aggregate size of 9.5mm, supplied in two batches. Concrete cylinders 100x200 mm and 150x300 mm were prepared and tested for its compressive and tensile strengths at the same time as testing of the slab specimens; concrete age of 29 months (Fig. 3.17). Yield stress and tensile strength of the reinforcing bars and shear bolts were obtained by testing (Fig. 3.18). The cyclic behaviour in compression of washers was also tested and the load-displacement curves were obtained. Material properties are shown on Tables

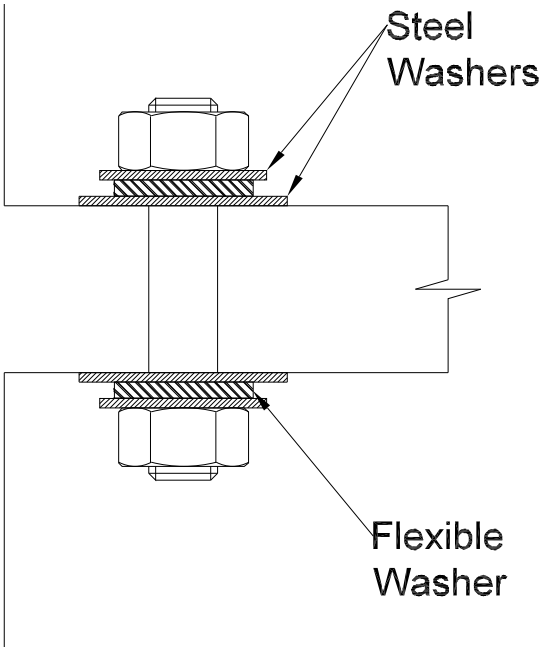

(a) Schematic of steel bolt and washers assembly

(b) Installed Bolts Assembly

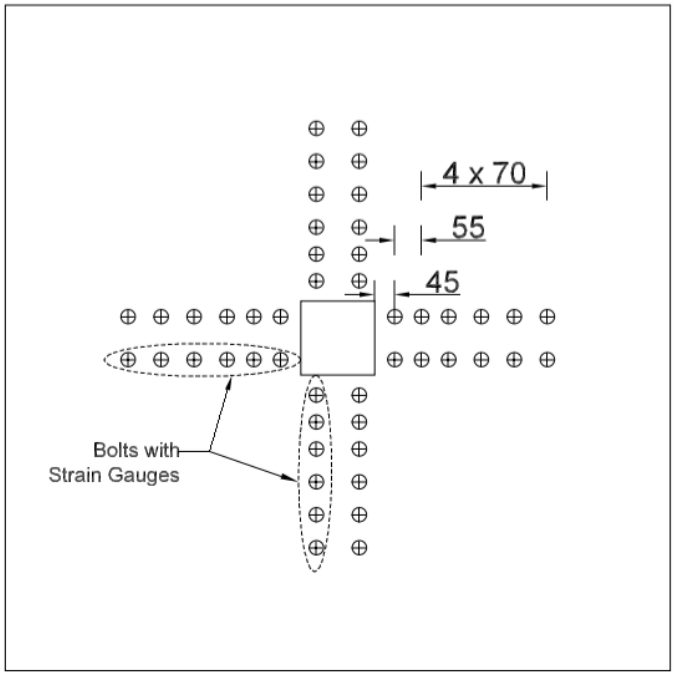

(c) Bolts Plan Configuration (4x2x6)

Figure 3.15: Shear Bolts Details

Figure 3.16: Cast Specimens in Humid Conditions

3.1 and 3.2. The tensile behaviour of the flexural rebars and the threaded rods and the compression behaviour of the washers are shown respectively in Figs. 3.19, 3.20 and 3.21.

3.3.5 Experimental Setup

3.3.5.1 Testing Frame

The testing frame, located in the structural laboratory of structures at the University of Waterloo, is shown in Fig. 3.22, and its main components are shown in Fig. 3.23 and 3.24. The main frame consists of four steel columns and the crosshead. Two horizontal hydraulic actuators, which are used to apply cyclic horizontal displacement on the top and bottom columns of the specimen, are installed on each side of the frame. Another

Figure 3.17: Cylinder Testing

vertical actuator is installed in the middle of the crosshead to apply a constant vertical load at the top of the concrete column. The second part of the frame, where the specimen is supported, includes a square ring beam, four supporting columns, and two top reaction beams. The concrete slab is supported on its bottom surface on four sides. On the slab top face, the two edges perpendicular to the loading direction are restrained by steel beams, fixed directly to the ground, to prevent lifting of the slab. Neoprene pads with a thickness of 25mm were installed between the concrete slab and the steel frame elements, to simulate the slab rotation at the contraflexure line of the continuous prototype building due to cyclic moment transfer.

The vertical actuator applied the load through a steel plate at the top of the column.

Figure 3.18: Tensile Testing of Flexural Reinforcement

The plate was pinned to the vertical actuator in order to allow horizontal displacements and there were steel rollers between the plate and the top of the column, to minimize any restraining. The horizontal actuators were connected to the top and bottom columns via steel collars. Further details of the frame may be found in [6].

3.3.5.2 Instrumentation

Five string pots, four linear variable differential transformers (LVDT's) and nine potentiometers, in addition to the three internal LVDT's of the actuators, were used to measure the displacements. Two string pots were horizontally installed at the top and

Table 3.2: Flexural and Shear Reinforcement Material Properties

Flexural Reinforcement		Shear Reinforcement		Washers	
Yield Stress (MPa)	Modulus of Elasticity (GPa)	Yield Stress (MPa)	Modulus of Elasticity (GPa)	Type	Modulus of Elasticity (kN/mm)
460	200	400	180	Nylon	50
				Neoprene	3

bottom column ends to measure the applied column lateral drifts (string pots 1 and 2 in Fig. 3.25(a)). To measure any possible horizontal shifting of the specimen, two string pots were installed in the horizontal loading directions (string pots 3 and 4). An additional string pot was vertically installed at the end of the bottom concrete column, to measure the displacement of the column end, relative to the ground (String pot 5). A series of displacement transducers were vertically installed on both top and bottom slab faces along two orthogonal directions. At three of these locations the transducers were aligned vertically and installed on both top and bottom surfaces to measure the vertical displacement difference, which was then used to estimate the shear crack width (Fig. 3.25(b)). All the instrumentation was installed onto a rigid steel frame, separated from the testing frame and installed directly on the laboratory floor, to avoid any influence on the measurements from the deformations of the frame itself.

Strains were measured on both flexural and shear reinforcement. Sixteen 5 mm long strain gauges were installed on the flexural reinforcement. Twelve shear bolts (shown in Fig. 3.15) were instrumented with strain gauges attached along the bolt stem. The threaded rods were filed at the gage location to achieve a proper smooth surface. Strain measurements on bolts in this case are mostly used to analyze the force on the shear bolts and not for the deformation, since most of the deformation happens through squeezing of the flexible washers.

3.3.6 Test Procedure

Each of the specimens was loaded in two main stages. A vertical load of 110 kN was first applied statically on the top of the upper column of the specimen at a loading rate

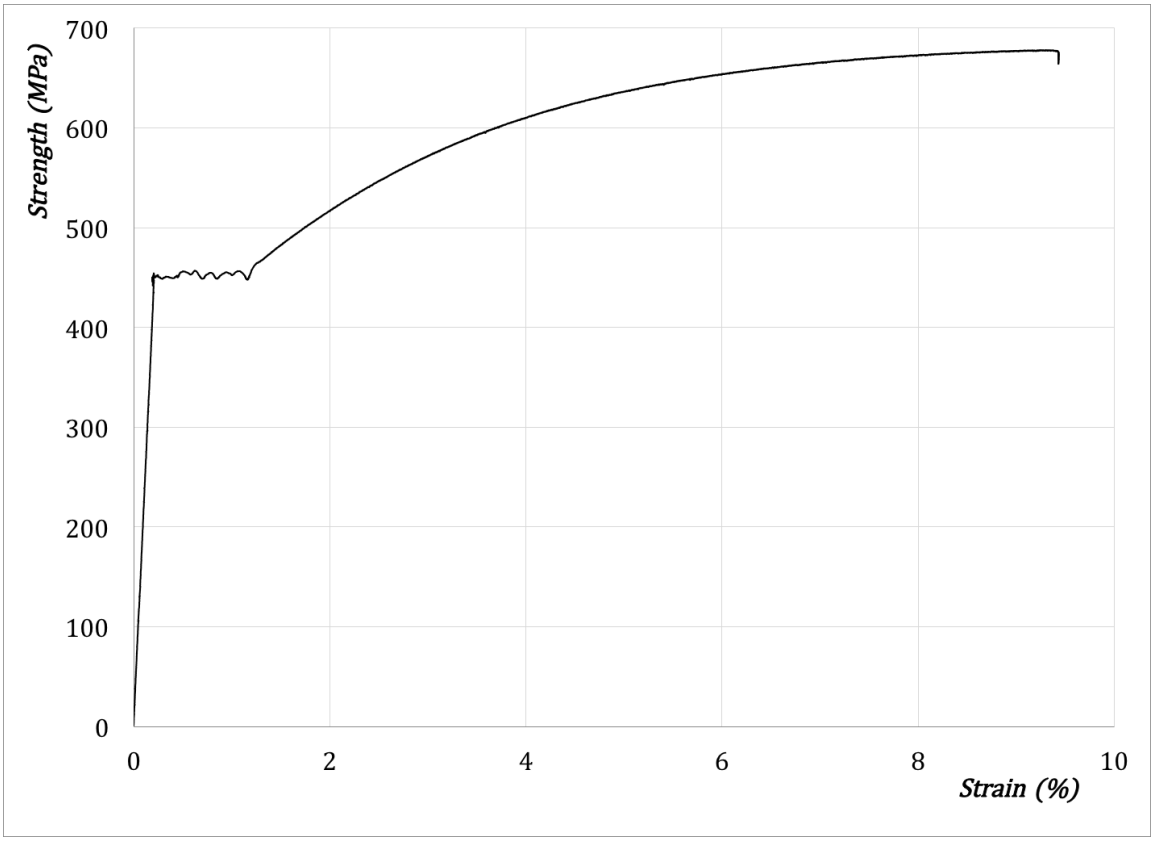

Figure 3.19: Tensile Behaviour of Flexural Rebar

of approximately 30 kN/min. This vertical load was then kept constant for the entire duration of the test, while the two horizontal actuators imposed drifts to the top and bottom column ends following the loading path shown in Fig. 3.6.

3.3.6.1 Horizontal Loading Path

The cyclic displacement path was designed to show stiffness degradation using multiple load cycles [6]. The load cycles were repeated three times at the same drift ratio, until the drift of 3%. A cycle of a small drift ratio of 0.5% was used between each group of three cycles to check the behaviour of the connection after experiencing large deformations, with regard to stiffness and strength degradation. Following the 3% drift, the loading path was applied in a monotonically increasing way at successive cycles without repetition. The applied displacement history is shown in Fig. 3.6.

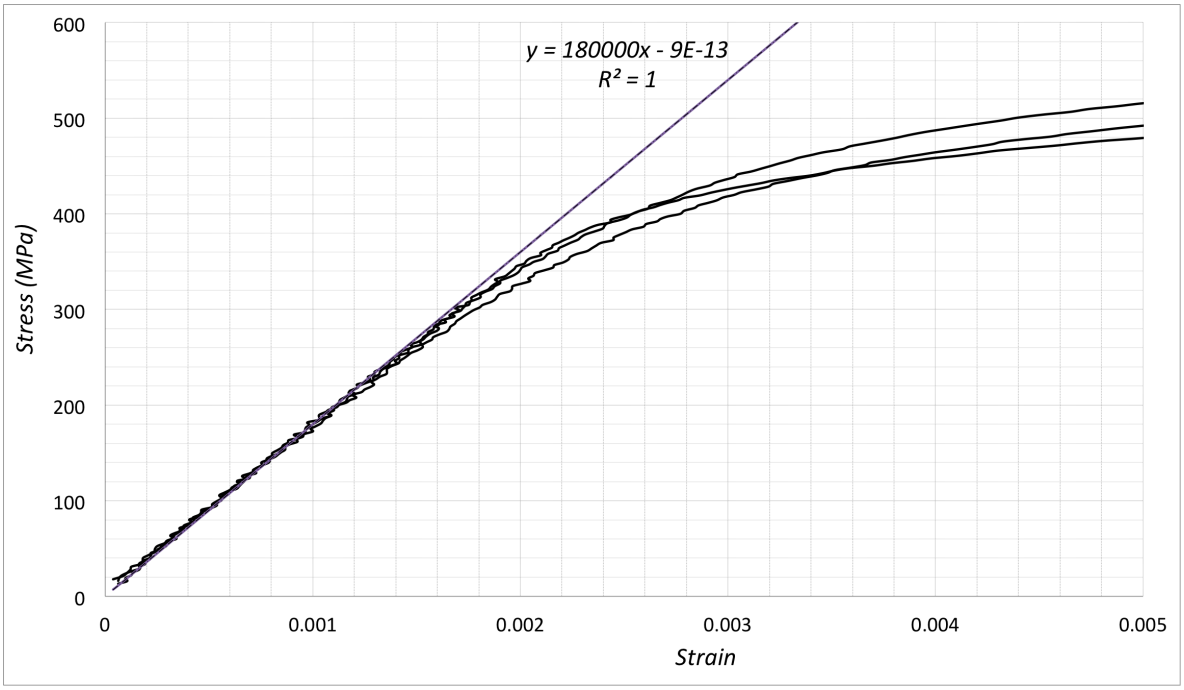

Figure 3.20: Tensile Behaviour of Steel Bolts

3.3.7 Test Results and Discussion

3.3.7.1 Moment vs. Drift Ratio

The unbalanced moments applied to the specimens were calculated by multiplying the two lateral forces, applied on each column end, by the distance from the application point to the centre of the slab: 625 mm. Similarly, drifts were calculated as the ratio of the applied horizontal displacement to the distance from the application point to the centre of the slab. All specimens failed in punching, as expected, considering they were over-reinforced in flexure.

Moment vs. horizontal drift ratios are shown in Figs. 3.26 to 3.28. As expected, the strength and the deformability of the connections were increased by the use of shear reinforcement of any type. The flexible washers, however, improved the ductility of the connection without considerably increasing its strength. Washers that allow large opening of cracks are not very efficient because they allow for higher strength degradation instead of introducing a flat plateau in the joint response curve.

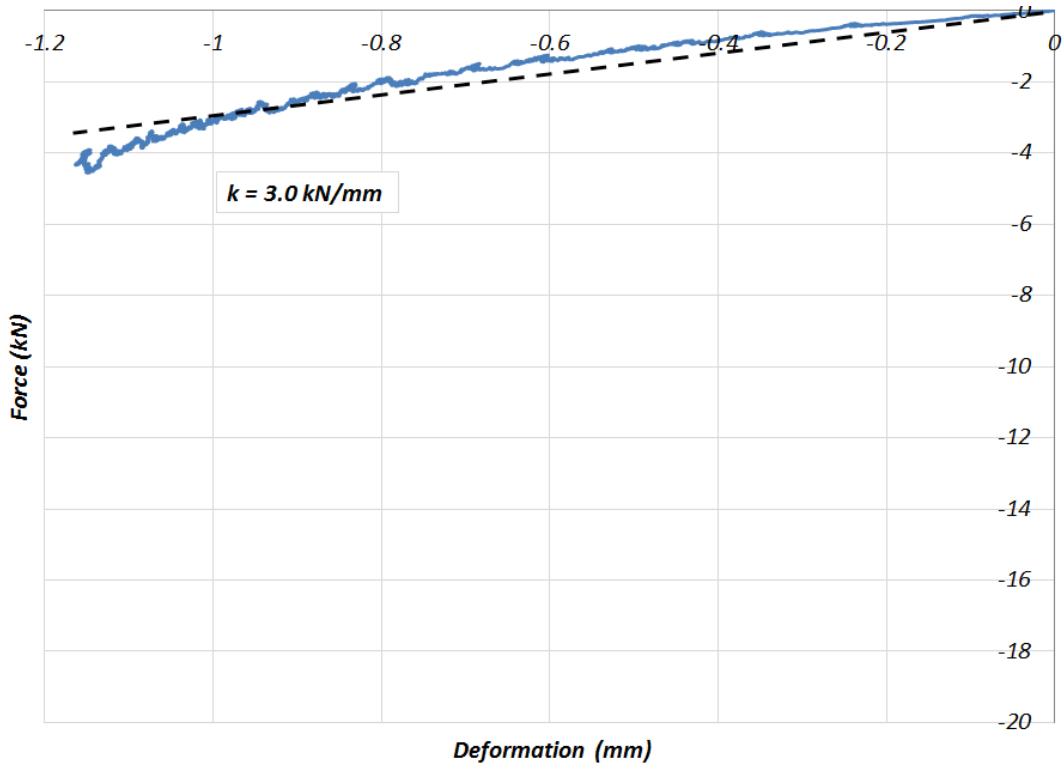

(a) Compression Behaviour of Neoprene Washers

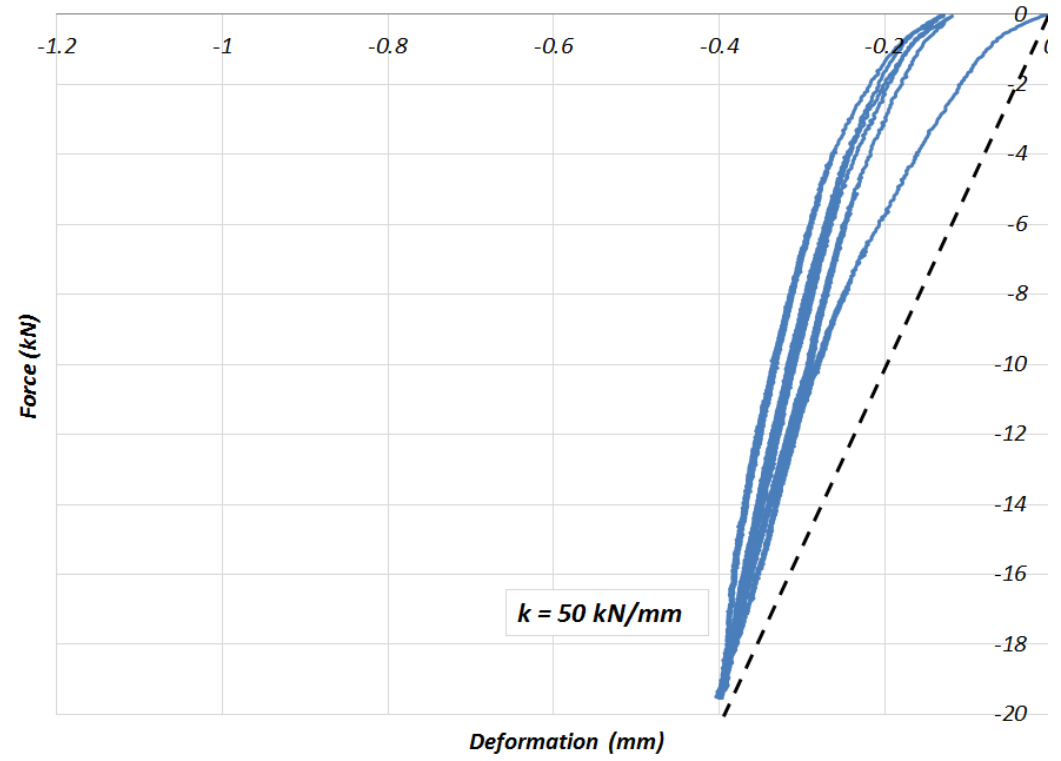

(b) Compression Behaviour of Nylon Washers

Figure 3.21: Testing of Washers in Compression

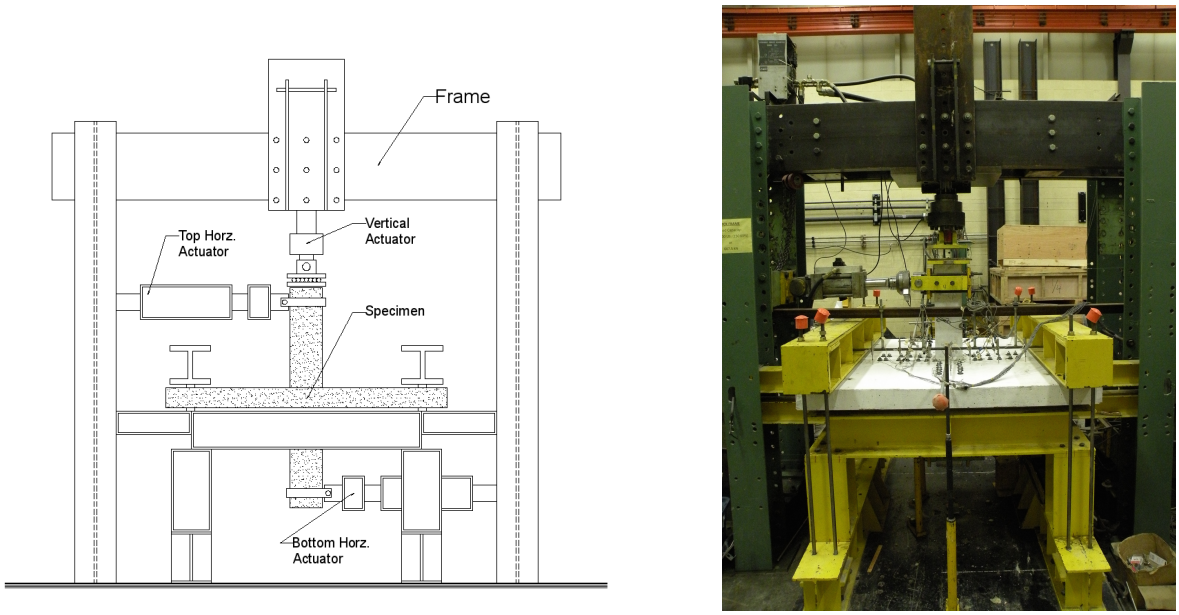

(a) Frame Sketch

(b) Frame Picture

Figure 3.22: Testing Frame

- Specimen SD02, which had very flexible washers of neoprene, did not experience higher strength; the punching failure happened at the same moment-drift level as the unreinforced specimen SD01. Further opening of shear cracks introduced strength degradation up to the drift of 3.5%, where the steel bolts were engaged, introducing hardening into the joint response. The use of thinner neoprene washers might be more efficient in having a plateau in the response, without increasing the strength. In that case, thinner neoprene washers would practically serve only to introduce a tolerance prior to the engagement of the stiff steel bolts.

- Specimen SD03 and SD04 seemed to have the most effective washers. The nylon washers, stiffer than neoprene, improved the strength of the specimen at low moment-drift, and the engagement of steel bolts was done prior to a drop in strength as in the case of specimen SD02. These specimens experienced a better plateau and lower pinching, in their moment-drift response.

- Specimen SD05, with double nylon washers, had a similar initial strength as SD03 and SD04, with a single nylon washer. The main difference was observed in the

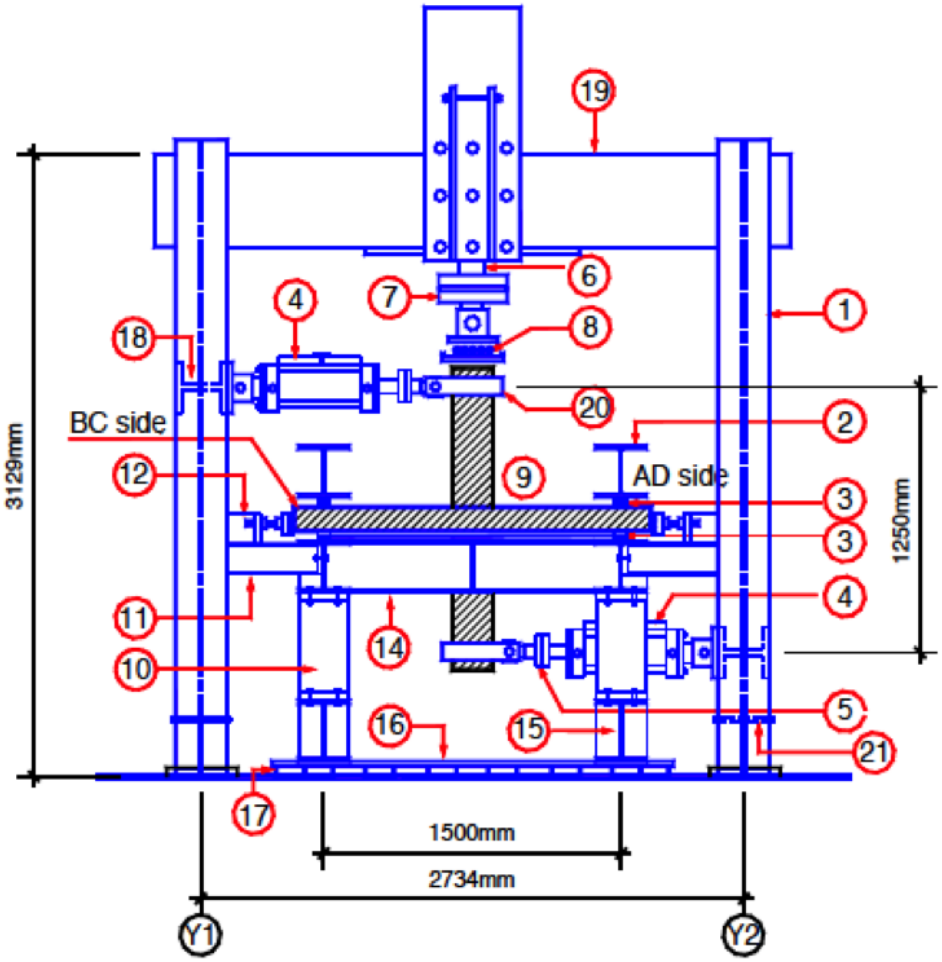

1. Column of steel frame (W310x86)
2. Top reaction beam (W250x89)
3. 1"x1" Neoprene pads
4. Horizontal actuator
5. Horizontal load cell (50 kip)
6. Vertical actuator
7. Vertical load cell (150 kip)
8. Steel pan and rollers
9. Concrete slab-column specimen
10. Supporting column (W250x89)
11. Bracing beam (W150x22)
12. Adjustable stopper (W150x22)
13. Reaction steel rods (ø22mm)
14. Support square ring beam (W250x89)
15. Base reaction beam (W310x73)
16. 1" thick steel base panel
17. Steel channels (C150x12)
18. Short beam for actuators (W250x73)
19. Channels of crosshead (MC460x86)
20. Collar system
21. Beam (W310x107, with end plates) connecting the two frame columns at the bottom, achored to the ground by four long bolts

Figure 3.23: Elevation A of the Testing Frame Setup [6]

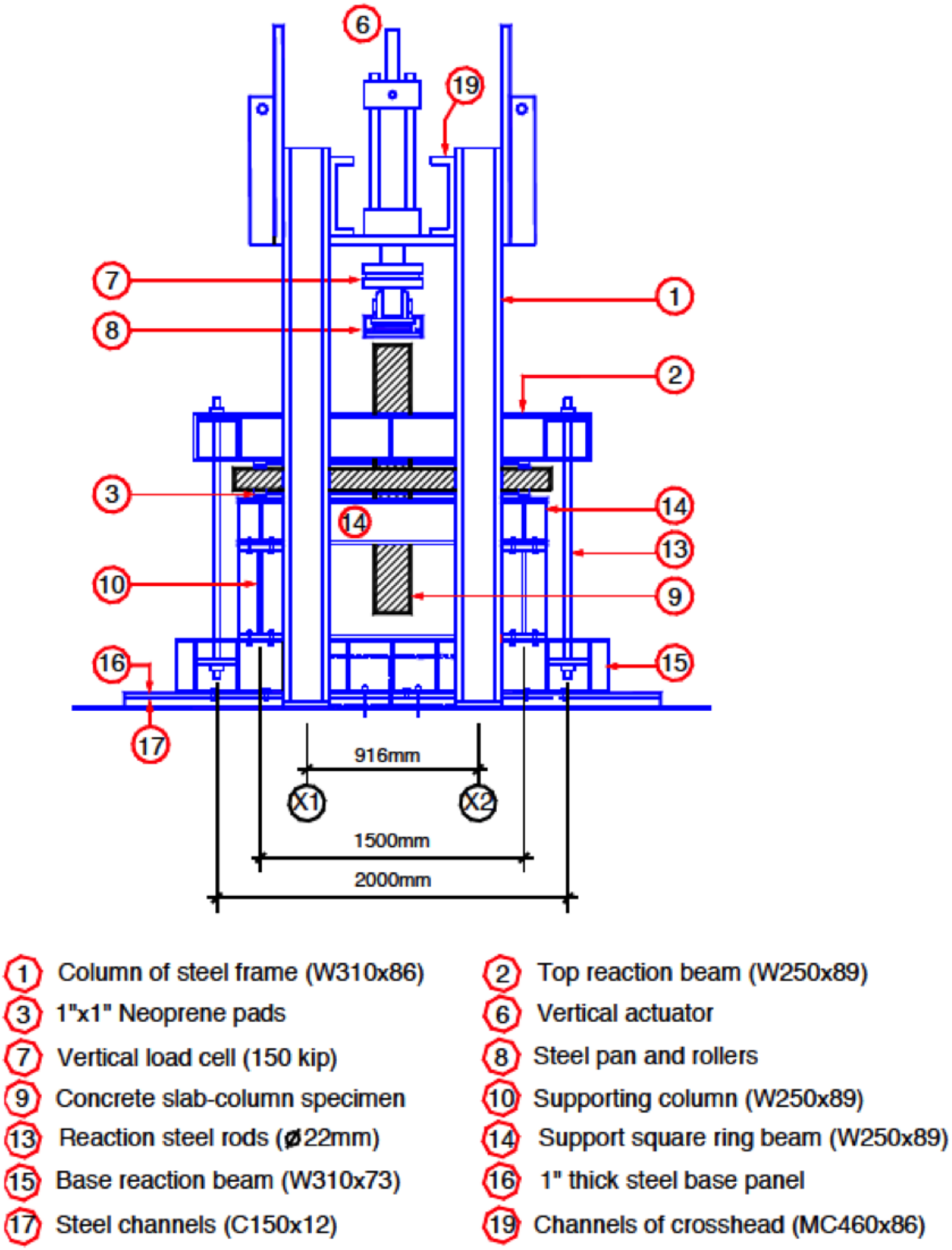

Figure 3.24: Elevation B of the Testing Frame Setup [6]

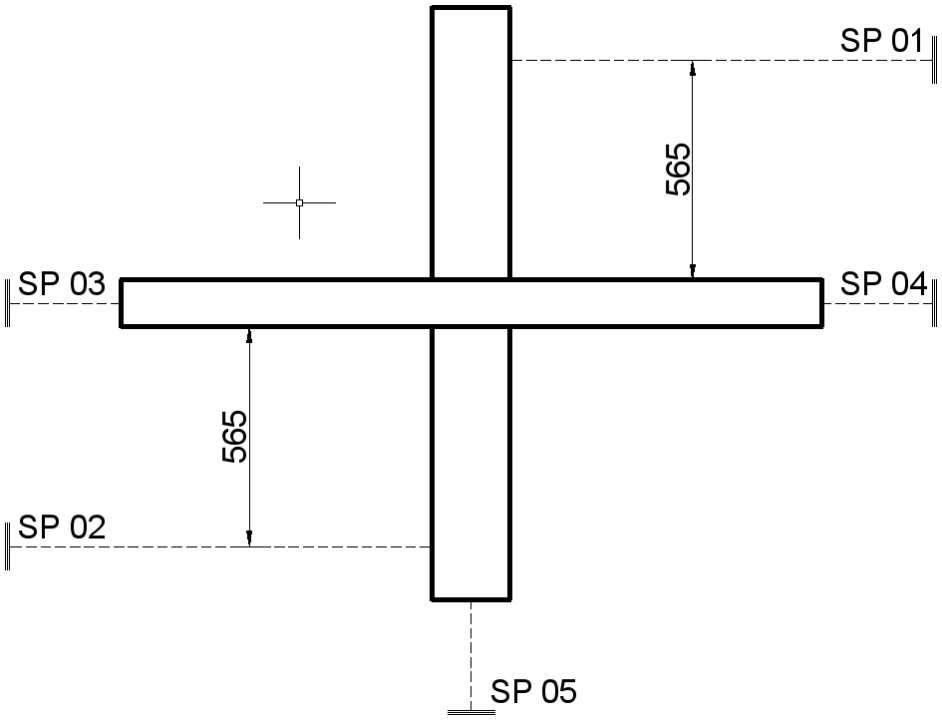

(a) Location of String Pots

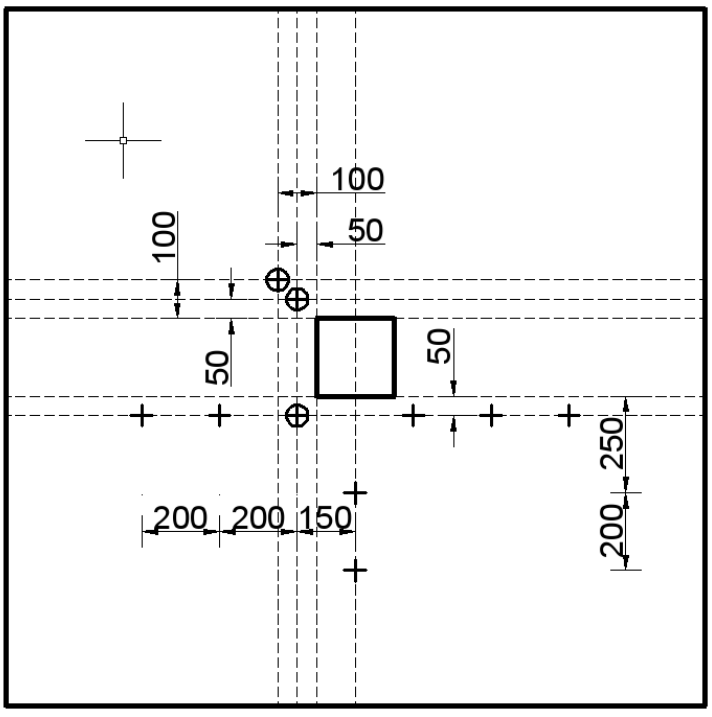

(b) Location of LVDT's ('+' - Top and '⊕' - Bottom)

Figure 3.25: Positioning of External Instrumentation

response at larger drift ratios, where the nylon washers kept deforming excessively, allowing further opening of shear cracks. This resulted in a quicker strength degradation, compared to specimens SD03 and SD04.

- Specimen SD06, having the stiffest reinforcement, had a higher strength, and also higher pinching. The steel bolts restrained the opening of cracks up to a drift of 4%, introducing a relatively linear behaviour of the connection. Since this is a large drift for practical structural applications, the joint would practically remain within the elastic range in a seismic event, without taking advantage of plastic deformations, introduced in the case of flexible washers.

The envelope curves of the Momment-Drift Response for all six tested joints are shown in Fig. 3.29. From this figure it may be observed that:

- All specimens had a similar stiffness up to a drift of 1.5%, which is within the range of normal loading
- The joint reinforced with steel bolts only provided a higher strength
- The joints reinforced with anchorage-controlled shear reinforcement were able to undergo the same lateral displacements at a lower strength.
- The ductility of the joints reinforced with anchorage-controlled reinforcement was considerably higher, as shown in Table 3.3.

Table 3.3: Drift Ductility

Specimen	δ_y	δ_{peak}	Ductility = $\frac{\delta_{peak}}{\delta_y}$
SD01	0.018	0.020	1.12
SD02	0.015	0.052	3.38
SD03	0.021	0.047	2.21
SD04	0.018	0.041	2.32
SD05	0.022	0.029	1.34
SD06	0.029	0.040	1.36

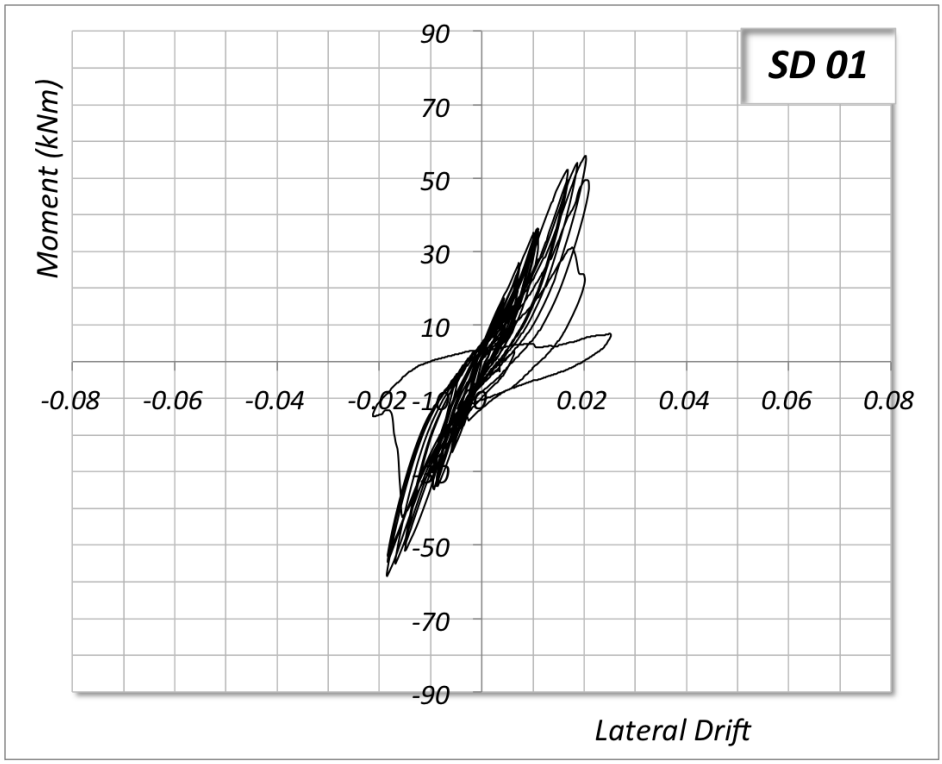

(a) SD01: (No Shear Reinforcement)

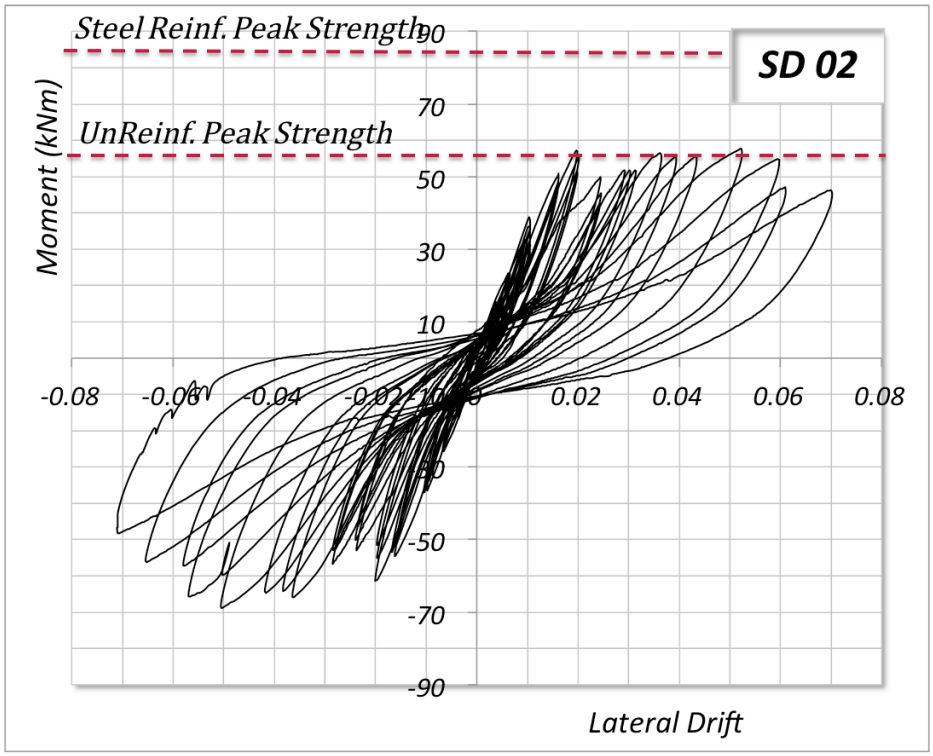

(b) SD02: (Single Neoprene Washer)

Figure 3.26: Moment-Drift Diagrams - SD01 & SD02

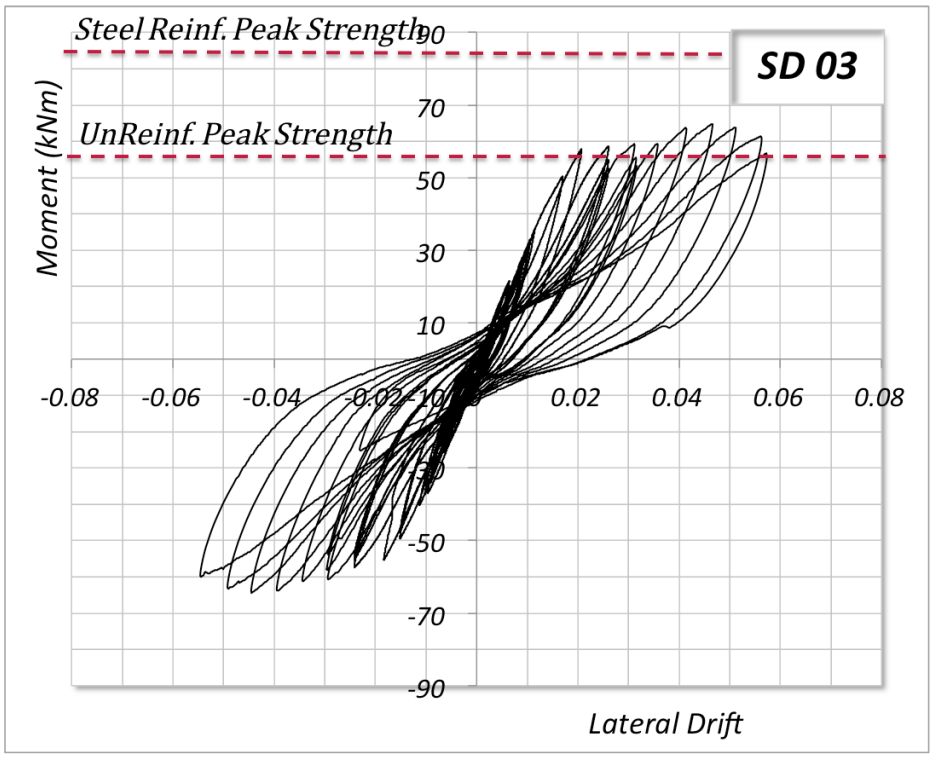

(a) SD03: (Single Nylon Washer)

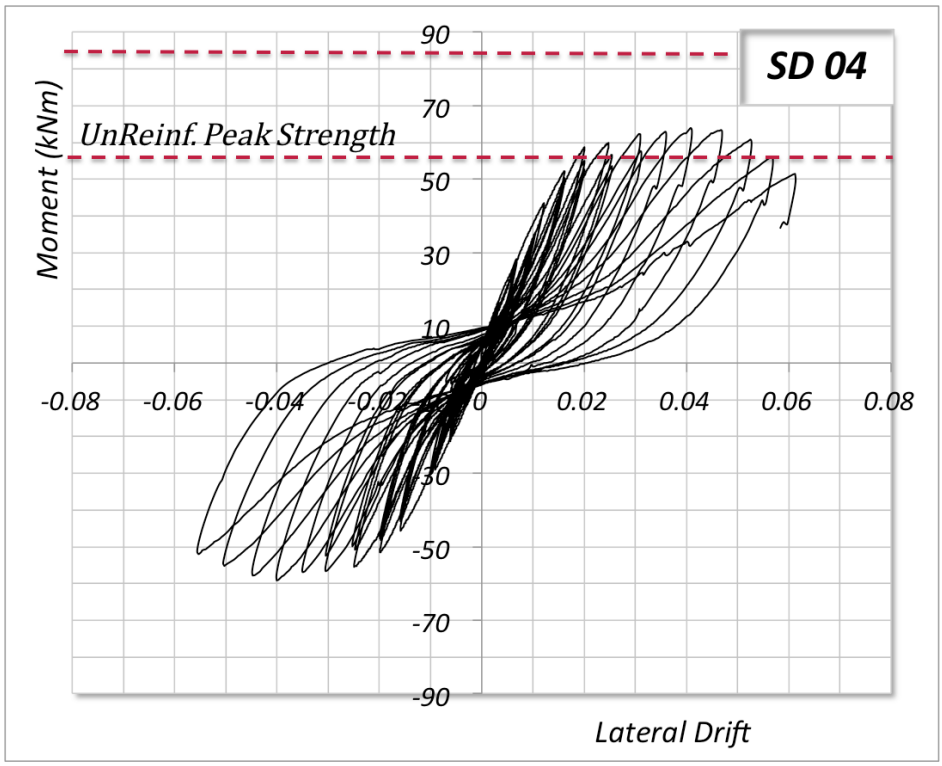

(b) SD04: (Single Nylon Washer)

Figure 3.27: Moment-Drift Diagrams SD03 & SD04

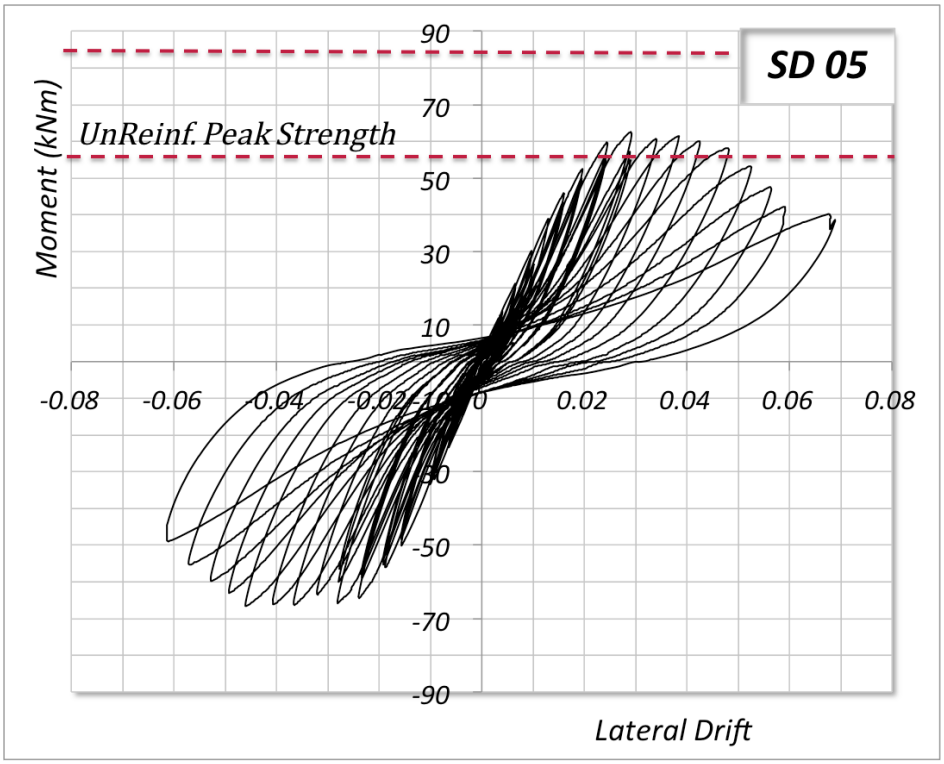

(a) SP05: (Double Nylon Washers)

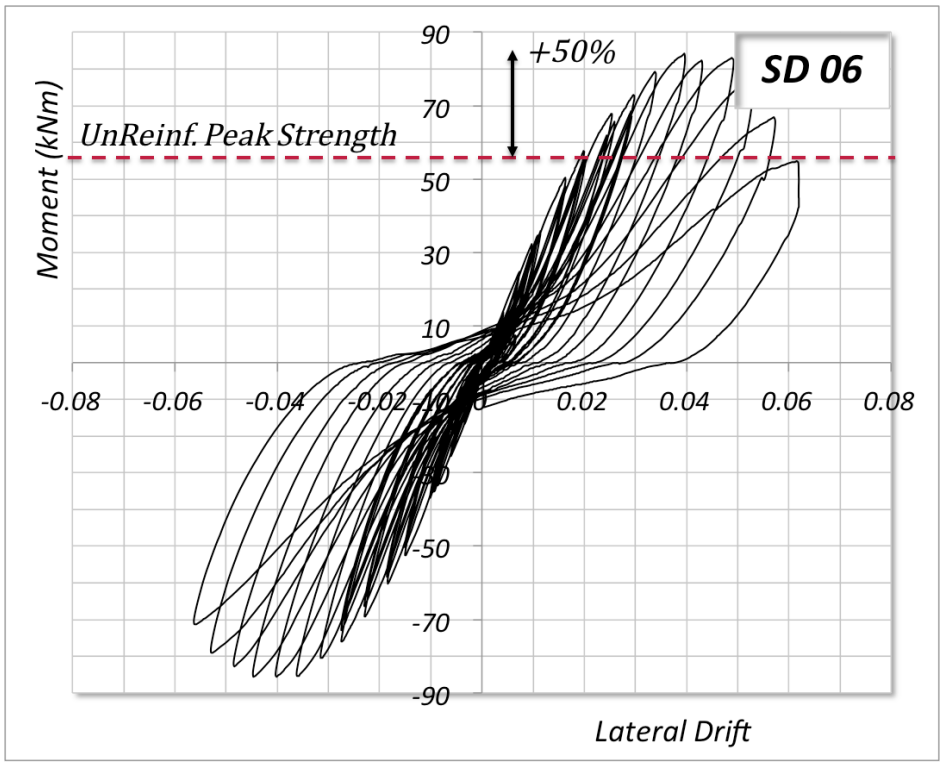

(b) SP06: (No Washers)

Figure 3.28: Moment-Drift Diagrams SD05 & SD06

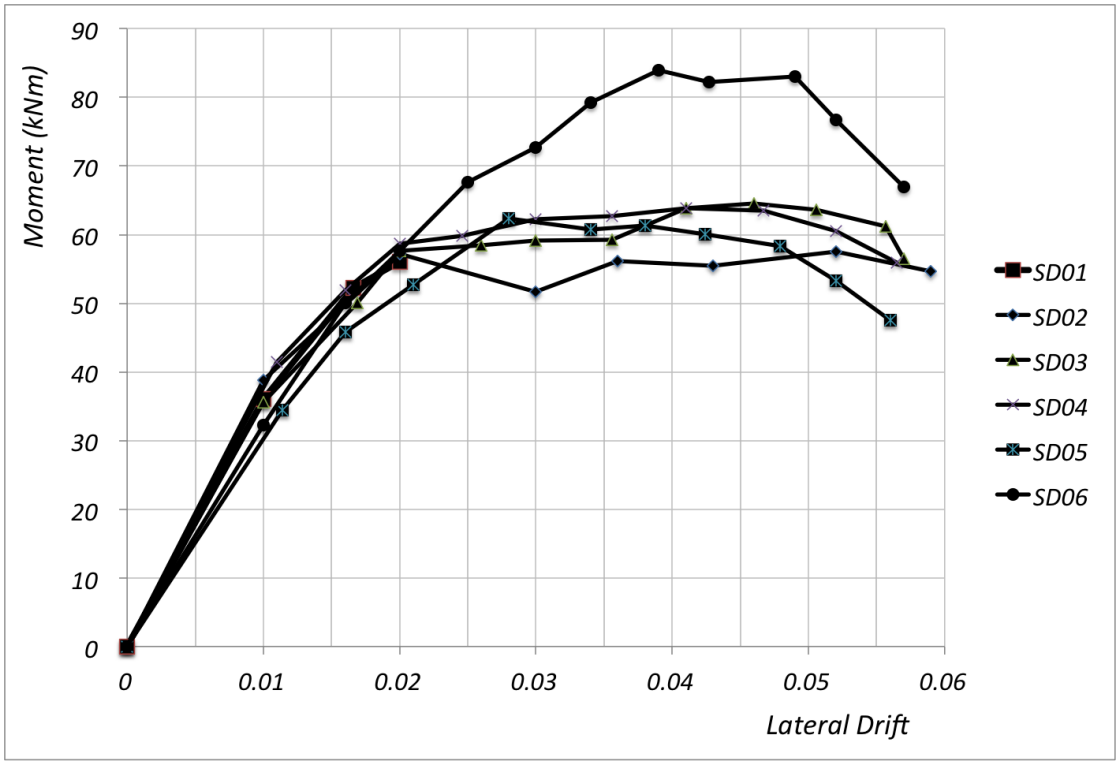

Figure 3.29: Envelope Curves of the Moment-Drift Response

3.3.7.2 Strain on Shear Bolts

Figs. 3.30 to 3.32 show the strain on the first bolt in the loading direction, which experienced the highest tensile stress and strain. From these graphs, shown for the typical specimens only, the following may be observed:

- The bolts in the two specimens with flexible washers (SD02 and SD04) did not experience any strain up to a drift of about 1.5%, because the deformation was experienced by the flexible washers, while the steel bolts without flexible washers (SD06) experienced a linearly increasing strain. The strain on the SD06 specimen was relatively lower.

- The bolts of the specimen with neoprene washers (SD02) experienced lower strain, since more deformation went into the washer compared to the stiffer nylon washers (SD04). In addition, SD02 allowed opening of cracks without high resistance after the drift of 1.5%. This was why the strength of SD02 plateaued compared to the

Table 3.4: Strength (kN) at Various Drift Ratios

Specimen	Drift Ratios				
	1%	2%	3%	4%	5%
SD01	36	57			
SD02	38	58	52	55	58
SD03	36	57	59	63	63
SD04	37	59	62	63	62
SD05	36	57	62	60	54
SD06	36	58	74	84	75

other specimens; similarly to the strain on the bolts.

- The bolts of specimen SD05 experienced low strain at large drifts because two nylons washers, compared to a single washer in SD04, experienced larger deformation, allowing for higher strength degradation of the connection.

3.3.7.3 Opening of Cracks

Figs. 3.33 to 3.35 show the opening of cracks. For large drifts (beyond 3%) the accuracy of LVDT measurements is not reliable due to large slab deformations and rotations and the LVDT locations. From these graphs, the following may be observed:

- Specimen SD01 failed immediately after an increase of crack opening since there was no shear reinforcement to provide the necessary strength.
- Opening of cracks for specimen SD02 was similar to specimen SD01, which was also reflected in their similar strength within this deformation range, until failure of SD01.
- Specimen SD04 showed the best performance because the cracks opened more than in specimen SD06, but less than the excessive opening in specimens SD01 and SD02. The nylon washer allowed a limited opening of cracks, also avoiding the sudden increase in crack openings observed in specimens SD01 and SD02, between 1.5% and 2.0%.

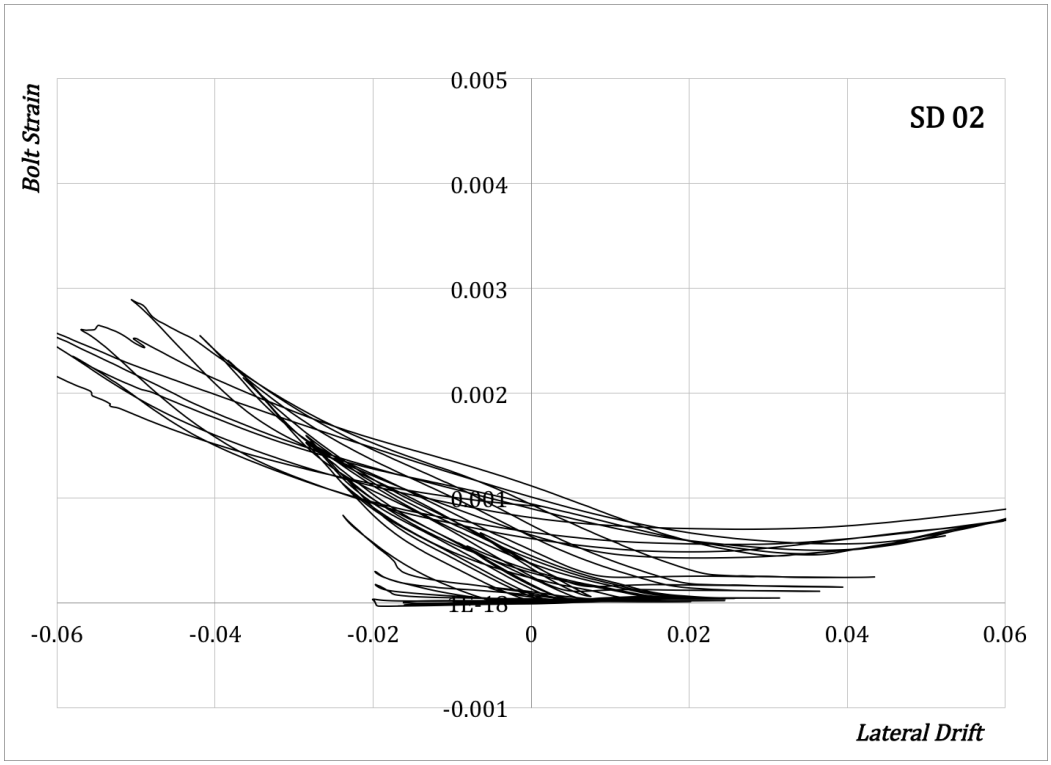

(a) SD02 Bolt Strain

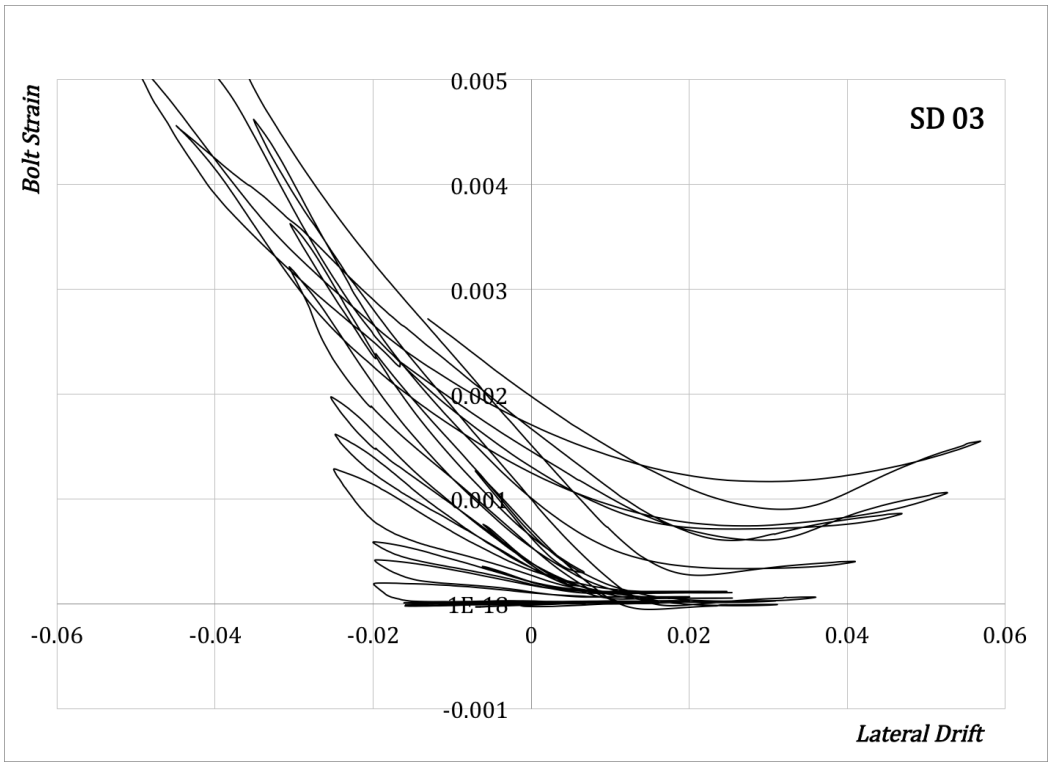

(b) SD03 Bolt Strain

Figure 3.30: Strain of Bolts During the Cyclic Loading - SD02 & SD03

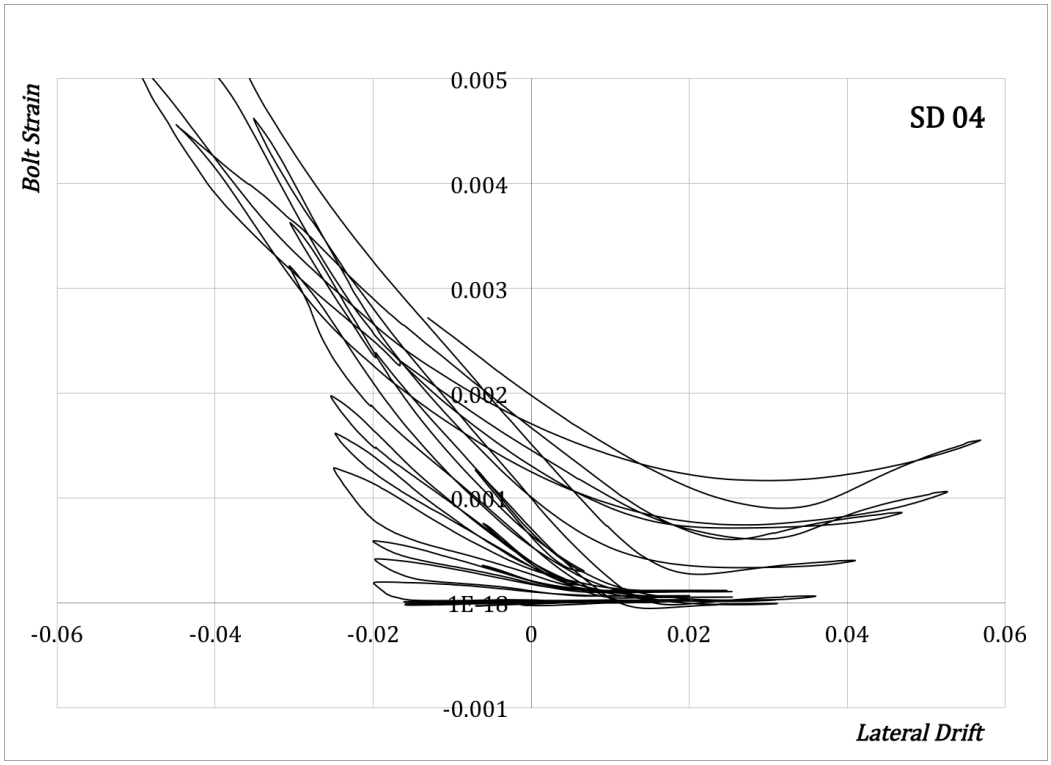

(a) SD04 Bolt Strain

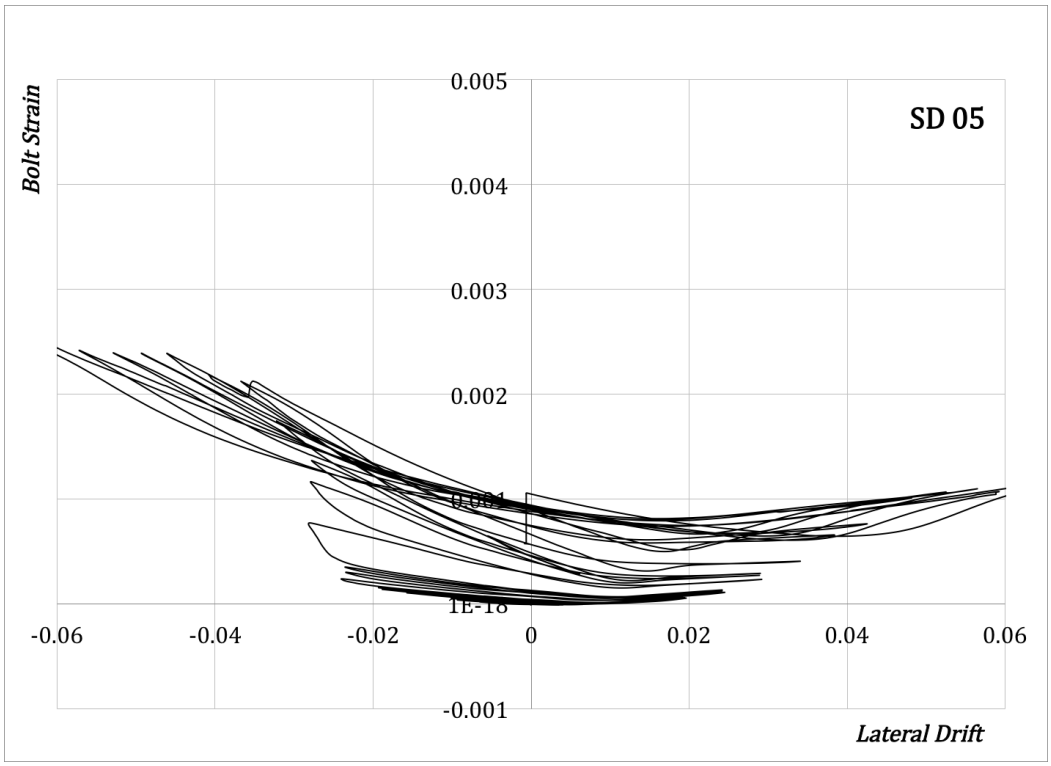

(b) SD05 Bolt Strain

Figure 3.31: Strain of Bolts During the Cyclic Loading - SD04 & SD05

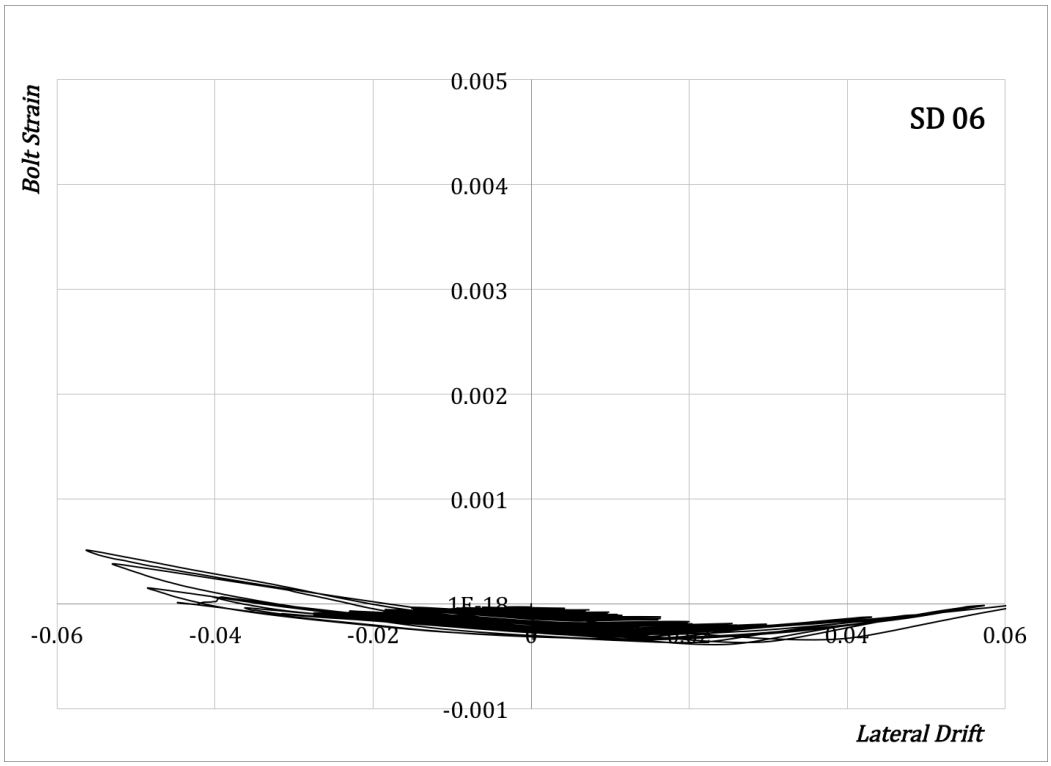

(a) SD06 Bolt Strain

Figure 3.32: Strain of Bolts During the Cyclic Loading - SD06

- The opening of cracks was considerably restricted in specimen SD06, reinforced with steel bolts without washers.

Pictures of slab surface cracks are shown in Figs. 3.37 to 3.39.

The experimental work showed that the use of anchorage-controlled shear reinforcement increases the ductility of slab-column joints without a commensurate increase in strength. Such connections would improve the seismic performance of flat plate systems, which is analytically investigated in Chapter 5.

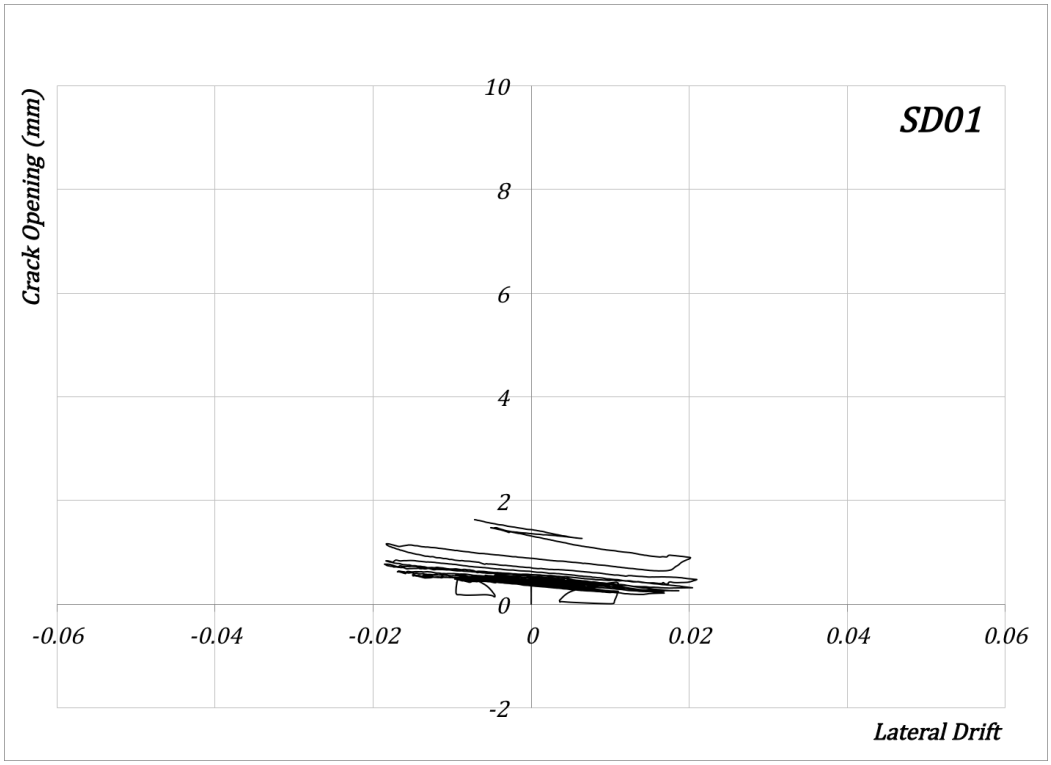

(a) SD01 Cracks Size

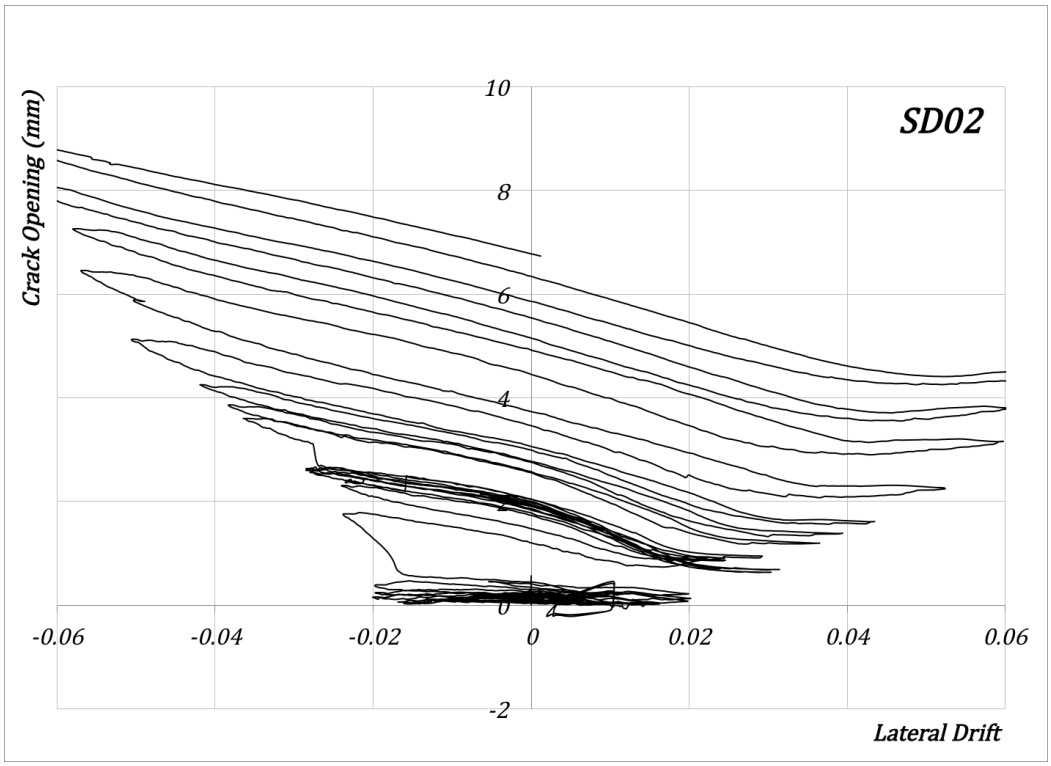

(b) SD02 Cracks Size

Figure 3.33: Opening of Cracks During the Cyclic Loading - SD01 & SD02

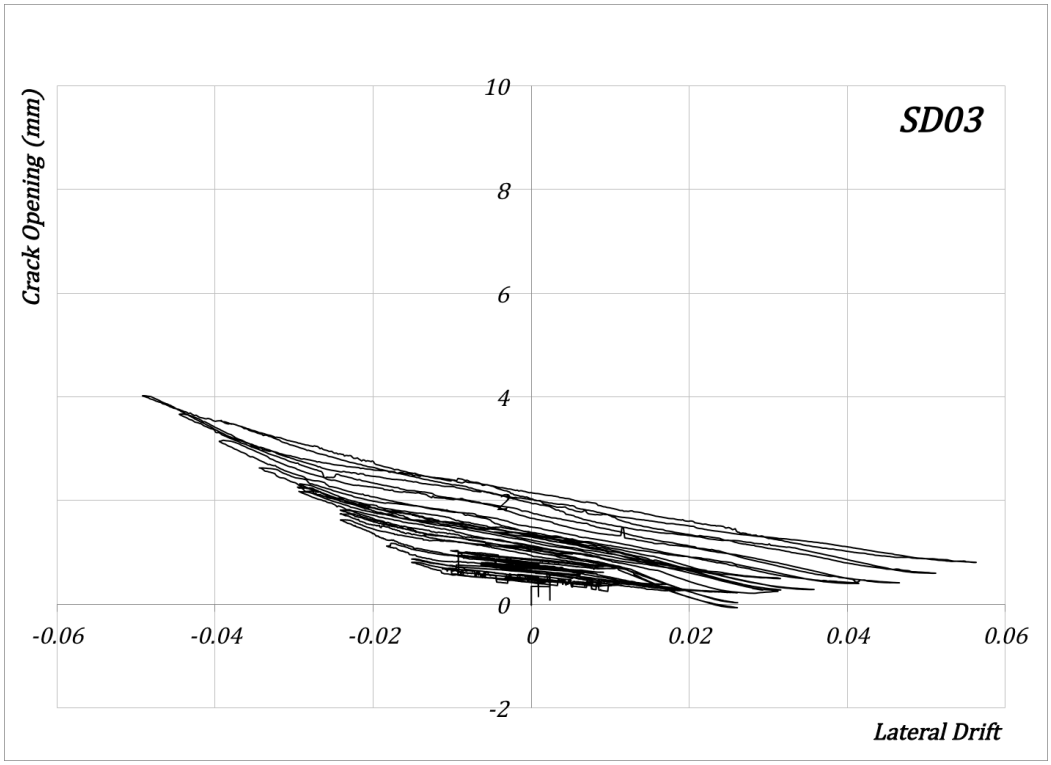

(a) SD03 Cracks Size

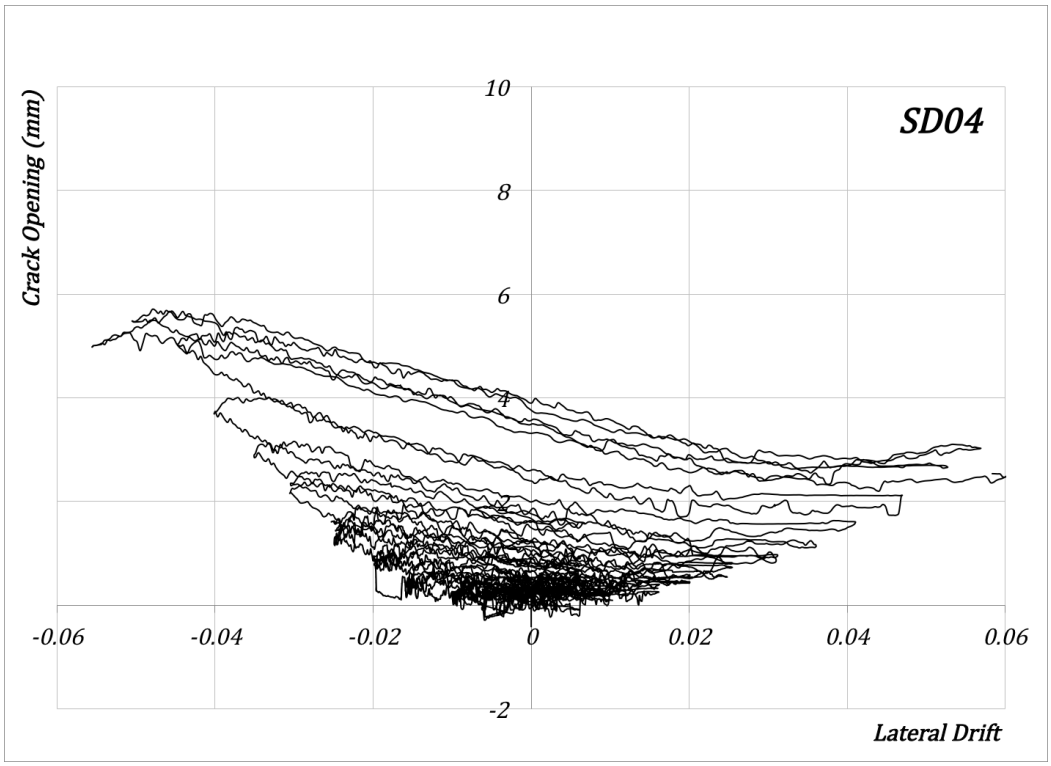

(b) SD04 Cracks Size

Figure 3.34: Opening of Cracks During the Cyclic Loading - SD03 & SD04

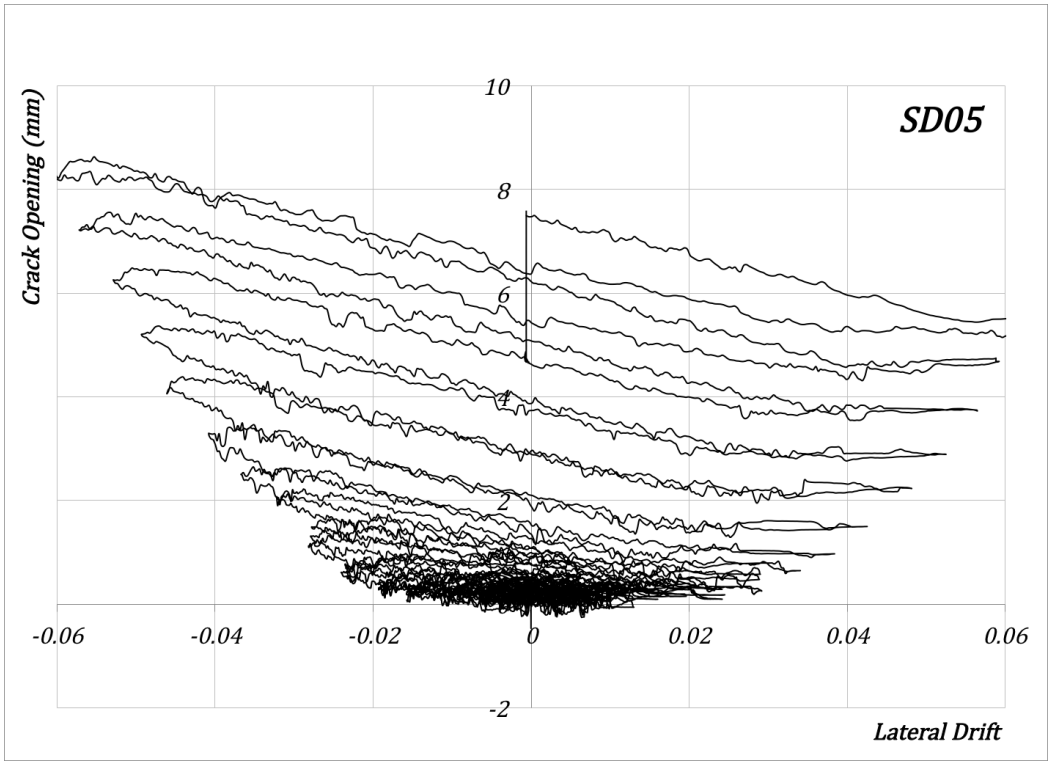

(a) SD01 Cracks Size

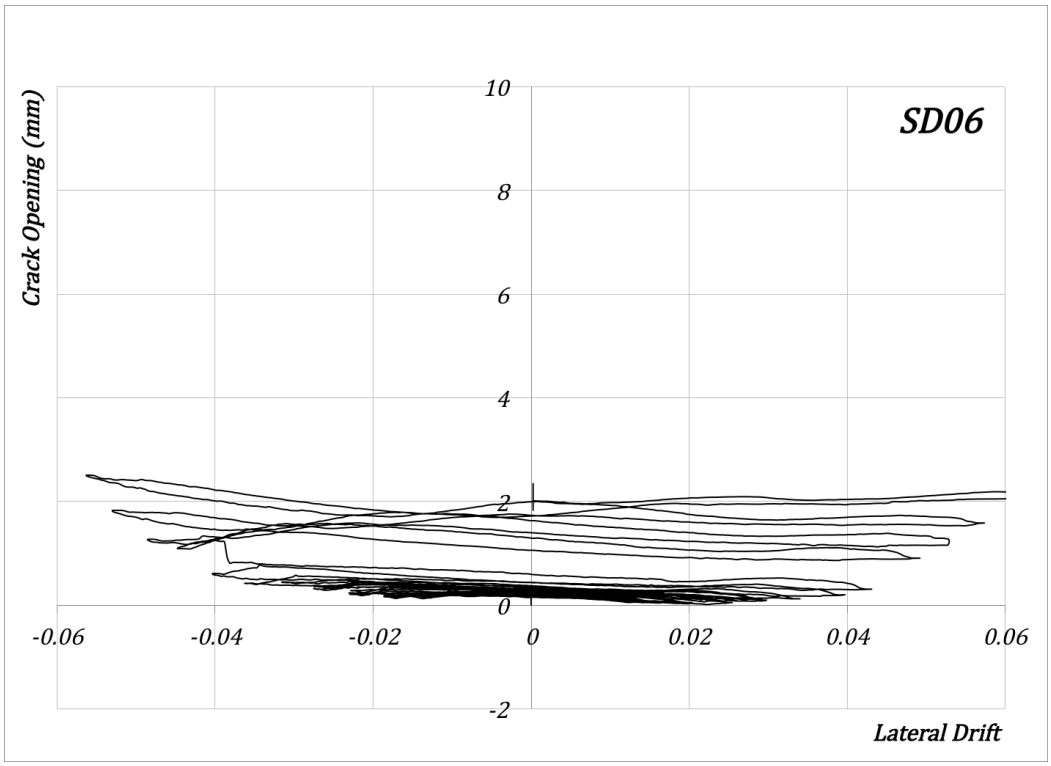

(b) SD02 Cracks Size

Figure 3.35: Opening of Cracks During the Cyclic Loading - SD05 & SD06

(a) Cracks at 1% drift

(b) Cracks at 2% drift

Figure 3.36: Progress of Cracks at the Bottom Surface of Slab SD02 (1 of 2)

(a) Cracks at 3% drift

(b) Cracks at failure

Figure 3.37: Progress of Cracks at the Bottom Surface of Slab SD02 (2 of 2)

(a) Cracks at 1% drift

(b) Cracks at 2% drift

Figure 3.38: Progress of Cracks at the Bottom Surface of Slab SD06 (1 of 2)

(a) Cracks at 3% drift

(b) Cracks at failure

Figure 3.39: Progress of Cracks at the Bottom Surface of Slab SD06 (2 of 2)

Chapter 4

Modelling of Slab-Column Connections

The objective of the analytical research presented in this chapter is to complement the experimental work by proving the value of the anchorage-controlled shear reinforcement in a more comprehensive way and show how it extends to full-scale structural frames. This part of the research is focused on:

1. A parametric investigation of the effect of the reinforcement crossing a crack on the crack opening and the shear slip, which shows the advantages of anchorage-cotrolled shear reinforcement at a micro level; along the crack interface. The analytical analyses are based on the Walraven model [61, 62] (Section 4.1).

2. The development of a large scale model of the slab-column joint to check the effect of the shear reinforcement on the lateral joint response. The crack interface response from point (1) was considered in modelling the slab-column interface (Section 4.2).

3. A parametric investigation of the effect of the response of individual joints behaviour on the global response of flat plate systems as assemblage of these joints (Chapter 5).

This combination of analyses enables the effect of the shear reinforcement type to be captured, starting from the crack interface opening, to the joint response, and then to

the global response of flat plate systems. Considering the complexities and nonlinearities involved, the models are intended to capture the joint behaviour at an acceptable level of accuracy to enable the parametric analyses of flat plate systems. The joint model is calibrated based on existing test data, from previous tests on cyclic loading of slab-column connections, with and without shear reinforcement. The associated computer programs are integrated into the open source finite element platform OpenSees [38].

4.1 Crack Interface Behaviour

The Walraven model [61, 62] captures the shear stress-slip behaviour along a crack interface using an aggregate interlock model, as shown in Fig. 4.1. This model was used to investigate the effect of the shear reinforcement on the response along the punching crack interface in a slab.

Fig. 4.1 shows the case of a particle (e.g. aggregate) in the cement matrix. The springs represent the reinforcement crossing the crack per unit area. w_0 represents the initial crack opening.
During a shear displacement, the particle penetrates into the cement matrix, causing crushing of the matrix and friction between the matrix and the particles. An additional opening of the crack size (Δw) generates tensile forces on the springs that are equivalent to the generated compressive stress (σ) per unit area of the crack plane. For the current crack opening, the compressive stress is calculated from the restraining stiffness of the extended springs, which is given as an input parameter depending on the reinforcement properties crossing the crack.

The modelling proceeds as follows:

- Crack faces are subjected to an incremental shear displacement $\Delta\delta$ (δ in Fig. 4.1(a)), the crack width $w_0 + \Delta w$ (w in Fig. 4.1(a)) remaining constant. The internal stress, σ, is compared to the external stress applied by the springs for the crack width ($w_0 + \Delta w$). If the internal stress is smaller than the external stress, the shear displacement δ is not large enough to be in equilibrium. This means that

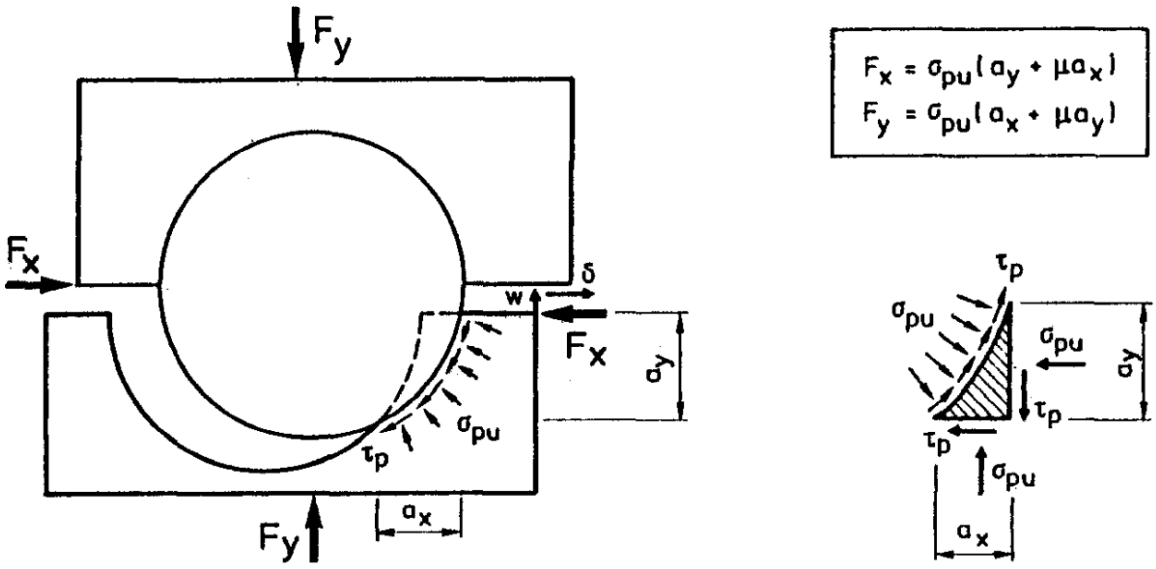

(a) Contact Mechanism at Shear Displacement

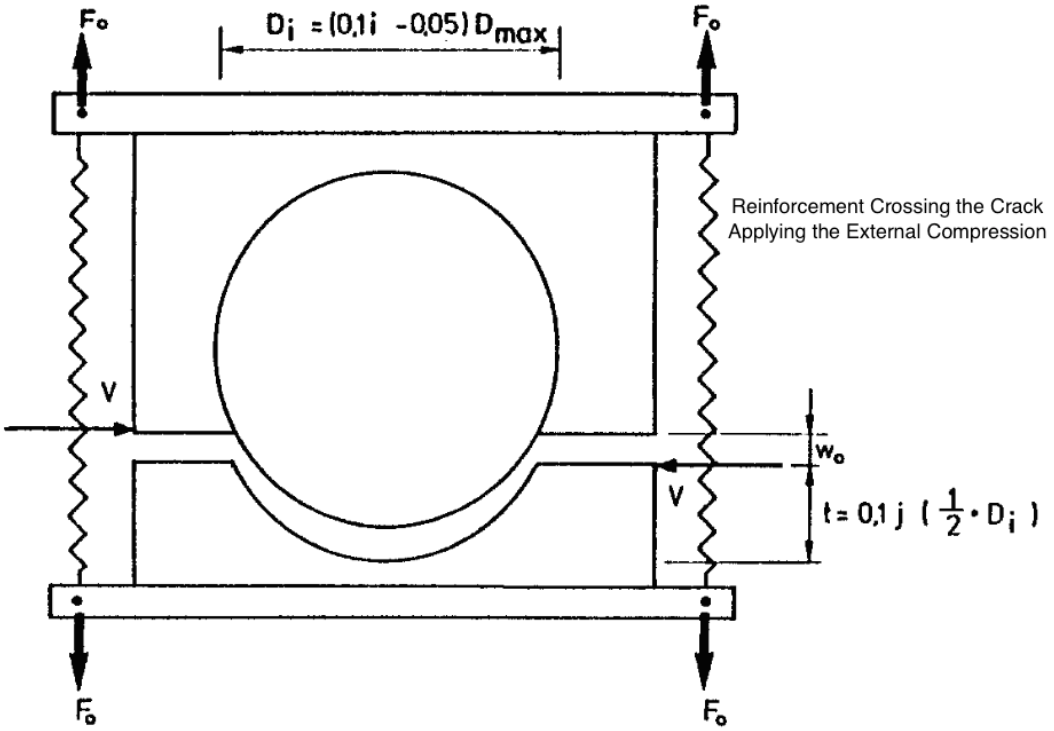

(b) Aggregate Interlock Model

Figure 4.1: Walraven Model [62]

a further shear displacement increment $\Delta\delta$ is necessary and the calculation has to be repeated for the new displacement status $(w_0 + \Delta w, 2\Delta\delta)$. This calculation is repeated until the internal stress is equal to the external stress provided by the springs that represent the reinforcement crossing the crack (Fig. 4.1(b)). This represents an equilibrium point.

- A further shear displacement increment would lead to an internal stress larger than the external stress provided by the restraining springs. This stress would further open the crack to $(w_0 + 2\Delta w)$, extending the springs and consequently there would be no equilibrium. In order to reach another equilibrium point, further shear displacement increments must be applied. Proceeding this way, the whole ascending branch of the $\tau - \delta$ relation is obtained. After the shear stress, τ, reaches the maximum shear stress of the loading cycle, unloading will occur. However, no immediate movement of the crack faces will occur because of the friction in the contact areas. A movement in backward direction will occur only when the maximum friction is exceeded. The value of δ for which no more contact between the crack faces exists can be found geometrically. The same procedure is repeated for loading on the opposite direction, which will be symmetric to the $\tau - \delta$ relation previously obtained.

- The calculation proceeds then with the next loading cycle, which is exactly the same as the first cycle. The only difference is that the crack faces are now damaged (abraded from the previous cycle, as shown in Fig. 4.2) and the two parts have to move further to get in touch. During each cycle, the crack faces are further damaged and the damaged faces need to be stored in the program memory for each cycle. More details on these calculations can be found in Appendix A.

The original Walraven model considers the reinforcement crossing the crack being perpendicular to the shear crack interfaces and linear elastic, while in this analysis the following modifications to this model are considered for the punching shear crack case:

- The shear reinforcement crosses the crack at different angles (depending on the

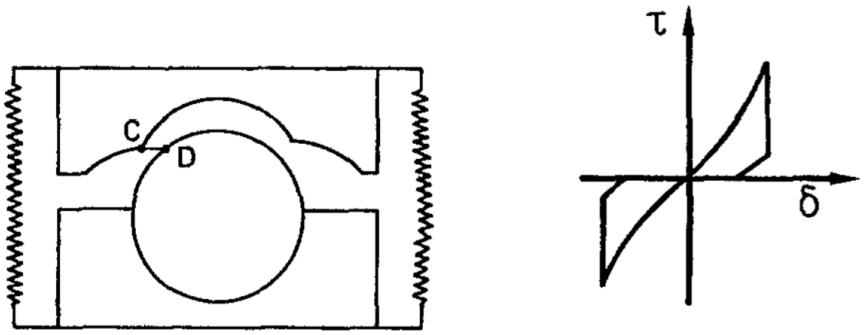

Figure 4.2: Damage of the Crack Interface

assumed punching crack angle) which may be considered accordingly in determining the stiffness of the representing spring.

- Different reinforcement behaviours have been considered for the springs to consider the effect of different shear reinforcement types.

- The opening of cracks following the first cycle does not considerably increase, as shown in Fig. 4.4 based on the test by Laible [31]. For this reason, and considering that the calculation of cyclic opening is computationally expensive, only the first cycle has been considered in this research to determine the properties of the Interface Shear Spring. Another alternative could be to assume a certain rate of crack opening increase or a larger crack as a representative of the average crack opening. This would require the investigation of more such test results, which is beyond the scope of this research.

4.1.1 Crack Interface Model Validation

Fig. 4.3 shows the results of a test conducted by Laible [31] and the respective calculated response, using the program described above. The main parameters were: $w_0 = 0.75mm$, $D_{max} = 38mm$ and $\mu = 0.2$. It may be observed that there is good agreement between the test and the model. The crack opening was 0.89mm (0.035in), which is also in good agreement with the crack opening for the first cycle, as shown in Fig. 4.4.

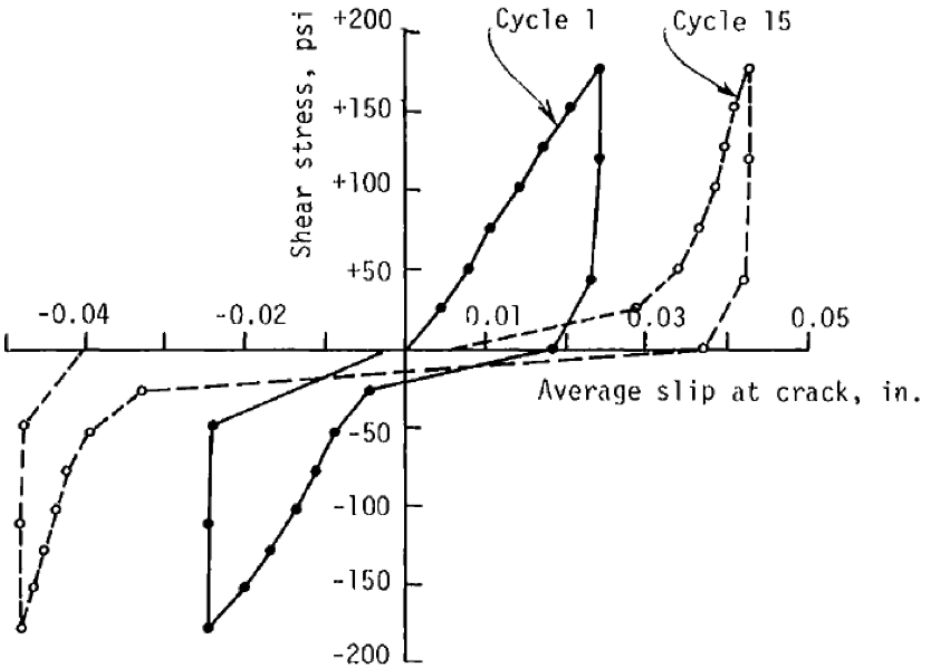

(a) Tested Shear Stress-Slip Response [31]

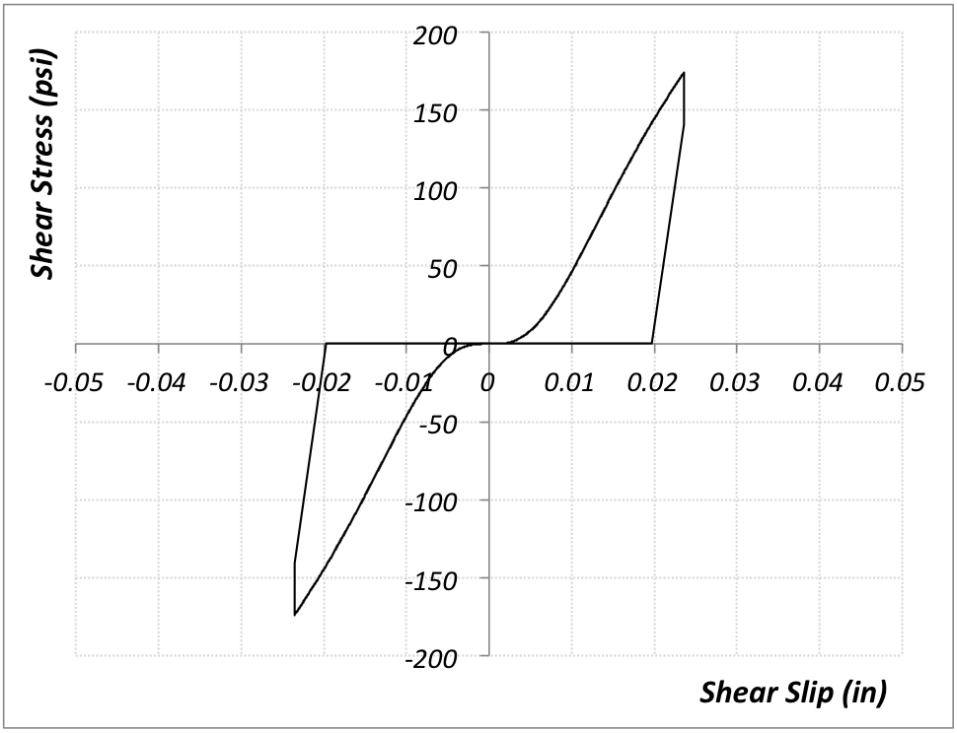

(b) Calculated Shear Stress-Slip Response

Figure 4.3: Comparison of Tested and Calculated Shear Stress-Slip Response

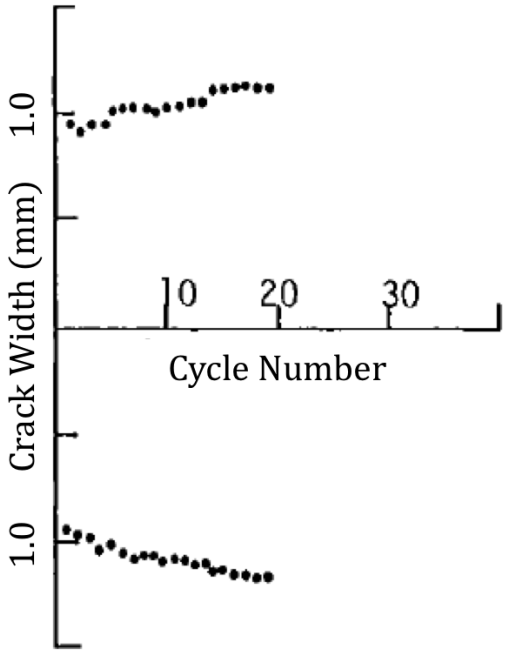

Figure 4.4: Cyclic Crack Opening [31]

Two parameters have been considered in the following sections:

- Effect of the reinforcement stiffness - Section 4.1.2.
- Effect of the flexible washers - Section 4.1.3.

4.1.2 Steel Bolts as Shear Reinforcement

Steel reinforcement only was considered first as the reinforcement crossing the crack (using the Walrave model [61]). The effect of the reinforcement stiffness and yielding has been considered for comparison purposes. The change in reinforcement stiffness would be achieved in practice by changing the bolt stem diameter and/or bolt spacing. For the recorded $V_u = 110kN$ and $M_u = 65kNm$ on the tested specimens and the respective dimensions, the shear stress ν_u is calculated using Equation no. 4.1.

$$\nu_u = \frac{V_u}{b_0 d} \pm \frac{\gamma_\nu M_u c}{J_c} = 3.0MPa \tag{4.1}$$

where:

b_0 is the critical shear perimeter

d is the effective depth of the slab

γ_v is the fraction of the moment that is transferred by shear stresses on the critical section, equal to 0.4 for a square column section

J_c is the polar moment of inertia of the critical shear section:

$$J_c = 2 \times \frac{b_1 d^3}{12} + 2 \times \frac{d b_1^3}{12} + 2(b_2 d)(\frac{b_1}{2})^2 = 1.85 \times 10^9 mm^4 \tag{4.2}$$

The stiffness of the springs (Fig. 4.1(b)) representing the reinforcement crossing the crack is also an input parameter and is determined as follows: Two shear bolts are considered for a crack interface with a rectangular shape $b_1 \times b_2$ where: $b_1 = c + d = 300mm$ and $b_2 = h_s/cos(45^o) = 170mm$ (Fig. 4.5). The stiffness per unit area of these springs has been calculated as the necessary force for a unit spring deformation of 1mm, divided by the area of the crack interface, and used as an input to the program as $4.7\frac{N}{mm^3}$. Fig. 4.6 shows the effect of the reinforcement stiffness on the shear stress-strain behaviour of the crack interface, with regards to shear slip and crack opening. The values of $k = 2, 3, 4$ and $5N/mm^3$ represent the stiffness of the steel bolts (without washers) crossing the crack. An initial opening of $0.5mm$ has been considered in these analyses. The *Walraven Model* requires an initial crack opening and $0.5mm$ was assumed in this case.

This parameter analysis shows that anchorage-controlled shear reinforcement would introduce higher ductility through larger opening of cracks, as well as larger shear slip resulting in higher interface friction. Since excessive opening of cracks would also result in failure, the following section introduces the flexibility through flexible washers, which allow larger, but limited, opening of cracks. The model may be used to consider the effect of other parameters, such as: aggregate size, concrete strength, etc.

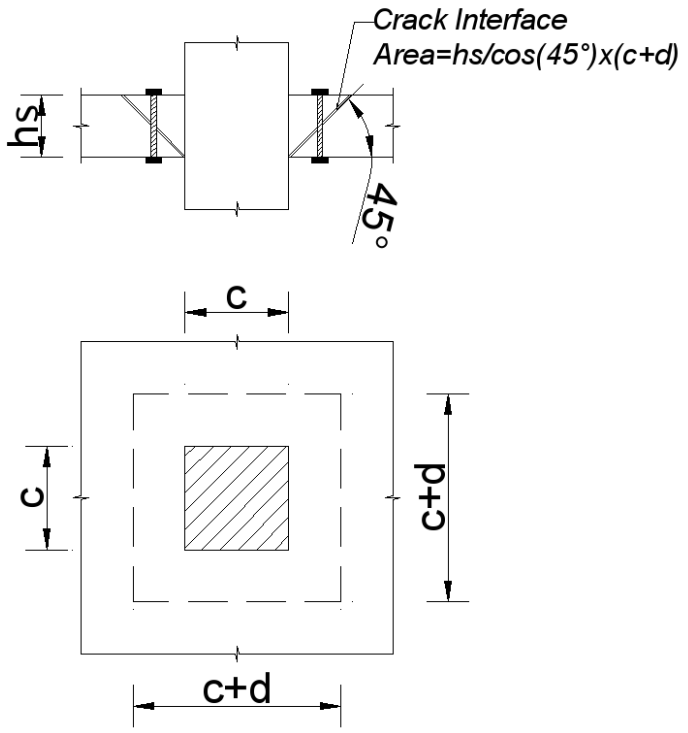

Figure 4.5: Crack Interface considered in the parameter analyses

4.1.3 Steel Bolts and Flexible Washers as Shear Reinforcement

A combination of steel bolts and flexible washers would result in springs connected in series crossing the crack, as shown in Fig. 4.7. Consequently the stiffness of the equivalent spring would be:

$$k_e = \frac{k_b \times k_w}{k_b + k_w} \tag{4.3}$$

where k_b is the bolt stiffness and k_w is the washer stiffness, determined from testing the washer in compression.

Fig. 4.8 shows the effect of washers on the crack interface response. In this case, thin washers of 0.2mm and 0.3mm, with negligible stiffness (assumed to be *zero* in the model), have been considered. The equivalent stiffness of the shear reinforcement is equal to *zero* until a deformation equal to the washer thickness is reached. After this point the equivalent stiffness is equal to the stiffness of the steel bolts. It may be observed that there is an increase in crack opening and shear slip, which would also introduce a higher

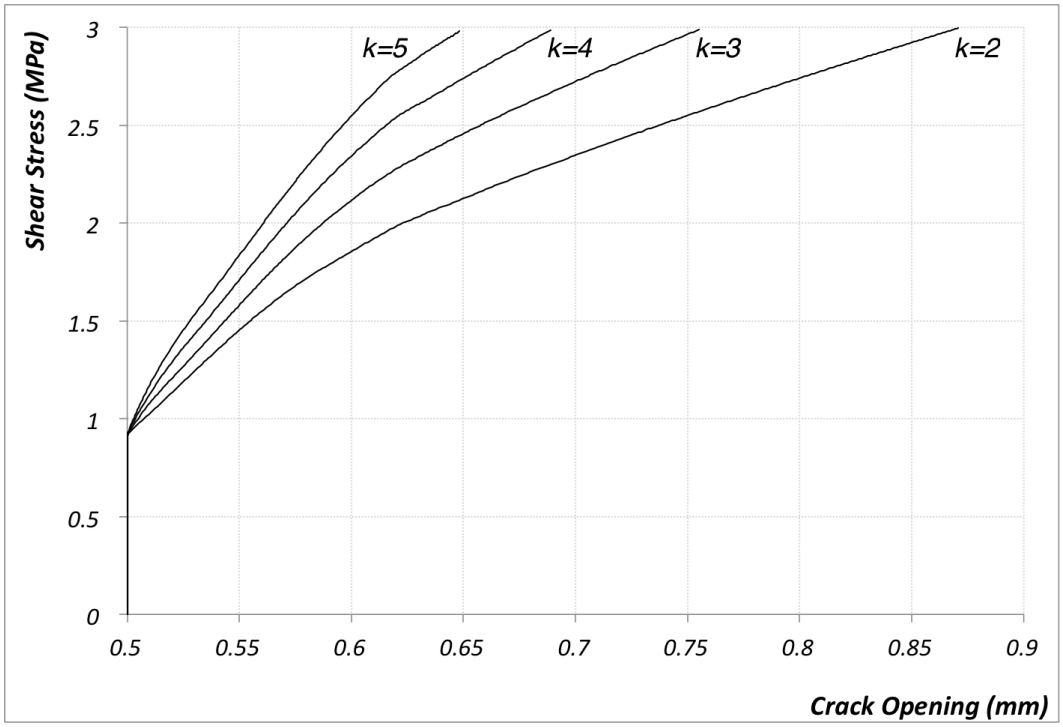

(a) Reinforcement Stiffness Effect on Shear Stress - Crack Opening Response

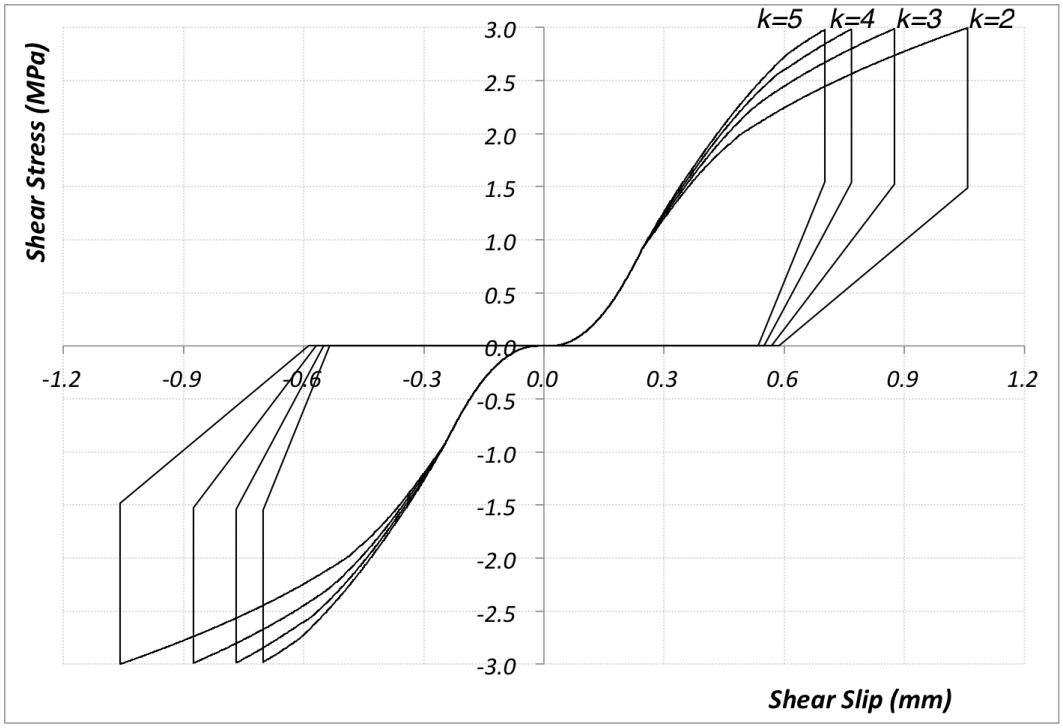

(b) Reinforcement Stiffness Effect on Shear Stress - Slip (δ) Response

Figure 4.6: Effect of Reinforcement Stiffness (k = 2 to 5 N/mm^3) on the Crack Interface Behaviour

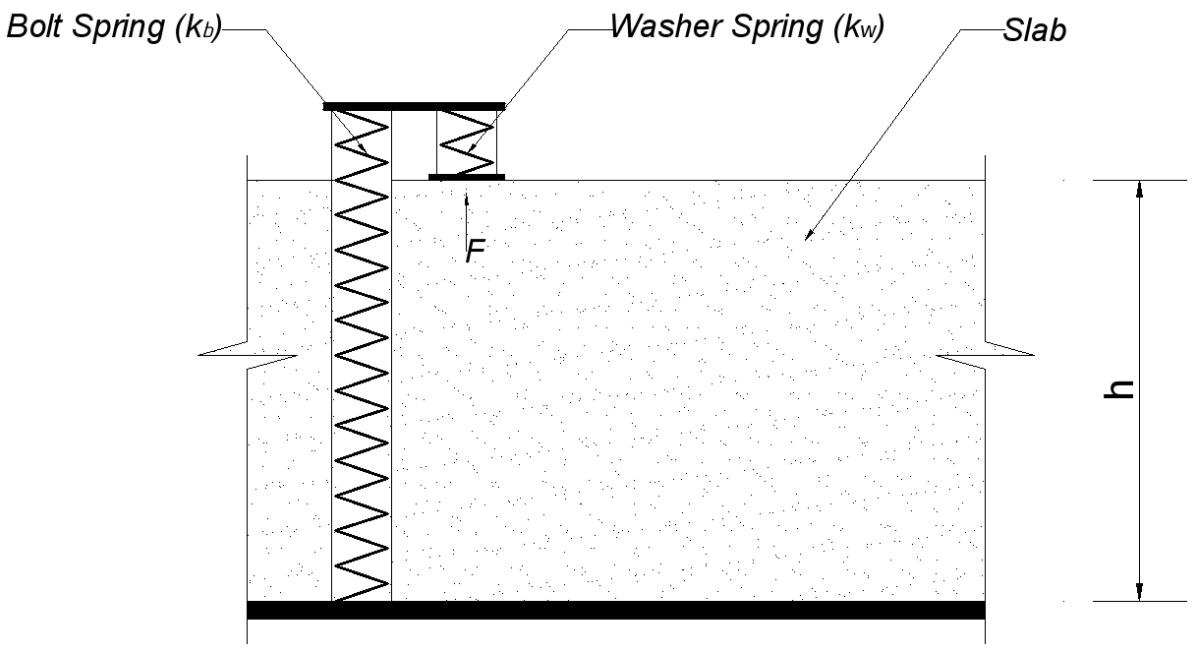

Figure 4.7: Configuration of Springs Representing the Shear Reinforcement

ductility of the crack interface response. The main advantage provided by the washers is in allowing for an additional crack opening, which is then *"locked"* by the stiff bolts, blocking any further considerable opening of cracks.

4.2 Slab-Column Joint Model

4.2.1 Introduction

In Section 4.1, the effect of shear reinforcement on the crack interface behaviour was analytically investigated. This section proceeds with the investigation of the effect on the slab-colum joint response through a large scale model of the joint. The joint model is calibrated based on the tested slab-column connections and is then used for the analytical investigation of frames, which cannot be practically tested in the lab. Shear transfer from the slab to the connection is modelled by the Walraven model [61, 62], while shear within the joint itself is modelled by the Modified Compression Field Theory [60]. A layered model is used to capture the flexural behaviour of the slab and columns, as

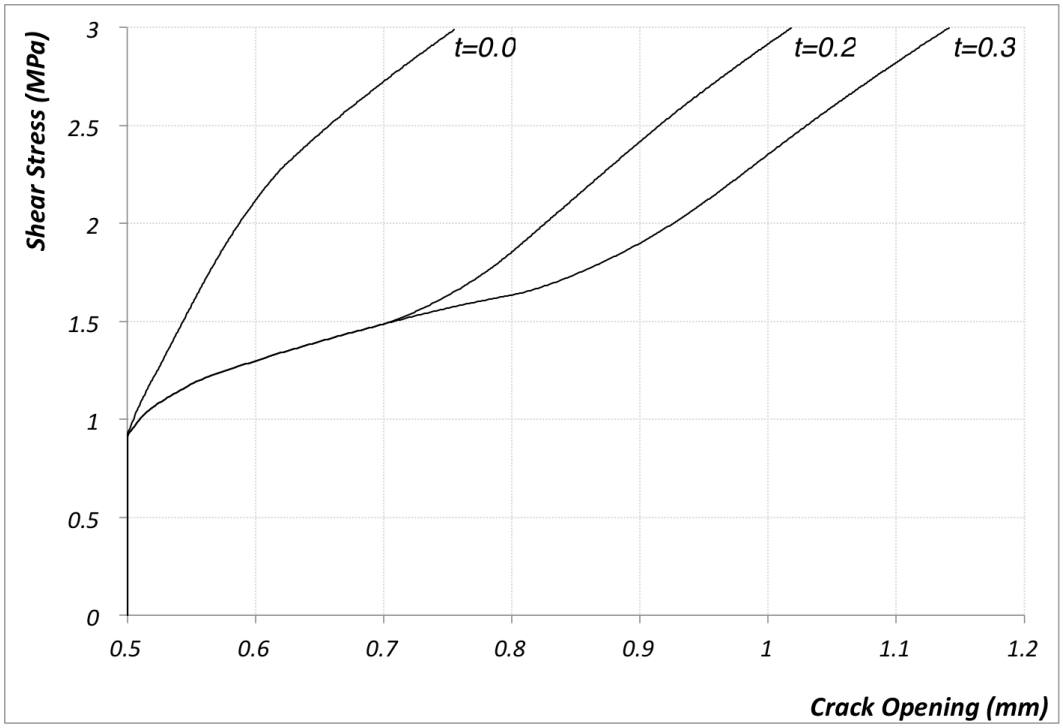

(a) Washer Effect on Shear Stress - Crack Opening Response

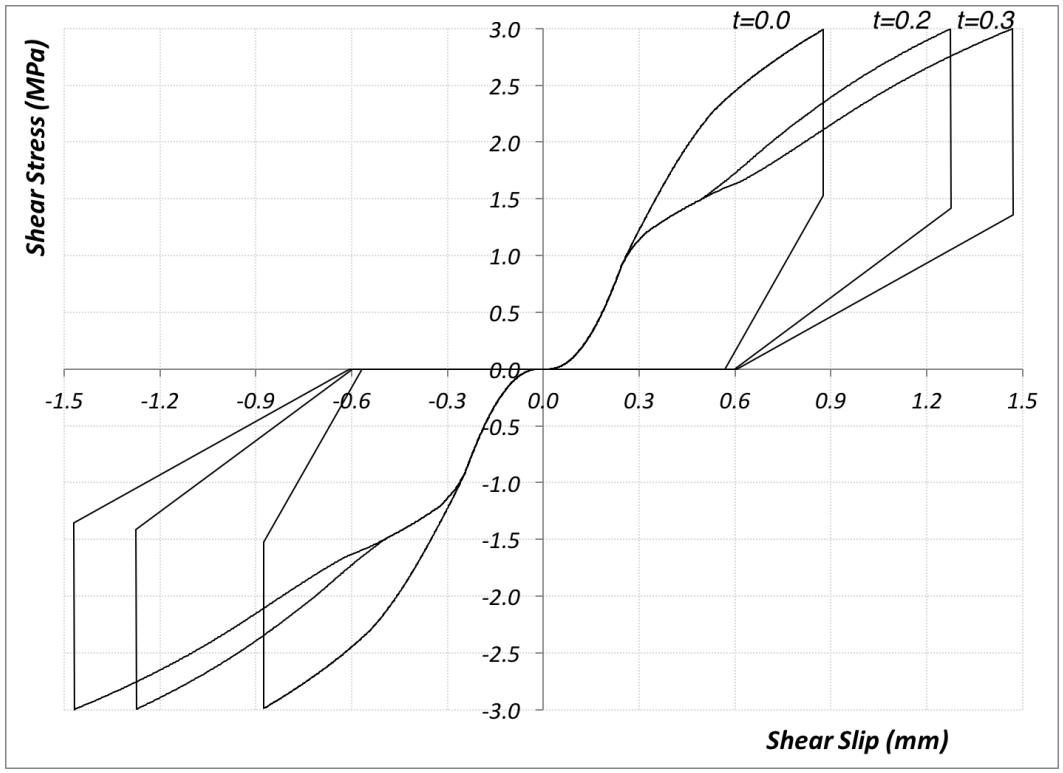

(b) Washer Effect on Shear Stress - Slip Response

Figure 4.8: Washer Effect (Thickness = 0.0, 0.2 and 0.3mm) on the Crack Interface Behaviour

one-dimensional elements.

A computer model of the joint enables the study of the effect of various connection hysteretic responses on the energy dissipation of the whole structural system and therefore the effect on the structural response, in terms of distribution of forces and total base shear. Different lateral load supporting systems were then investigated with the aim of determining the hysteretic response needed at slab-column connections for best performance, as described in Chapter 5.

In order to simulate the behaviour of the tested slab-column connection, shown in Fig. 4.9, a non-linear simulation has been carried out in OpenSees. OpenSees was chosen as a powerful open source platform also for the analysis of frames as assemblage of these joints, which is described in Chapter 5.

The connection model is composed of the following elements:

1. two non-linear beams (representing the slab-beams).
2. two non-linear columns.
3. one joint super-element, as shown in Fig. 4.10, which is composed of the following subcomponents:
   (a) one shear panel spring, which is intended to simulate strength and stiffness loss associated with shear failure of the joint core (Modified Compression Field Theory).
   (b) four interface shear springs, which are intended to simulate loss of shear-transfer capacity at the joint-slab and joint-column interface (Walraven Model).
   (c) eight bar-slip springs, which are intended to simulate stiffness and strength loss associated with bond-strength deterioration for slab and column longitudinal reinforcement embedded in the joint core.

Modelling of each of the above-mentioned elements is described in more details in the following sections.

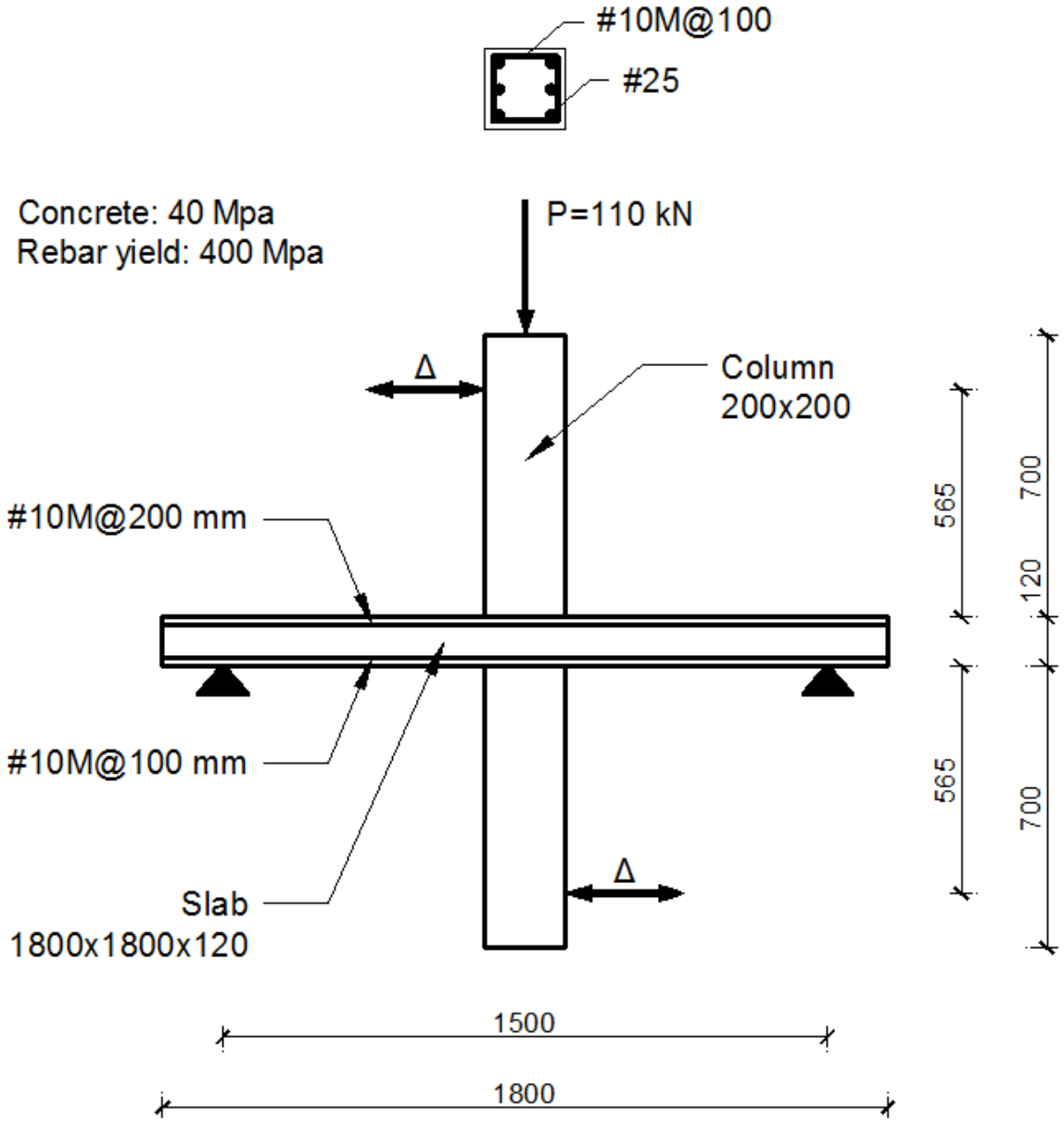

Figure 4.9: Slab-Column Joint Specimen

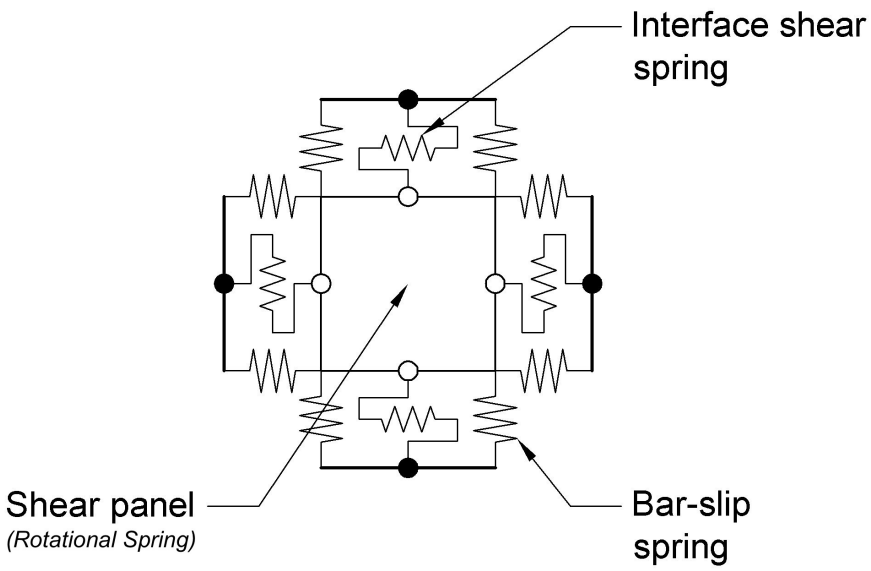

Figure 4.10: Joint super-element

4.2.2 Modelling of Joint Elements

4.2.2.1 Modelling of Slab-Beams and Columns

Columns and slab-beams have been modelled by displacement-based non-linear beam column elements, with co-rotational geometric transformation and five GaussLobatto integration points along the element length. Concrete has been modelled by a uniaxial constitutive model with tension softening (Concrete02 material, available in OpenSees), shown in Fig. 4.11. For the columns, concrete properties for the fibres confined by stirrups have been computed using the modified Kent-Park procedure [30]. For the slab-beams, the confinement has been neglected considering the configuration of reinforcement within the slab. Reinforcement steel has been modelled by the GiuffreMenegottoPinto model (Steel02 material, available in OpenSees), shown in Fig. 4.12. A fibre model has been used for the cross section [55], as shown in Fig. 4.13.

4.2.2.2 Constitutive Models of Joint Springs

The response of the springs of the super-element has been determined based on the guidelines given by Lowes et al. [34], as described in the following sections.

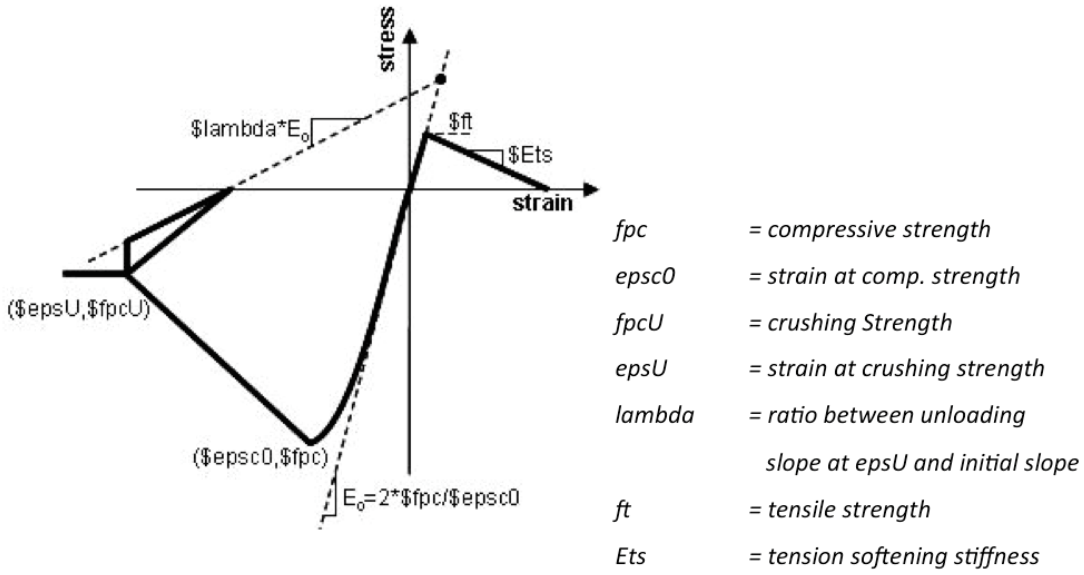

Figure 4.11: Concrete02 Material (adapted from the OpenSees Manual [38])

The Bar-Slip Response

The bar-slip spring (Fig. 4.10) is intended to simulate the bond response of the slab and column longitudinal reinforcement embedded in the joint core. The Bar-Slip material available in OpenSees, calibrated on test results from Eligehausen [15] and Hawkins [24], has been used. The model considers strength and stiffness degradation at the bonding interface. Once the slip demand exceeds 3mm, strength deterioration due to cyclic loading initiates. Reloading and unloading stiffness deterioration are also simulated (Fig. 4.14).

The following parameters are needed to define the response (more details can be found on the OpenSees manual [38]):

- compressive strength of the concrete
- yield strength of the reinforcing steel
- modulus of elasticity of the reinforcing steel
- hardening modulus of the reinforcing steel
- development length of the reinforcing steel

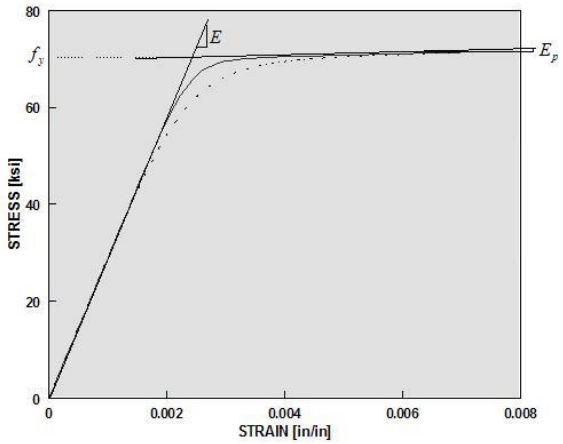

(a) Material parameters

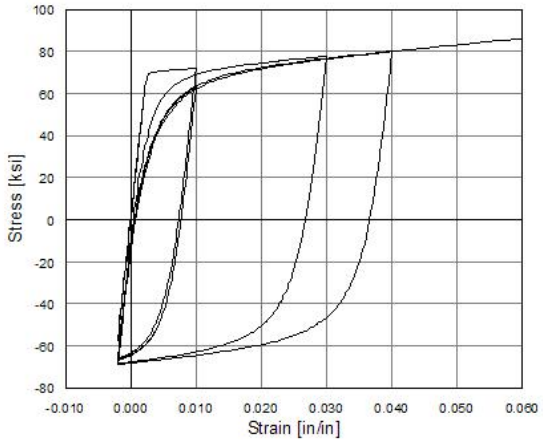

(b) Hysteretic response without Isotropic Hardening

Figure 4.12: Steel02 Material (adapted from the OpenSees Manual [38].)

- diameter of the reinforcing steel
- number of anchored bars
- dimensions of the beam or column
- bar location (beam top, beam bottom or column)

The Shear Panel Response

The Shear Panel (the rotational spring in Fig. 4.10) is modelled using a symmetric multi-linear moment-rotation relationship, using the Pinching4 material available in OpenSees, with the envelope response shown in Fig. 4.15.

The envelope properties (four typical $(M-\theta)$) points are determined based on the Modified Compression Field Theory (MCFT), proposed by Vecchio and Collins [60]. MCFT provides shear stress vs. shear strain (τ-γ) response for a reinforced concrete panel, subjected to pure shear only. The panel, in this case, is defined by the vertical plane of the slab-column joint, as shown in Fig. 4.16. The (τ-γ) relationship can be

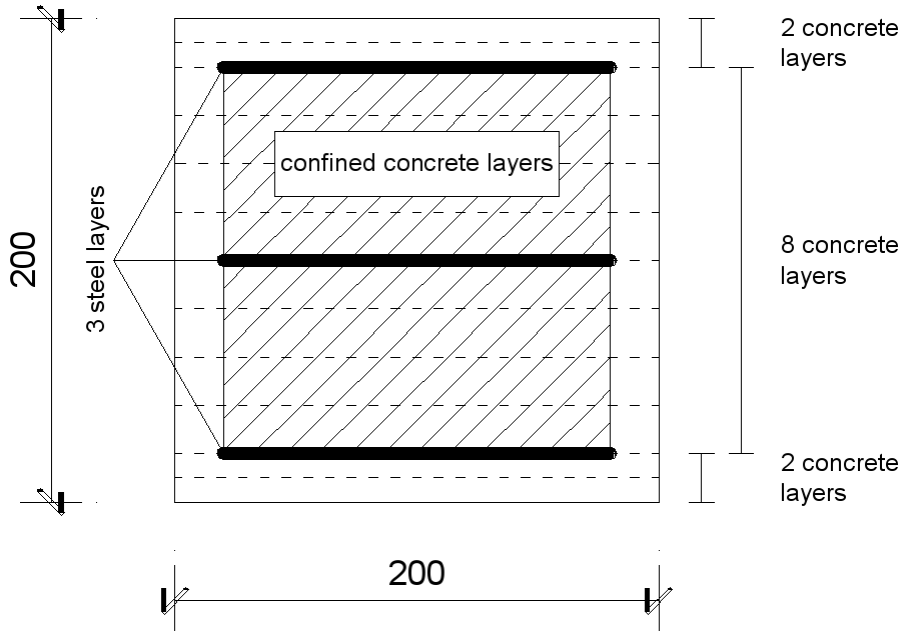

(a) Column Fibre Model

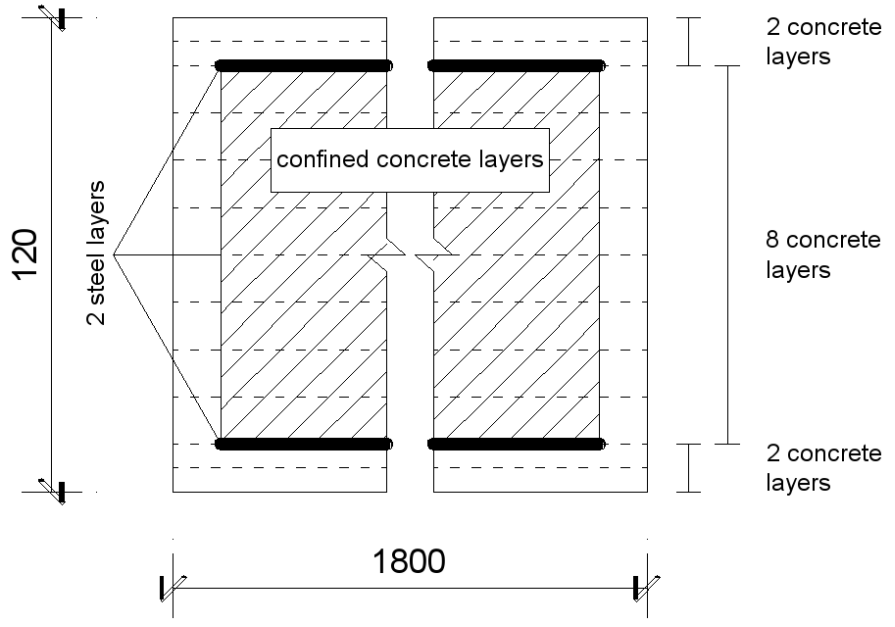

(b) Slab-Beam Fibre Model

Figure 4.13: Fibre Models for the Frame Elements

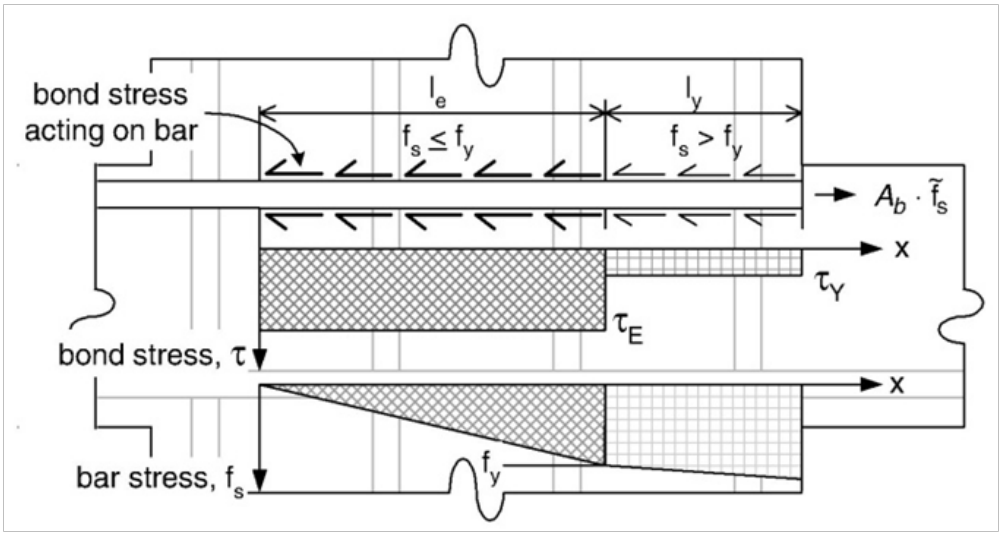

(a) Bond and bar stress distribution for a reinforcing bar anchored in a joint

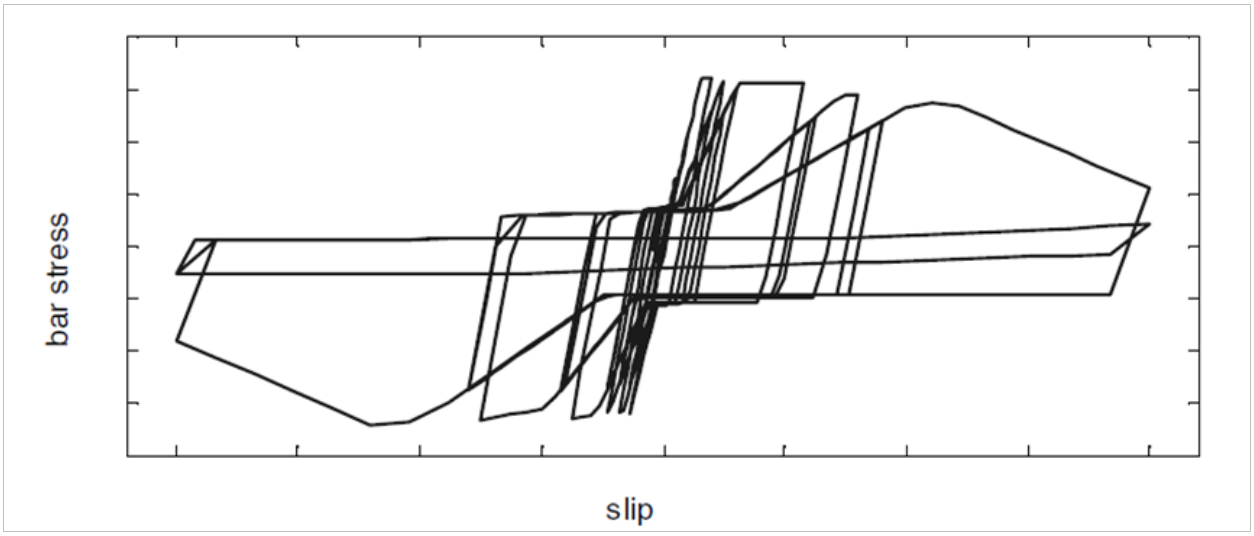

(b) Stress-Slip Response

Figure 4.14: Bar-Slip Spring Model [34]

converted into a moment-rotation $(M - \theta)$ relationship according to:

$$M = \tau \cdot Vol_{joint} \tag{4.4a}$$

$$tan\theta = \gamma \tag{4.4b}$$

where $Vol_{joint} = col_{height} \times col_{width} \times slab_{height}$ is the volume of the intersection of the slab and column.

This material model can also consider the deterioration of the material response under cyclic loading with regard to unloading and reloading stiffness and strength. However, in this analysis this degradation has been neglected since the shear panel within the joint is relatively small and very well reinforced. Consequently, the degradation is expected to be negligible. Greater degradation of both stiffness and strength are expected at the slab portion around the column. This degradation has been captured by the spring representing the response at the interface between the joint and the slab-beam element. This way, the model becomes more flexible in considering the effect of various types of shear reinforcement in the slab around the column. The effect of this reinforcement on the strength of the shear panel and consequently the joint itself is considered by adjusting the width of the shear panel accordingly.

Interface Shear Spring

For the *Interface Shear Spring*, the Walraven model has been considered as described earlier in Section 4.1. A shear force-slip response is calculated with this model based on the shear reinforcement technique.

4.2.3 Boundary Conditions

The tested specimen is a two-way slab freely supported on the four edges, with two steel beams restraining its corners against lifting. In this research the slab is modelled as a beam, as part of a 2D model. To have an equivalent response of the simplified beam

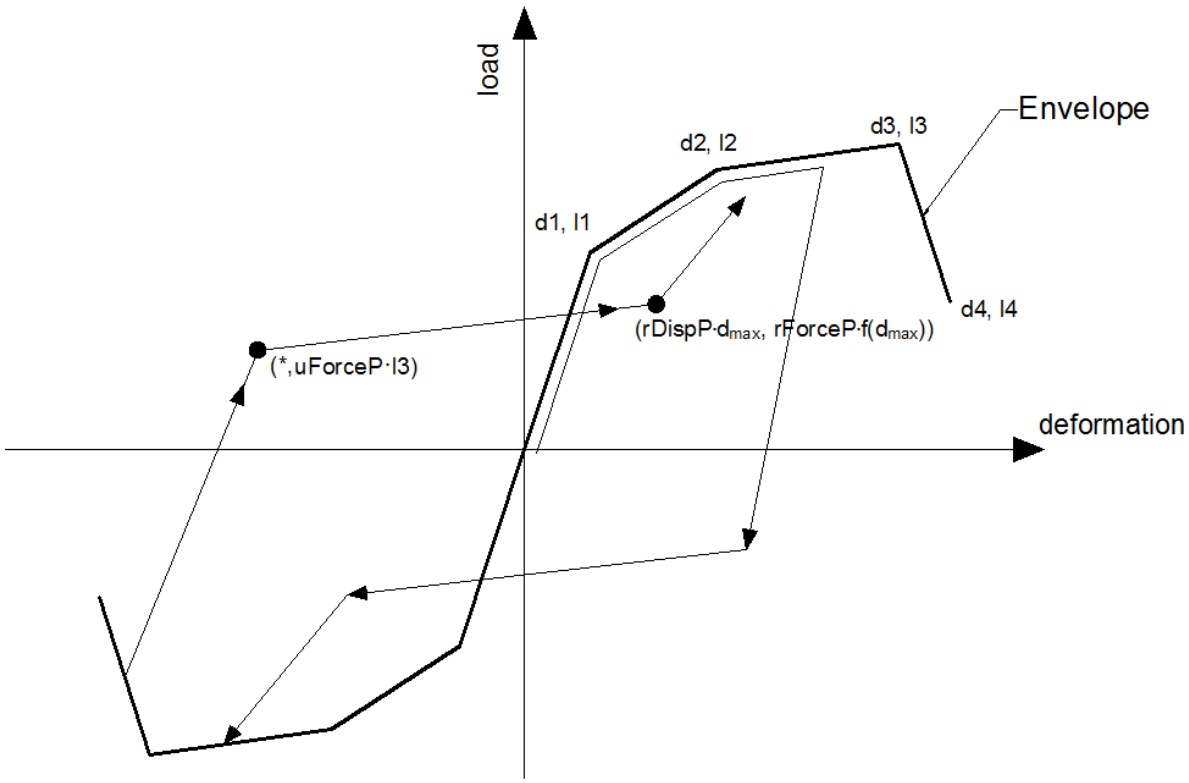

Figure 4.15: Pinching4 Material Model [38] (details in Appendix B)

model, the boundary conditions have been considered as fixed on both sides (Fig. 4.17), based on the following analyses:

- The bending moment of a two-way slab, freely supported and subjected to a central concentrated load P, is:

$$M_{max} = \frac{P}{2} \times \frac{l^2}{4} = \frac{Pl^2}{8} \tag{4.5}$$

  This bending moment is equal to the value of the bending moment on a fixed beam with a concentrated load. If the other effects (torsion etc.) are considered, the bending moment of the slab would be even lower, making the fixed beam a better model than a freely supported beam.

- For the typical case when the slab is subjected to a UDL, w, the bending moment would be $M_{max} = \frac{wl^2}{27.4}$ [36]. This is also very close to the equivalent fixed beam case, where $M_{max} = \frac{wl^2}{24}$, compared to the freely supported beam where $M_{max} = \frac{wl^2}{8}$.

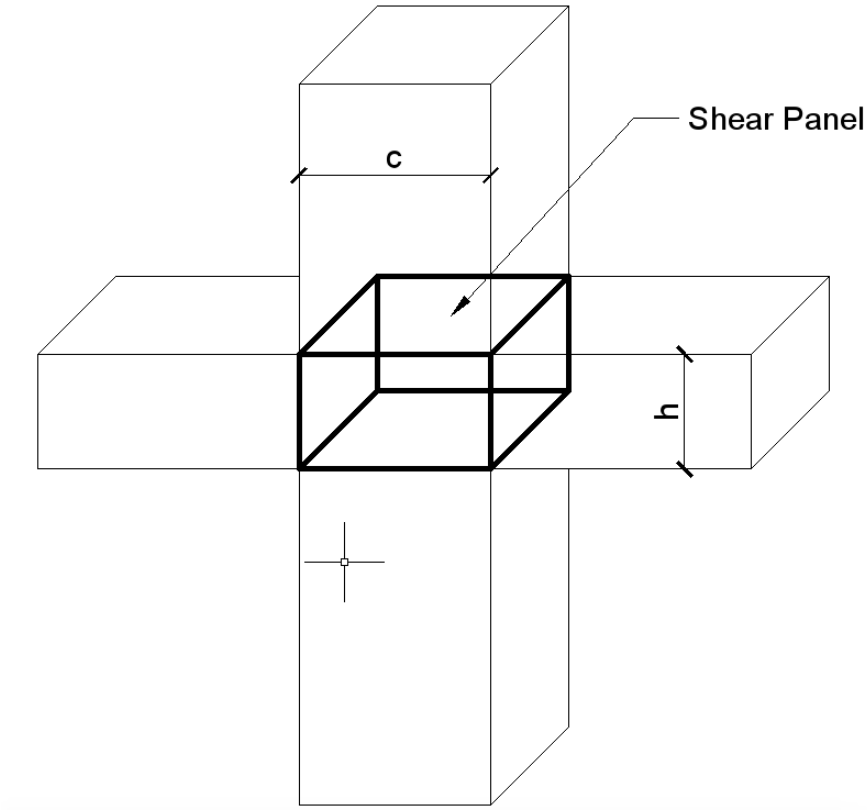

(a) Shear panel definition (column-slab intersection)

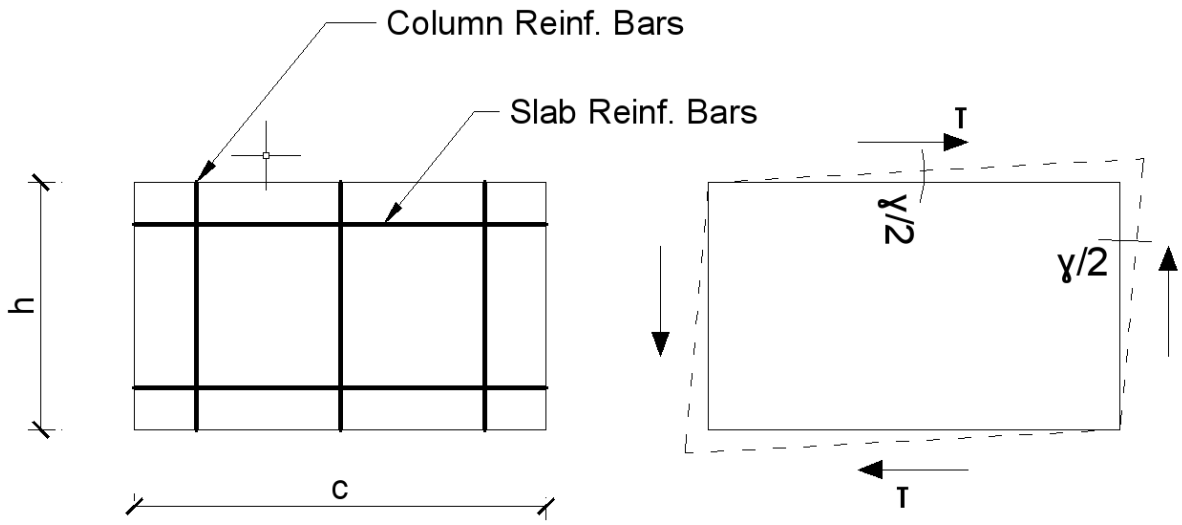

(b) Shear panel reinforcement and deformations

Figure 4.16: Joint Shear Panel

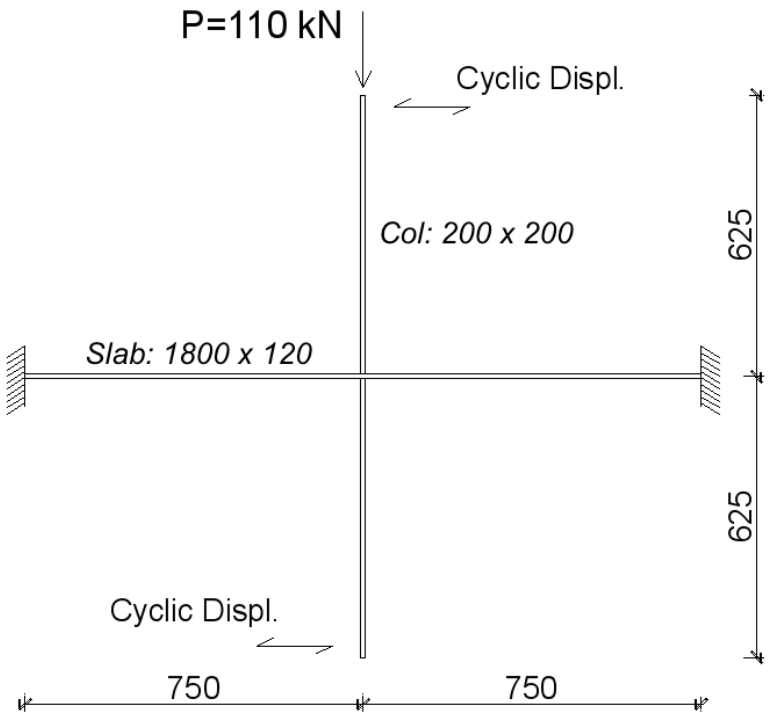

Figure 4.17: Boundary Conditions

The modified boundary conditions will introduce a different distribution of forces on the slab-beam elements, but the total response of the structure will be more realistic.

4.2.4 Analytical Examples

This section describes an analytical investigation of the effect of the shear reinforcement on the joint response. Being a macro-level model, the investigation is mostly qualitative to determine the effect of the stiffness and flexible washers. The models are based on the tested specimens, described in Chapter 3, and shown in Fig. 4.9. All dimensions, loading, material and reinforcement properties, are the same as used in those tests. The boundary conditions of this model are shown in Fig. 4.17, fixed on both ends of the beam.

4.2.4.1 The effect of the shear reinforcement stiffness on the joint response

Four one-dimensional elements represent the columns and slab-beams and a joint super-element represents the non-linear behaviour of the joint. The frame elements have been modelled as described in Section 4.2.2.1. The joint model has been further described below.

Loading

First, a gravity load of 110 kN was applied statically on the top of the column, which was kept constant throughout the analysis. A cyclic displacement was then applied on the top and bottom of the columns, following the displacement path shown in Fig. 3.6.

Shear panel

The shear panel properties have been determined based on the Modified Compression Field Theory. Membrane 2000 [5] was used for the shear load-deformation response. The panel in this case is the panel defined by the intersection of the slab and column. The thickness of this panel has been determined by considering the thickness of the panel within the column, equal to 200 mm. The reinforcement of the panel in directions x and y represent the reinforcement of the slab and the column, respectively, located within this panel, as shown in Fig. 4.16.

Bar-slip springs

The bar-slip springs have been modelled as described in Section 4.2.2.2, based on the reinforcement and materials properties of the tested specimen. These springs are however relatively not important in this case, because all longitudinal reinforcement goes through the joint and elements have been over-designed in flexure. Consequently, no slip degradation is expected, as also observed from the tests. The model would however consider such failure for a corner connection, or anywhere else where the flexural reinforcement could slip from the joint core.

Interface shear springs (ISS)

The four interface shear springs of the joint model have been divided in two types:

- The springs at the interface of the columns with the joint core have been modelled as simply linear elastic, considering that this interface is relatively stiff and does not experience any significant degradation.
- The springs at the interface of the slab-beams with the joint have been modelled based on the Walraven Model, as further described below.

The main parameter to be determined in this model is the stiffness of the spring that represents the stiffness of the reinforcement crossing the crack. For one side of the punching cone as the shear interface, with two shear bolts crossing the interface, the calculations would proceed as following:

- The area of the crack interface for an assumed crack angle of 45° would be $A_{ci} = 49,220mm^2$.
- The force T_b on the two bolts due to a unit deformation of 1mm, would be:

$$T_b = 2 \times A_b * E_b \times \frac{1mm}{h_s} = 2 \times 45.6 \times 180,000 \times \frac{1}{120} = 137,000 \frac{N}{mm} \tag{4.6}$$

  where A_b and E_b are the cross sectional area and the modulus of elasticity of the shear bolt, respectively. For a crack opening of 1mm, this force would be:

$$T_b' = \frac{T_b}{cos(45°)} = 194,000 \frac{N}{mm} \tag{4.7}$$

  where $T_b^{'}$ is equivalent to the stiffness provided by the bolts in the direction perpendicular to the crack interface (the force introduced for a unit opening of the crack).

- The linear stiffness of the reinforcement is then converted into a stiffness per unit area of the crack interface to be compatible with the required input in the Walraven

model, as follows:

$$k_s = \frac{T_b'}{A_{ci}} = \frac{194,000}{49,220} = 3.94\frac{N}{mm^3} \tag{4.8}$$

The rest of the parameters of the model are related to concrete properties, as described in Section 4.1. The response along the crack interface is determined as described in Section 4.1.2 for a spring stiffness of $3.94\frac{MPa}{mm}$. Subjected to a stress of 3MPa, the calculated max slip is 0.75mm, which would represent the stiffness along the crack interface as $3MPa/0.75mm = 4\frac{MPa}{mm}$. This response is then converted into a vertical force-displacement response, which is the necessary input for the ISS of the super-joint model. For a punching area of:

$$A_s = 4 \times (c + d) \times d = 4 \times (200 + 90) \times 90 = 104,000mm^2 \tag{4.9}$$

it would result in:

$$V_s = A_s \times \tau = 104,000 \times 4.0 = 416\frac{kN}{mm}. \tag{4.10}$$

The stiffness of the two interface shear springs, being in series, would then be 416/2 = 208 kN/mm.

The simulated response of the tested slab-column connection is shown in Fig. 4.18. Compared to the tested response the simulation shows a similar strength, but a relatively higher stiffness. In order to check the effect of an increase in ISS stiffness, a similar simulation was conducted with a stiffness of 300 kN/mm and other parameters being the same. The simulated response, shown in Fig. 4.19, shows an increase in both strength and stiffness.

4.2.4.2 The effect of flexible washers on the joint response

This model is similar to the model of the joint described in Section 4.2.4.1, except for the different behaviour of the Interface Shear Spring. The response of this Spring is now more flexible due to the introduction of the flexible washers on the shear reinforcement. Considering the response shown in Fig. 4.8(b), a quadrilinear behaviour has been assumed for the ISS Response, as shown in Fig. 4.20. The *'stiffness gap'* between 0.3 and

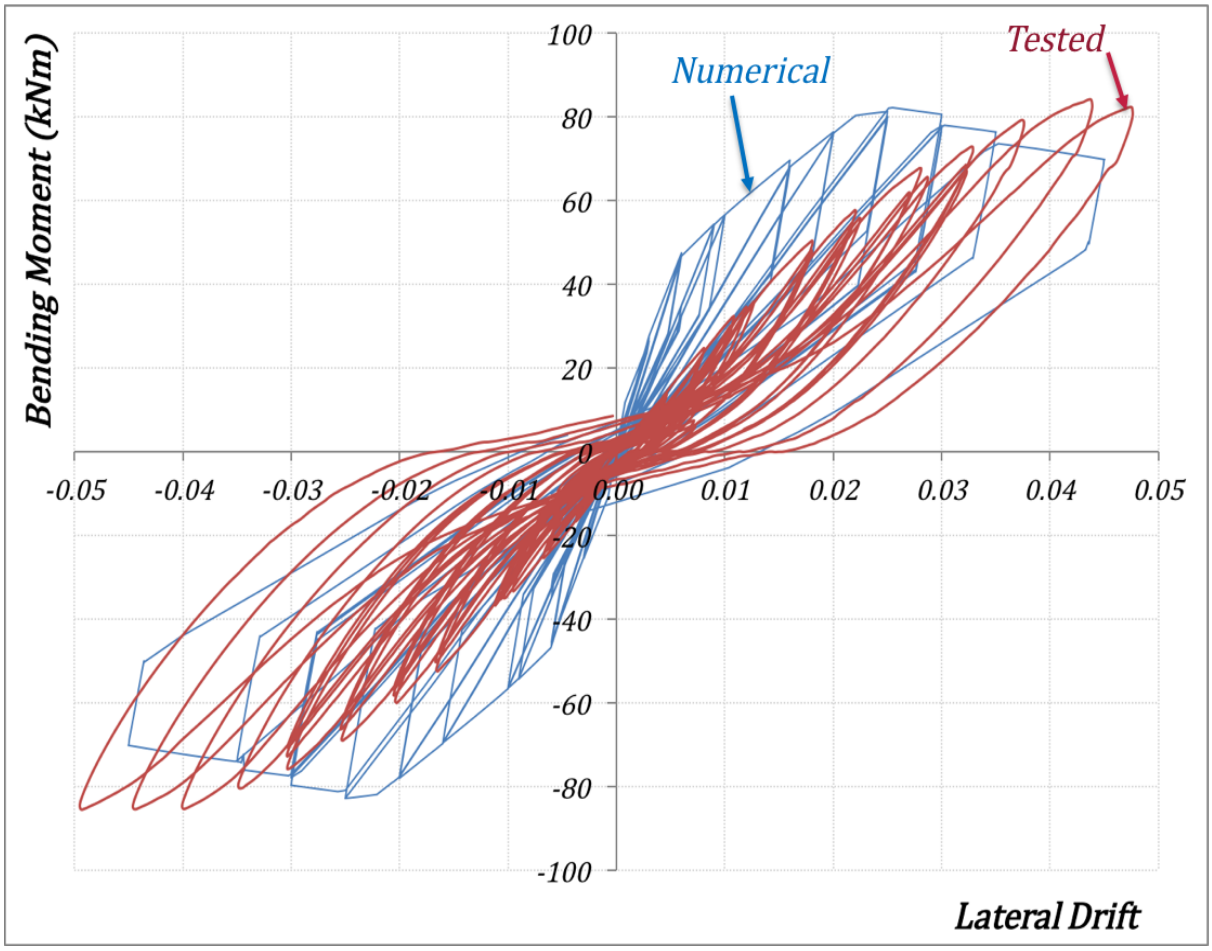

Figure 4.18: Slab-Column Joint Reinforced with Steel Bolts Only

0.8mm considers the effect of the washer which allows for a deformation without load (a 3mm washer, which is the thickness of washer for the tested specimen, introduces an additional "slip" of 0.5mm in Fig. 4.8(b)). The washer has been assumed to engage at a deformation of 0.3mm, which is the point when the slab loses strength due to punching cracks occurring inside the slab, activating the shear reinforcement. Beyond a deformation of 1.0 mm, the Interface Shear Spring has been assumed to lose stiffness due to yielding of the shear reinforcement. A washer stiffness of $k_w = 0$ has been used in this case, considering the negligible stiffness of neoprene.

The simulated lateral load-displacement response of the connection is shown in Fig. 4.21. From this graph it may be observed that the connection now has a lower strength than the original connection, due to increased deformation allowed for by the ISS. This

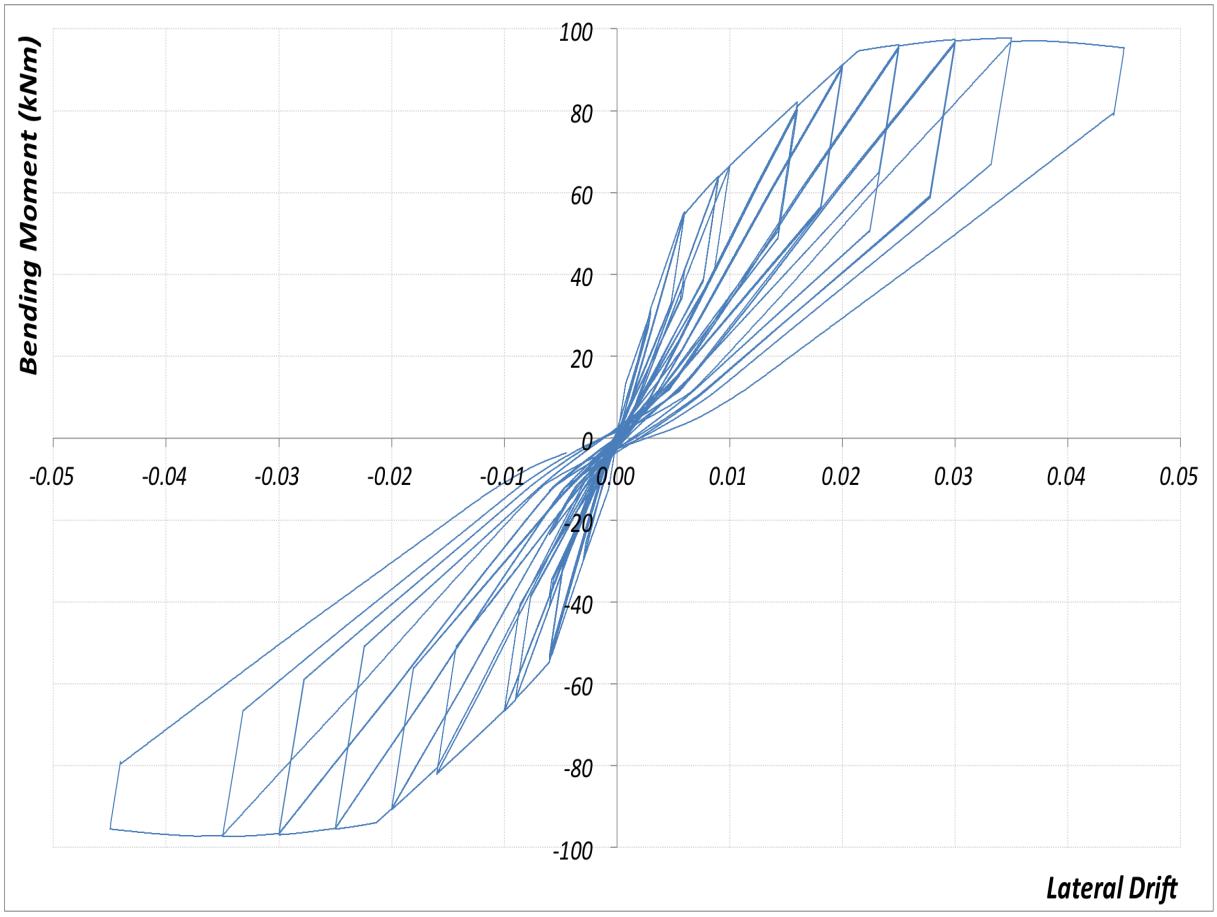

Figure 4.19: Slab-Column Joint Reinforced with 50% Stiffer Bolts than the Case in Fig. 4.18

deformation is *"locked"* once the washer has completely deformed and the connection regains stiffness and experiences similar deformability afterwards. The plateau introduced in the response is considered to be the advantage of using washers, resulting in higher ductility in the response of the connection. In addition, less pinching is observed, particularly for lower loading cycles (of higher practical importance). Compared to the tested specimen reinforced with washers the analytical model provides a higher strength, of about 10%.

Both analytical responses (Figs. 4.18 and 4.21) show a higher stiffness than the respective tested responses. This is a result of the assumed boundary conditions, which increase the flexural stiffness of the slab-beams (being fixed at the ends). In addition, the initial stiffens of analytical responses is typically higher because of inaccuracies in

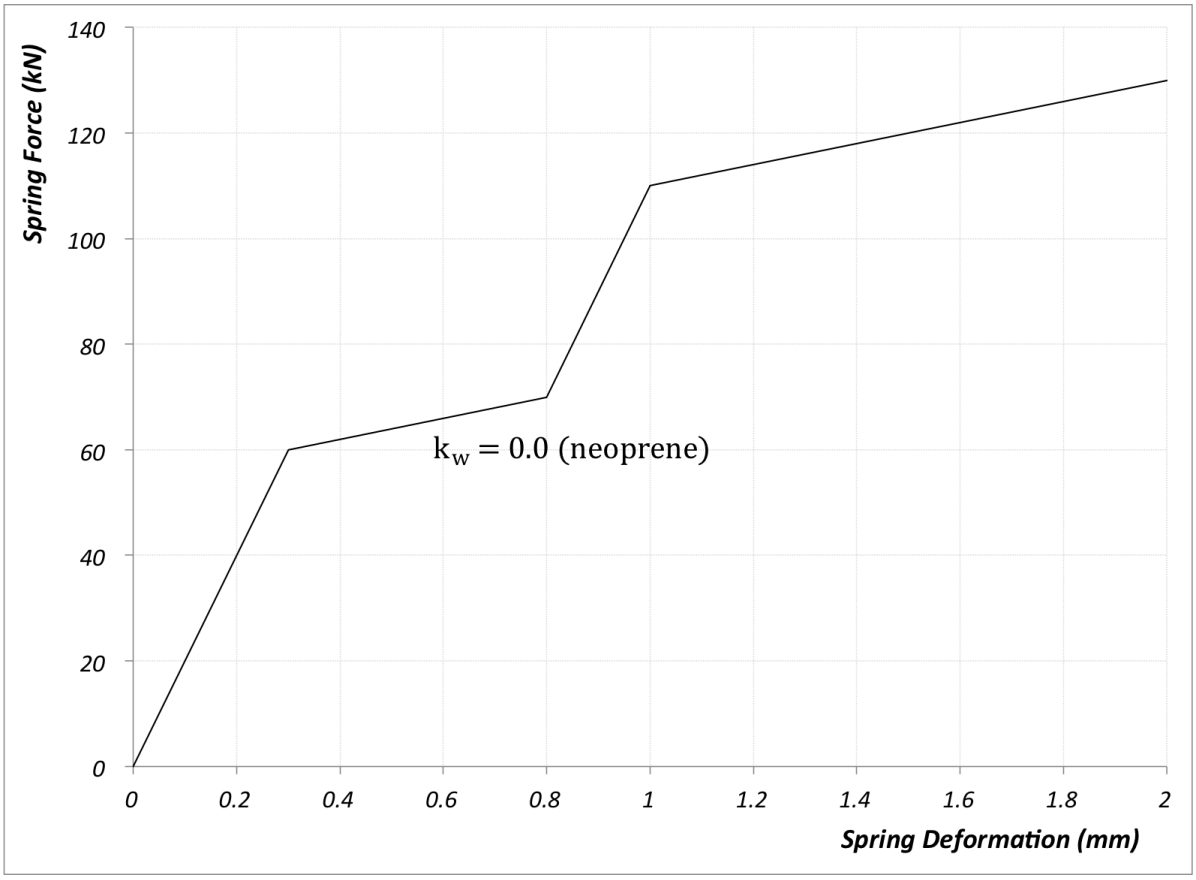

Figure 4.20: Interface Shear Model for the case with a Flexible Washer (kN/mm)

lab measurements, related to frames and instrumentation not perfectly tightened.

The slab-column joint model, which involves also the crack interface model, may be used to capture the response of slab-column joints, which is then incorporated into the modelling of flat-plate frames as further described in Chapter 5. This would be an acceptable alternative when test results of slab-column joints are not available.

Due to the large scale nature of these models, involving the various assumptions discussed previously, they are not intended to accurately predict the behaviour of slab-column joints. They may, however, be used successfully for parametric analyses, especially if test results of a similar specimen are available.

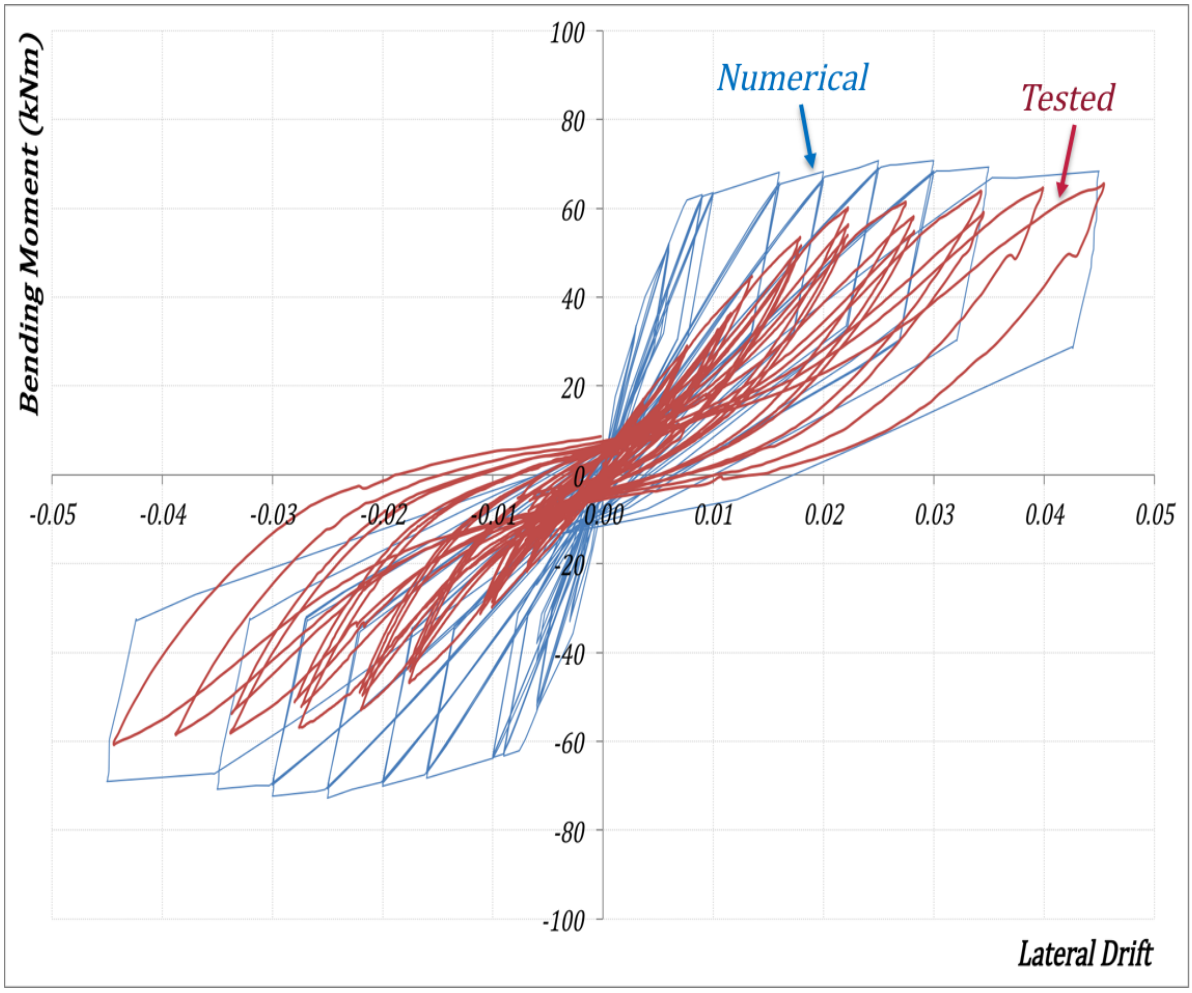

Figure 4.21: Slab-Column Joint Reinforced with a Combination of Steel Bolts and Flexible Washers

Chapter 5

Modelling of Flat-Plate Systems

This Chapter is focused on the analytical investigation of the effect of the slab-column joint response on the global response of a frame. The prototype frame from which the joint specimens were taken from [6] has been analyzed initially (Section 5.3), followed by the analyses of a more general five-storey, six-bay frame (Section 5.4). Three typical joint responses, shown in Fig. 5.1 have been considered in this model, taken from the experimental part of this research. The responses captured from the tested specimens (as previously described in Chapter 3) have been simplified into two envelope elastic-perfectly plastic responses for the case with flexible washers and a quadri-linear curve for the stiffer response, with steel bolts only. A failure criterion has been used such that the material representing the joint behaviour fails if a rotation of 0.06 is achieved. From that point on, values of 0.0 are returned for the tangent stiffness and stress. This also enables the simulation of the progressive collapse of the frames.

The frame analyses in this Chapter are based on responses of tested slab-column joints. When such test results are not available, the necessary joint response can be determined as described in Chapter 4.

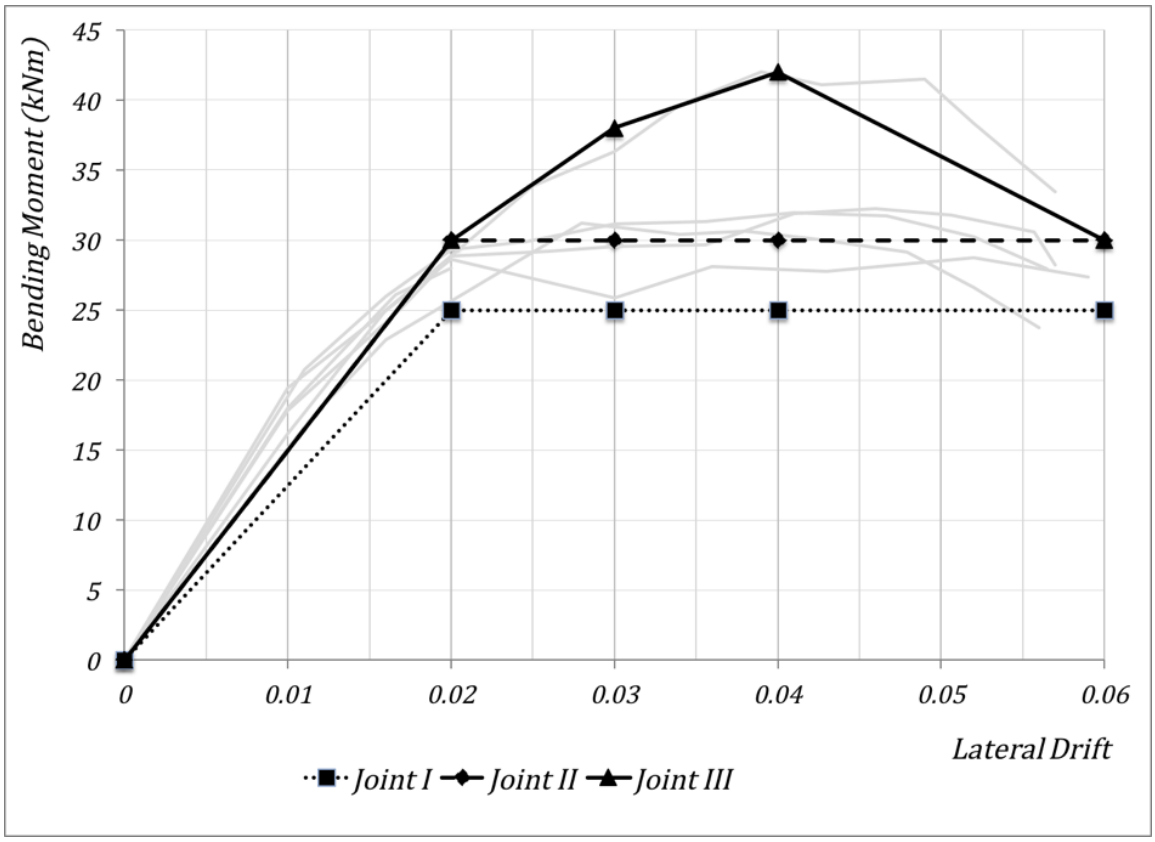

Figure 5.1: Frame Spring Behaviour

5.1 Model Description

Two dimensional frames with different combinations of springs, number of floors, and loading types and levels, were analysed to check the sensitivity of the frame response. Three types of analyses were considered: nonlinear static pushover, nonlinear static cyclic loading by applying specified cyclic displacements, and nonlinear dynamic time history analyses.

5.1.1 Modelling of Columns

The internal flexible columns have been modelled by displacement-based nonlinear beam-column elements, with co-rotational geometric transformation and five GaussLobatto integration points along the element length. Concrete has been modelled by a uniaxial

constitutive model with tension softening (Concrete02 material, available in OpenSees), shown in Fig. 4.11. Concrete properties for the fibres confined by stirrups have been computed using the modified Kent-Park procedure [30]. Reinforcing steel has been modelled by the GiuffreMenegottoPinto model (Steel02 model, available in OpenSees), as shown in Fig. 4.12. A fibre model has been used for the cross section [55], considering three types of fibres: confined concrete, unconfined concrete, and steel, as shown in Fig. 4.13.

5.1.2 Modelling of Slab-Beams

Slab-beams have been divided into three segments. The two end segments have been modelled as very stiff, with an artificially high modulus of elasticity, and the central segment has been modelled as a linear elastic beam element. The dimensions of the slab-beam have been determined based on the effective slab width theory. The rigid segments are used because that portion of the slab has already been included in the response of the slab-column joints, represented by the rotational spring in Fig. 5.2. The column does not need such adjustments, since the column of the tested specimen was over-dimensioned and over-reinforced, resulting in negligible deformations.

5.1.3 Modelling of Joint Springs

Two rotational springs have been used on each beam-column node, one on each side of the column (Fig. 5.2). The tested moment-rotation response has been used for the springs behaviour for the three-storey frame (Section 5.3), split into the two springs in series. For the five-storey frame (Section 5.4) the response has been adjusted for the slab thickness and amount of reinforcement designed for the frame analysed. This adjustment has been done by analysing the curvature of the slab and scaling the tested response accordingly. Only the slab curvature has been considered since the deformation of the over-reinforced column has been negligible in the tested specimens.

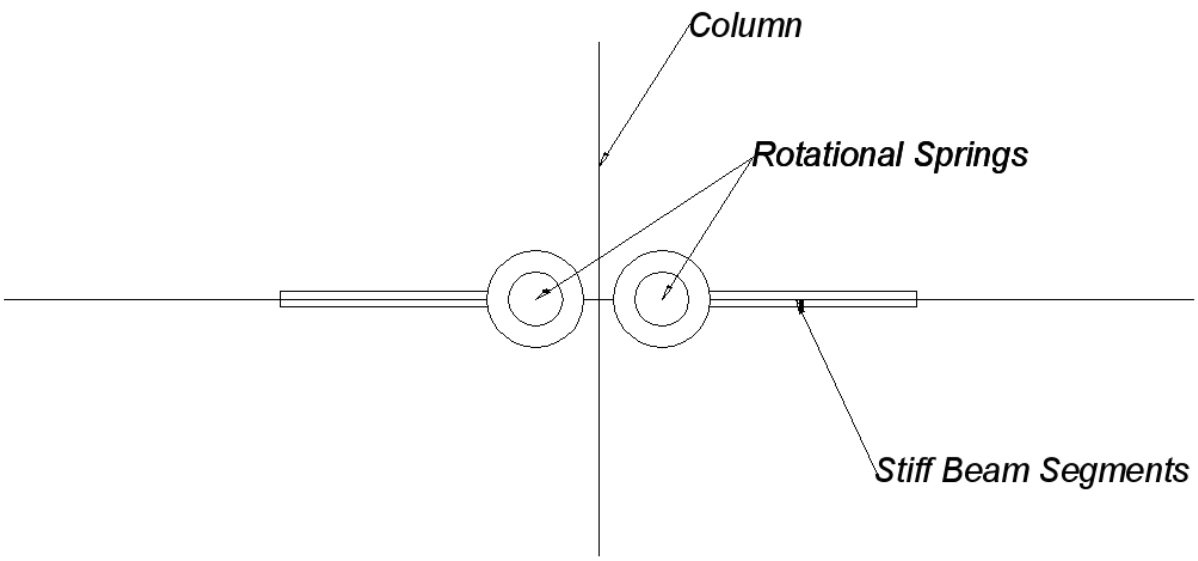

Figure 5.2: Rotational Springs on Each Side of the Column

This combination of two springs, instead of the super-element used for the joint model in Chapter 4 (Fig. 4.10) was considered because the frame would otherwise be relatively insensitive to the Interface Shear Spring Response. The flexural stiffness of the slabs at the frame joints would be mostly dictated by the bar-slip springs. This was not the case in the joint model where the couple of ISS springs introduces a resisting bending moment, which is more effective due to the boundary conditions related to the fixity of the slab-beams ends. One solution to this would be the modification of the bar-slip response as a function of the ISS response, but this would make the analysis of such frames computationally expensive. These two different approaches enable the analysis of joints at a more detailed level, while allowing for the analysis of frames as assemblage of these joints, by introducing the response of the individual joint to the behaviour of the frame joints.

5.1.4 Output Data

The following output is monitored during the analyses to check their sensitivity on the input springs response:

- Base shear force on each of the vertical elements.
- Stress-strain response of the column fibres (steel and concrete).
- Moment-rotation response of the springs.
- Nodal displacements, rotations, velocities, accelerations, etc.

5.2 Frame Model Validation

The computer model is a TCL code in a parametric form to enable the analysis of frames with an arbitrary number of stories, bays, element dimensions, etc. To validate this model, the flat plate frame tested by Fick [18] was analyzed and the model results were compared to the test results. The analyzed structure is a three-storey ($3 \times 10ft$), two-bay ($2 \times 20ft$) flat plate frame, with $18in$ square columns and a $7in$ thick slab, as shown in Fig. 2.9. More details can be found in [18].

The analytical and tested response in Fig. 5.3 show a good agreement with regard to the total base shear of the frame ($155kips$ ($690kN$) vs. $154kips$ ($685kN$), respectively, for a max. displacement of $10.8in$ ($280mm$)). The total base shear is the main parameter investigated in the following frame analyses, making this model of acceptable performance.

5.3 Analyses of the Prototype Three-Storey Frame

5.3.1 Pushover and Cyclic Displacement Analyses

The frame shown in Fig. 5.4 represents the prototype three-storey frame, from which the lab specimens were based [6].

First a nonlinear pushover analysis was conducted. The frame was subjected to a vertical load on each node and then to an increasing horizontal load, applied on each of the floors, on the side column, up to failure. The three joint responses (Fig. 5.1) were

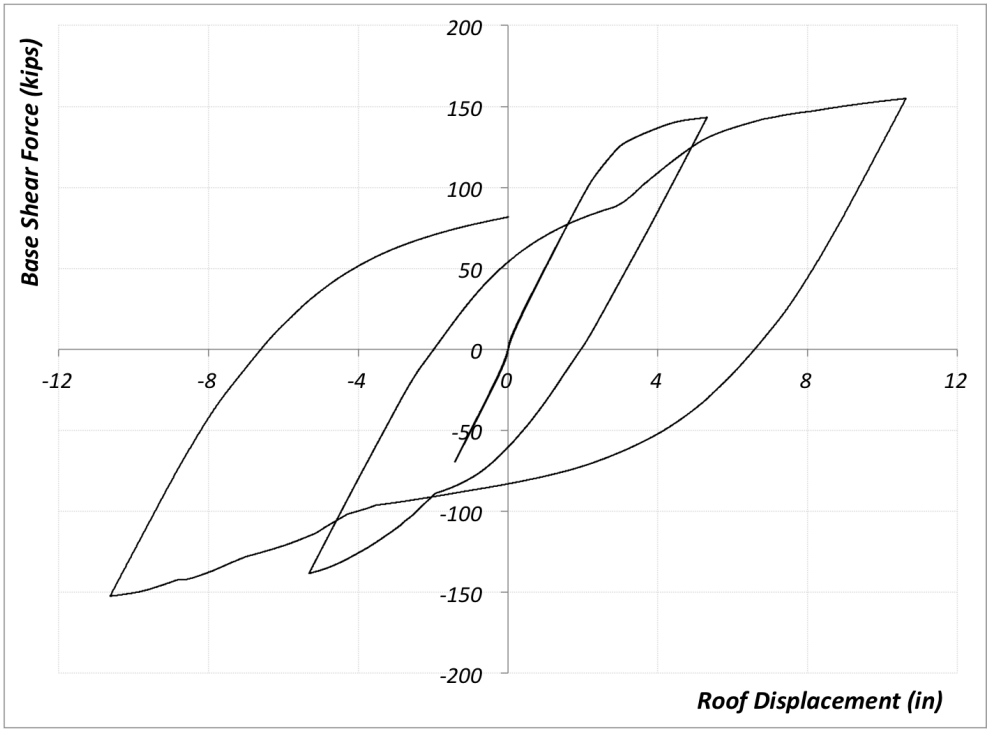

(a) Analytical Results

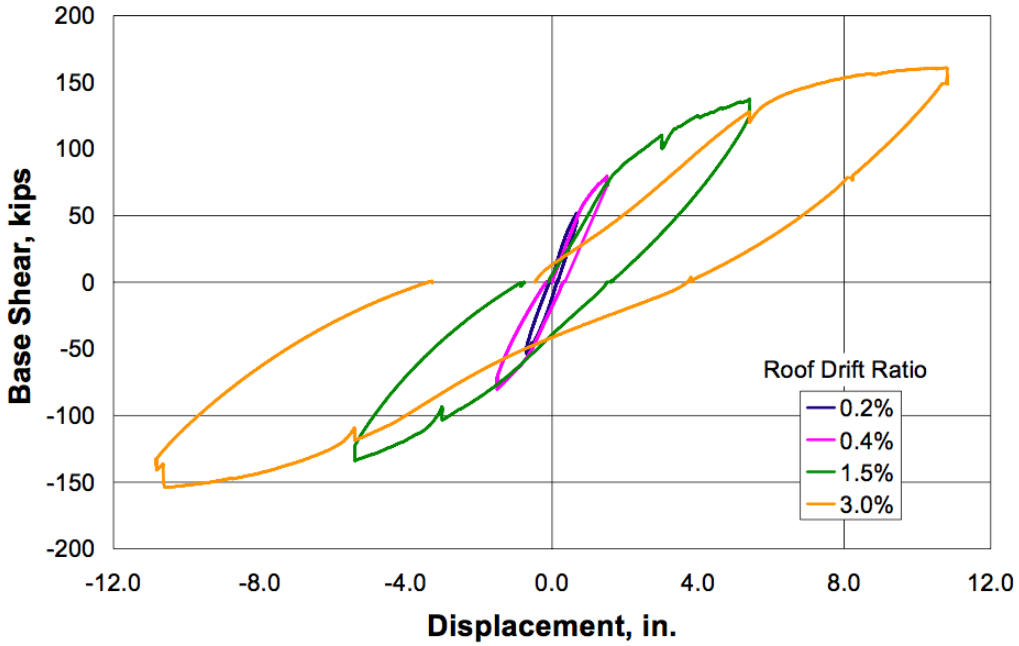

(b) Test Results [18]

Figure 5.3: Base Shear vs. Roof Displacement for the frame by Fick ([18])

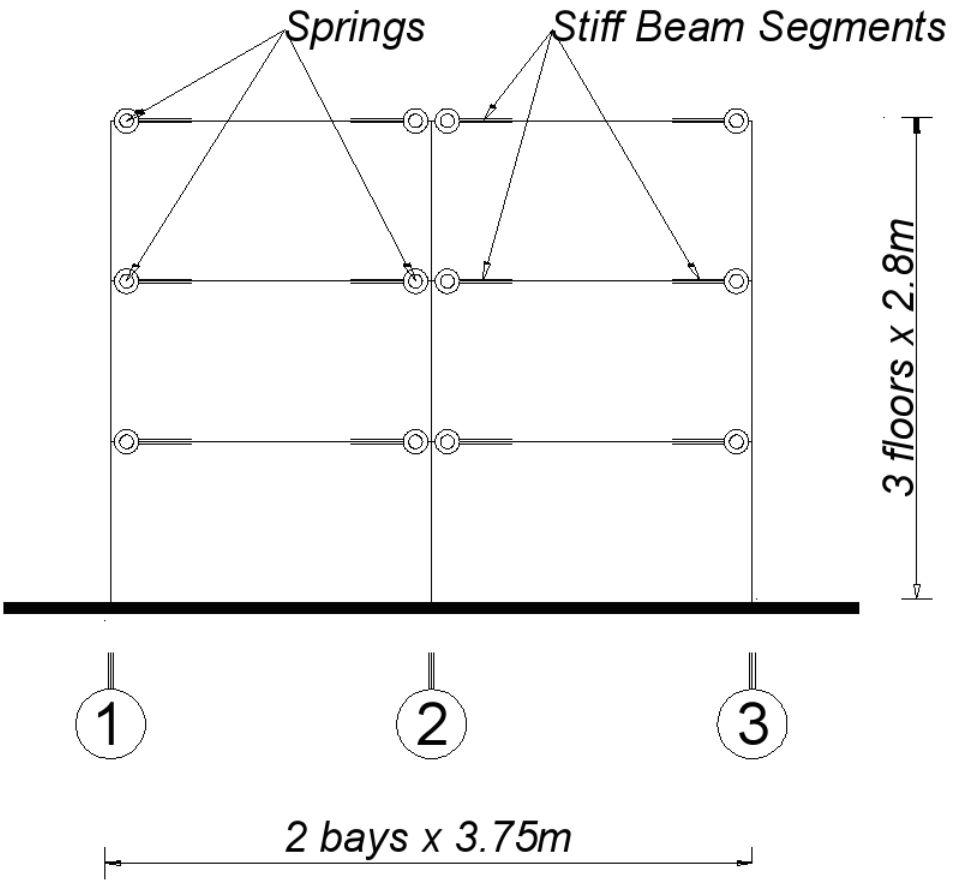

Figure 5.4: Prototype Frame

alternatively used for comparison, and the total base shear was recorded, to check the effect of the joint behaviour. The results of this analysis are shown in Fig. 5.5. From these analyses, as expected, it may be observed that for the frame with flexible springs, the base shear force is lower, with a peak load of 80% of the stiffer frame.

Following the push-over analyses, the same three-storey frame was subjected to a gravity load at each node and then to a specified cyclic displacement at a top node, following the same path used for the tested specimens (Fig. 3.6). The lateral force-drift responses are shown in Fig. 5.6. Similarly to the pushover analyses, it may be observed that for the frame with flexible joints, the base shear force is lower, with a peak of 77% of the stiffer frame.

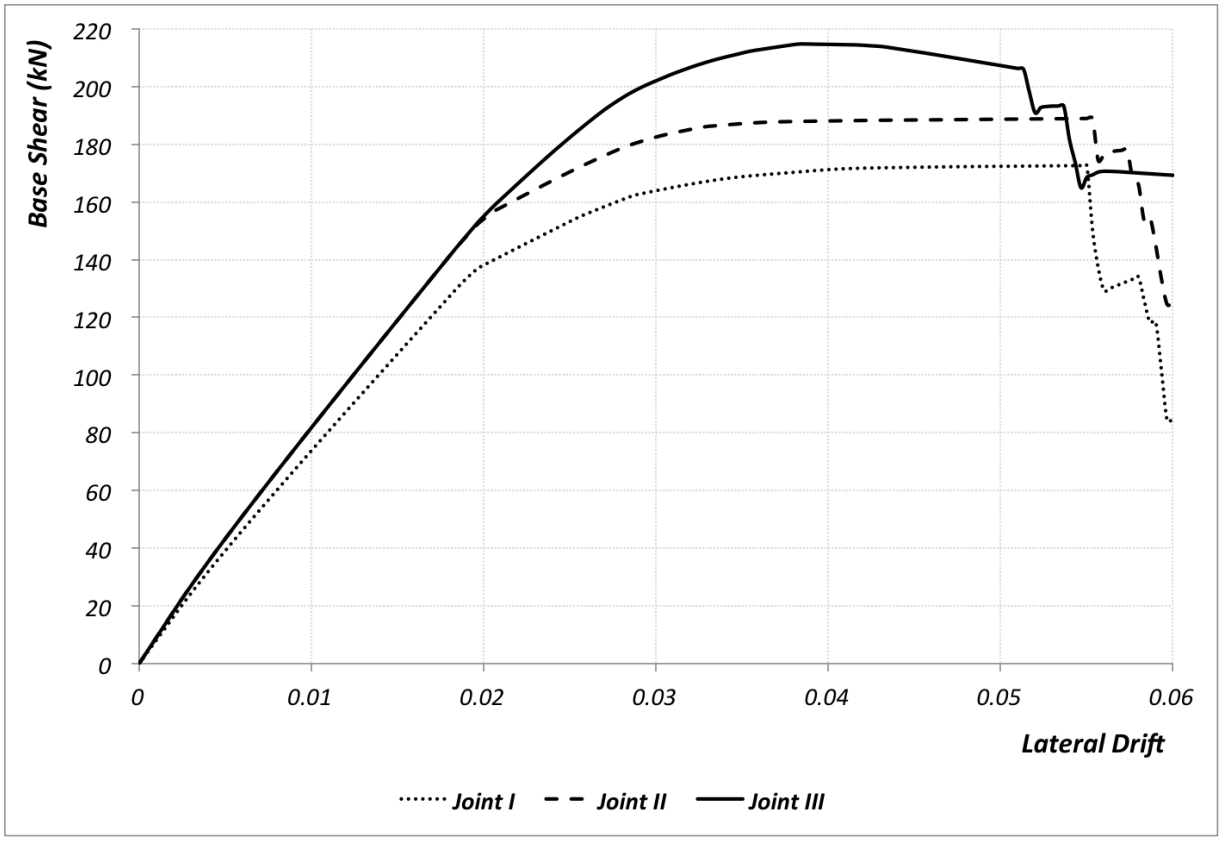

Figure 5.5: Pushover Analysis: Force-Displacement Behaviour

5.3.2 Time History Analyses

The 3-storey structure was subjected to ground acceleration, using the El-Centro 1968 record (Fig. 5.7). Rayleigh damping proportional to the initial stiffness matrix was considered, except for the springs for which damping was set to *zero* due to their negative stiffness at large deformations. The recorded base shear force is shown in Fig. 5.8 for two types of spring responses (joints I and III). From this graph it may be observed that the peak base shear for the frame with stiff joints is 15% higher than in the case with flexible joints. For the initial cycles, no difference is observed, since the behaviour of the springs is the same up to 2% lateral drift. It is beyond the drift of 2% that the structure behaves better in the case of flexible joints due to the *'yielding'* of the slab-column connections. For the same reason, the difference in base shear becomes higher as the peak load becomes higher, making this a more efficient seismically responsive structure when subjected to

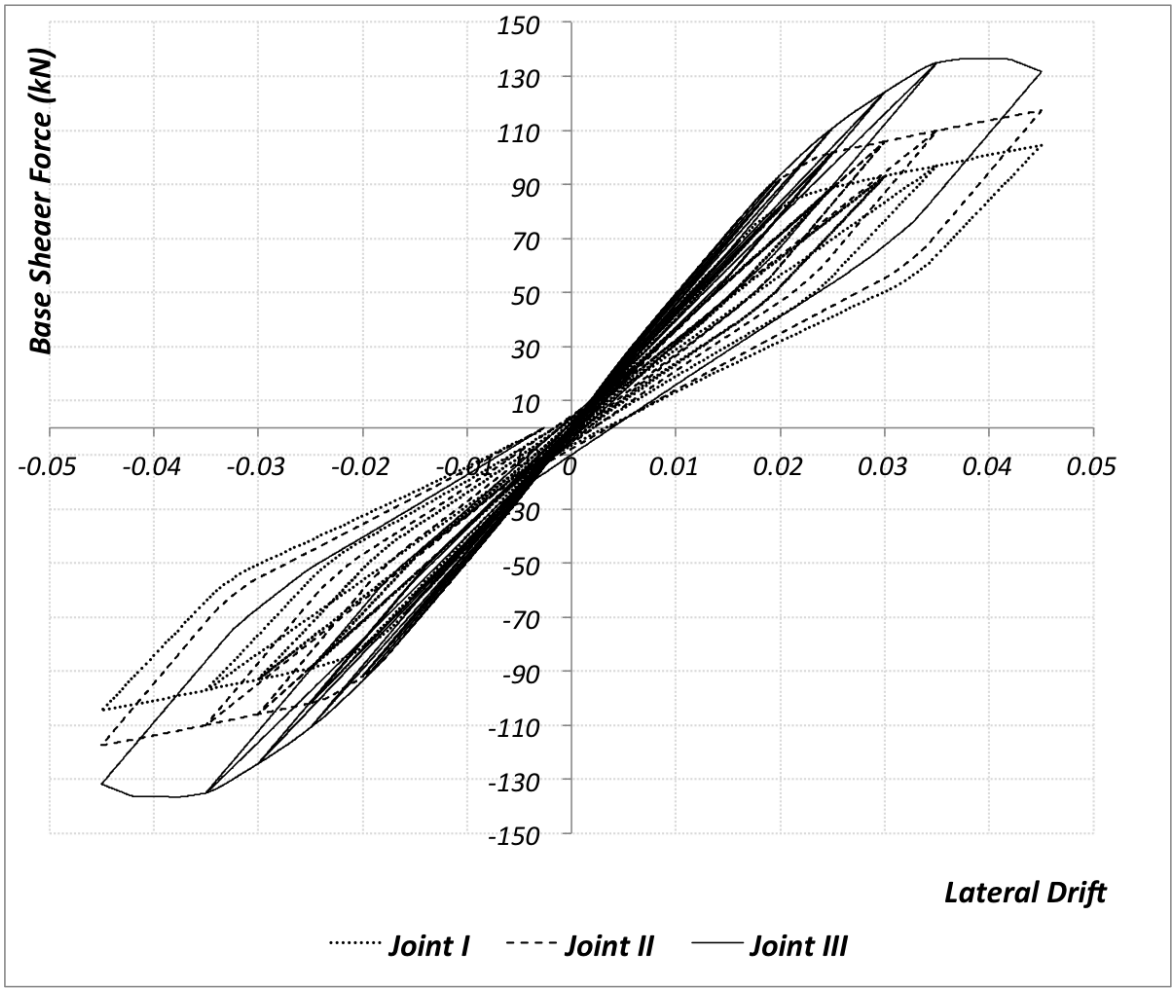

Figure 5.6: Cyclic Displacements Applied at the Top Node

an earthquake. A difference of 15% on the peak base shear is not very representative for the quantification of the joint effect since it would depend on the ground acceleration considered for the analysis. For a more comprehensive analysis, Incremental Dynamic Analyses were considered, as described in the following paragraph.

Incremental Dynamic Analyses (IDA)

For a more comprehensive analysis, Incremental Dynamic Analyses were performed, in order to consider various earthquake records. In performance-based earthquake engineering (PBEE) the estimation of the Mean Annual Frequency (MAF) of exceeding a specified structural demand or a certain limit-state capacity is of great interest. IDA has

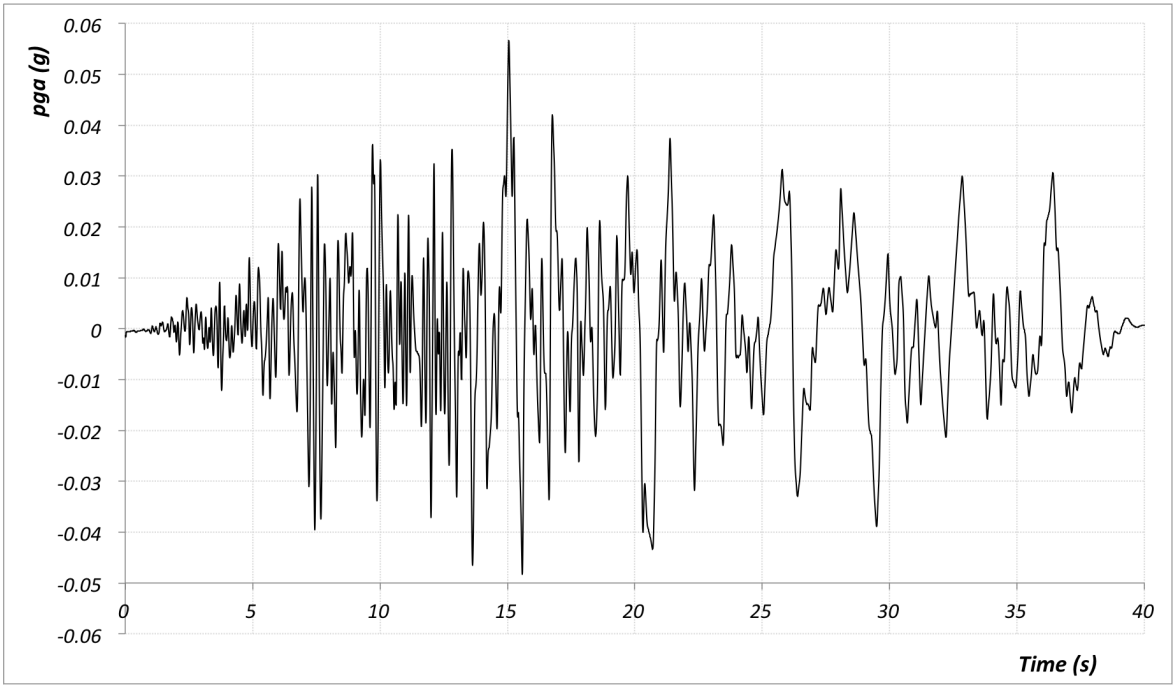

Figure 5.7: El Centro Earthquake, 1968

been used as an efficient method to accomplish this task. A set of 20 ground motion records, listed in Table 5.1, were considered.

Twelve analyses have been performed per each record, scaling the ground motion with respect to the Peak Ground Acceleration (pga), stepping from 0.1 to 1.2g. This resulted in $12 \times 20 \times 3 = 720$ analyses for all three joints considered, taking about 2,500 CPU-hours for each run. IDA curves were then generated, by interpolating these twelve points, for each record. Curves showing the total base shear vs. the peak ground acceleration (pga) are shown in Fig. 5.9, for each of the 20 records.

Limit states on IDA curves need to be defined to proceed with performance calculations. There are several alternatives for defining limit states; two limit states have been considered here:

- *Immediate Occupancy*, defined by the initiation of yielding of the column longitudinal reinforcement. Based on a pushover calculation, the column reinforcement yields at a total base shear force of 150 kN.

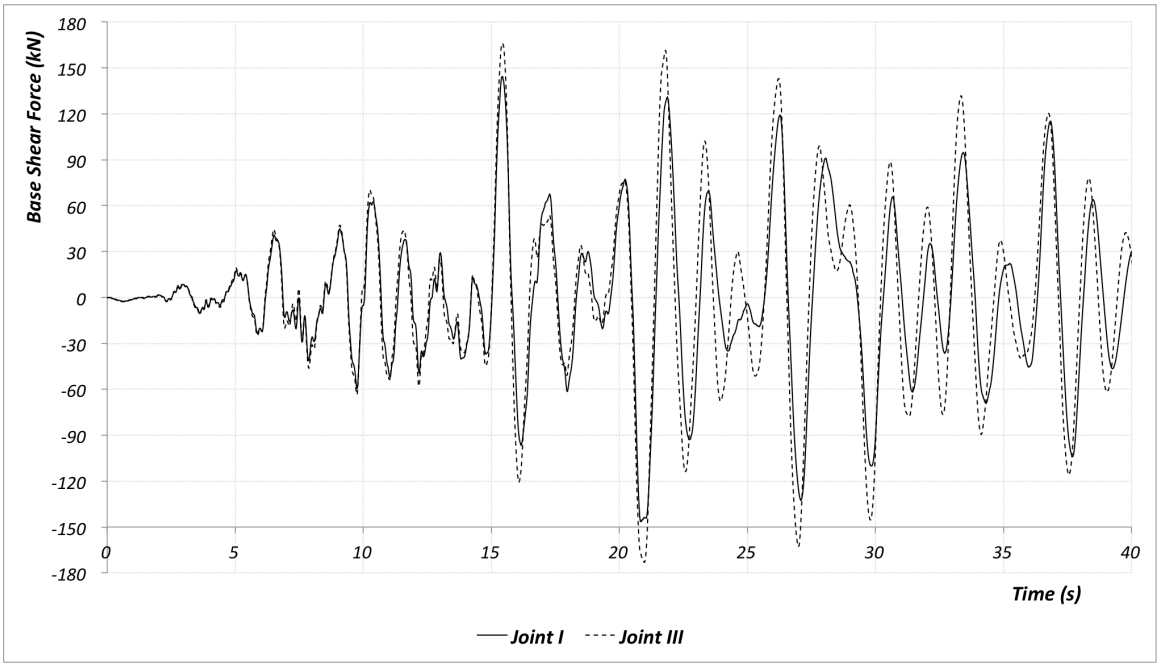

Figure 5.8: Time History (3-storey): Base Shear Force (17% difference on Peak Load)

- *Collapse Prevention*, defined by a total base shear force of between 200 kN and 250 kN, which may be considered as *'yielding'* of the structure, considering Fig. 5.9.

By summarizing the IDA Curves, generating 16%, 50% and 84% fractile IDA curves (corresponding to the *mean-one standard deviation*, *mean*, and *mean+one standard deviation*, respectively, for each of the cases (flexible and stiff joints)), as shown in Fig. 5.10, we may observe the advantages of using flexible joints. Total base shear is considerably lower in the case of frames with flexible joints.

In PBEE, MAF of exceedance for the limit states is an important parameter for the performance evaluation of each structure. The method proposed by the Pacific Earthquake Engineering Research Center has been considered in this research. These calculations involve the MAF of exceeding a given pga, which are available from conventional PSHA Curves. A structure located in Los Angeles, CA, has been considered, and the respective Hazard Curve is shown in Fig. 5.11. MAF is calculated based on Equation 5.1:

Table 5.1: The suite of twenty ground motion records used

No.	Event	Station	ϕ^o	M	$R_{rup}(km)$	$PGA(g)$
1.	Northridge, 1994	LA, Baldwin Hills	090	6.69	29.9	0.239
2.	Imperial Valley, 1979	Compuertas	285	6.53	15.3	0.147
3.	Imperial Valley, 1979	Plaster City	135	6.53	30.3	0.058
4.	Loma Prieta, 1989	Hollister Diff. Array	255	6.93	24.8	0.279
5.	San Fernando, 1971	LA, Hollywood Stor. FF	180	6.61	22.8	0.195
6.	Loma Prieta, 1989	Coyote Lake Dam Dow.	285	6.93	20.8	0.179
7.	Imperial Valley, 1979	Calipatria Fire Station	225	6.53	24.6	0.129
8.	Northridge, 1994	LA, Hollywood Stor. FF	360	6.69	24.0	0.358
9.	Loma Prieta, 1989	Anderson Dam Downst.	340	6.93	20.3	0.239
10.	Loma Prieta, 1989	Hollister South & Pine	000	6.93	27.9	0.370
11.	Loma Prieta, 1989	Sunnyvale Colton Ave	360	6.93	24.2	0.207
12.	Superstition Hills, 1987	Wildlife Liquefaction Arr.	090	6.54	23.9	0.179
13.	Imperial Valley, 1979	Chihuahua	282	6.53	7.29	0.254
14.	Imperial Valley, 1979	El Centro Array #13	230	6.53	22.0	0.139
15.	Imperial Valley, 1979	Westmoreland FS	180	6.53	15.3	0.111
16.	Loma Prieta, 1989	Halls Valley	090	6.93	30.5	0.115
17.	Superstition Hills, 1987	Wildlife Liquefaction Arr.	360	6.54	23.9	0.208
18.	Imperial Valley, 1979	Compuertas	015	6.53	15.3	0.187
19.	Imperial Valley, 1979	Plaster City	045	6.53	30.3	0.043
20.	San Fernando, 1971	LA, Hollywood	090	6.61	22.8	0.225

$$\lambda_{LS} = \int_{x=0}^{x=+\infty} F_{IM}(x) |\frac{d\lambda_{IM}(x)}{dx}| dx \tag{5.1}$$

where $|\frac{d\lambda_{IM}(x)}{dx}|$ is the PGA gradient and $F_{IM}(x)$ is the Cumulative Distribution Function of the PGA-value of limit-state capacity. By inverting the calculated λ_{LS} we can get the return period of limit-state exceedance. The results of these calculations are shown in Table 5.2.

From these results it may be observed that the Mean Annual Frequency of exceeding any of the limit states is higher for the stiffer joints. In addition, the higher the limit state, the higher this effect is, making the flexible joints more advantageous for higher

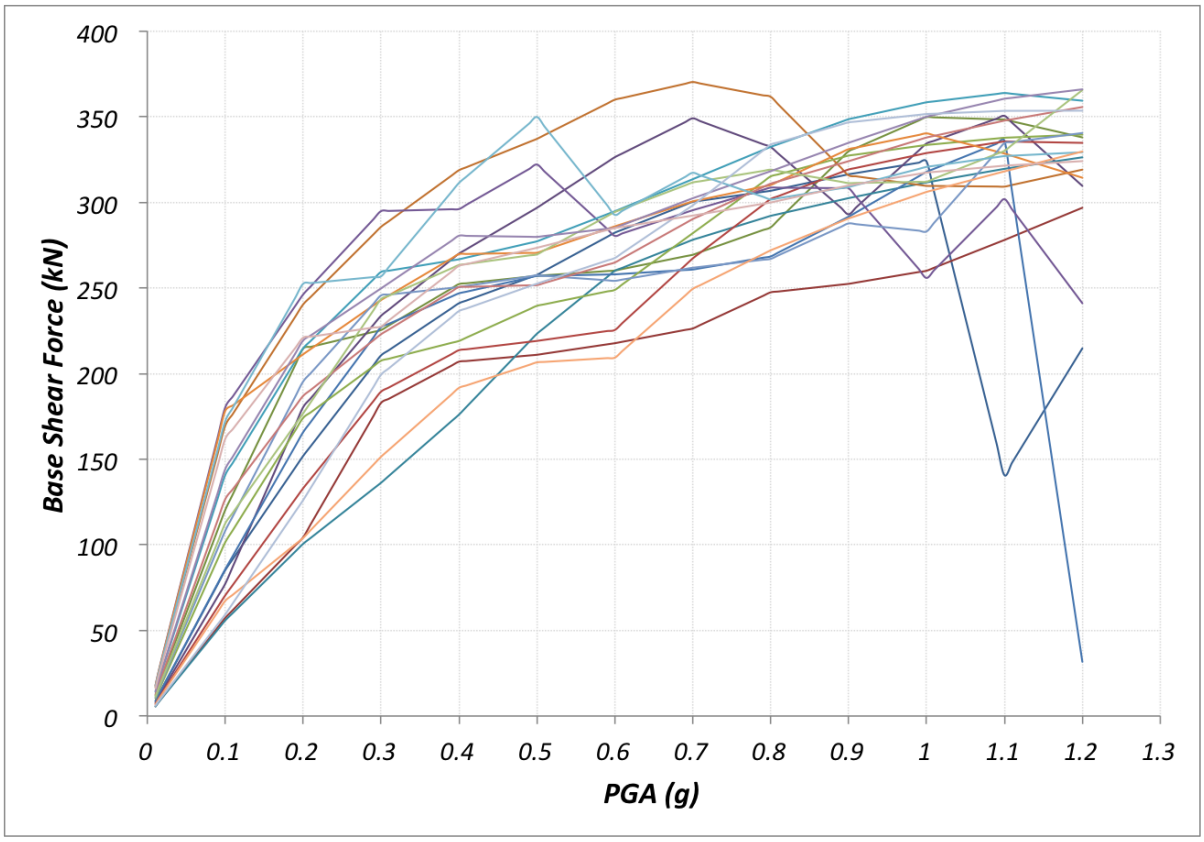

Figure 5.9: IDA Curves

seismic forces.

5.4 Analyses of a Five-Storey Frame

A more complex structure consisting of 5 storey and 6 bays (Fig. 5.12) was analyzed to parametrically check the effect of the joints. The following assumptions were considered in this case:

- The columns have dimensions of 600 x 600mm.
- The slab has a thickness of 250mm, reinforced with 15M@200mm.
- The joint responses captured from the test have been scaled up by a coefficient of 4 ($M^{'} = 4M_0$ for the same rotation θ), considering that the current slab has

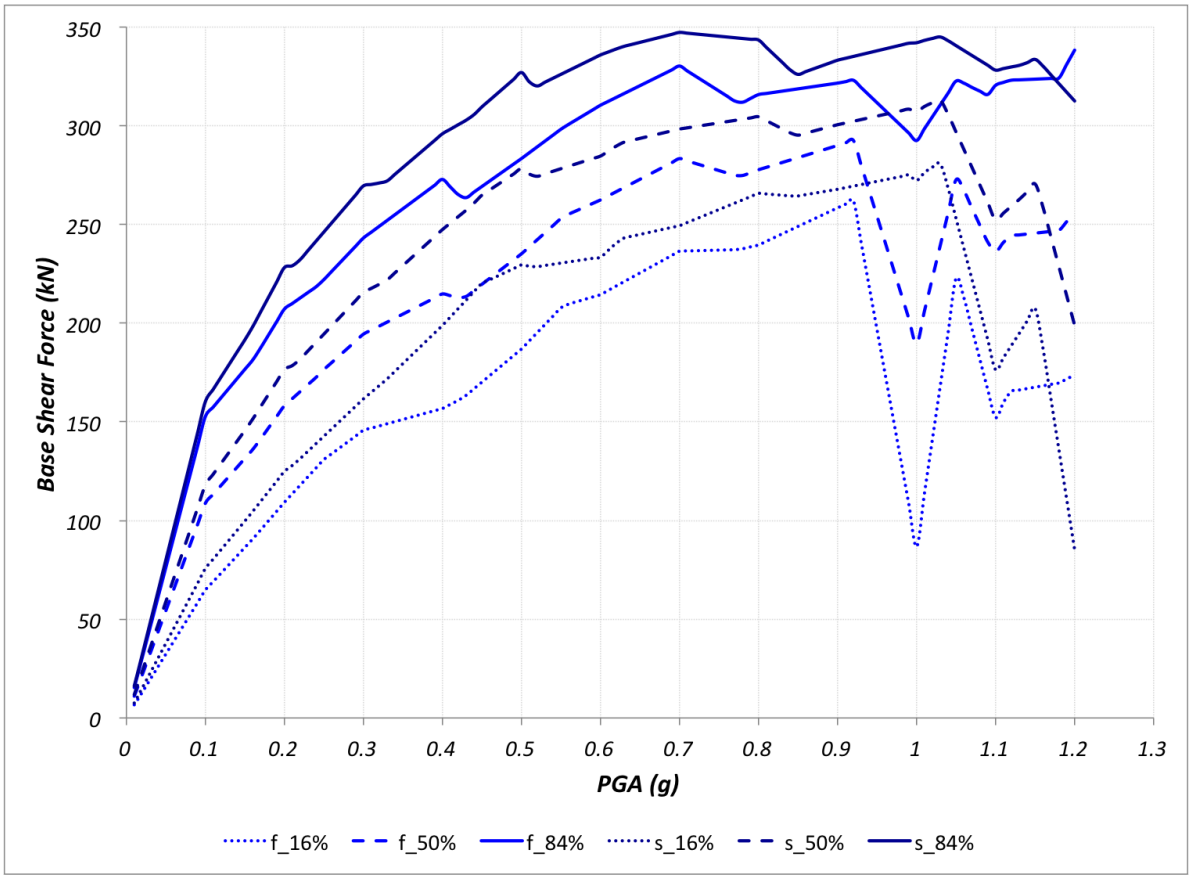

Figure 5.10: IDA fractiles (16%, 50%, 84%)

a thickness of $2t_0$ and flexural reinforcement of $2A_{s0}$, which would result in an increase of flexural strength of about 4 times.

- The recorded seismic ground acceleration has been scaled up to achieve a lateral drift of 3+%, to capture the effect of the different joints (by forcing their behaviour into the yielding plateau).

For each frame the following springs combination was considered (naming flexible springs as type F and stiffer/stronger springs as type S:

- F-type springs on each internal column.
- A combination of S-type springs with F-type springs on column #4 only.
- S-type springs on each internal column.

(a) Base Shear V=150 kN

	Joint I	Joint II	Joint III
MAF of exceedance	0.009082	0.011859	0.011950
return period (years)	110	84	83

(b) Base Shear V=200 kN

	Joint I	Joint II	Joint III
MAF of exceedance	0.003851	0.005095	0.005751
return period (years)	260	196	174

(c) Base Shear V=250 kN

	Joint I	Joint II	Joint III
MAF of exceedance	0.001152	0.001475	0.002108
return period (years)	868	678	474

Table 5.2: MAF of exceedance and return periods for the three types of springs for the 3-storey frame

These combinations of springs enable the evaluation of the change in total base shear, the distribution of base shear among stiff and flexible columns, and the distribution of base shear among the internal flexible columns when their springs vary in stiffness and strength.

The time history of the total base shear force is shown in Fig. 5.13. From this graph it may be observed that a slab-column joint reinforced with stiff shear bolts would result in an increase of 18% of the base shear force on the flexible columns due to the higher stiffness and strength of the joints.

The use of flexible joints on the central column only resulted in a decrease of the shear force on this column. The decrease is dependant on the floor location of the column; with the difference being higher on the upper floors as shown in Table 5.3. This also shows that the effect of the joint response on the distribution of forces is higher for lower buildings, since in higher frames the differences are neutralized; the more floor levels and structural elements, the higher the possibilities for redistribution of internal forces.

This effect on the distribution of forces among columns may be taken advantage of by designing flexible columns with flexible joints where architecturally required, while transferring the shear force to the adjacent structural elements.

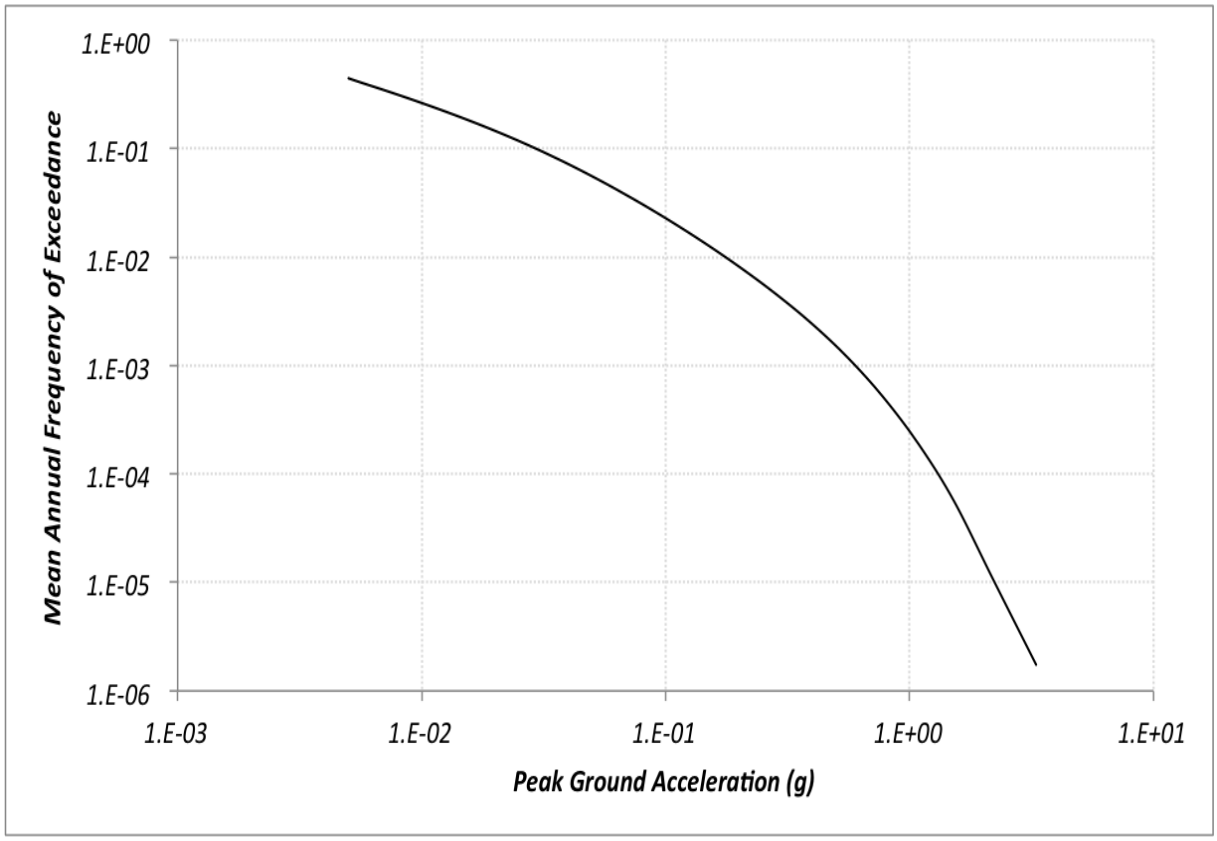

Figure 5.11: Hazard Curve, Los Angeles, CA

If the dimensions of the central column are changed from 600x600mm to 500x500mm (considering the lower forces on this column as a result of the flexible joint), it is observed the base shear force on the central column decreases to 75% of the adjacent column. The base shear on columns C4 and C3 changes from 234 kN and 224 kN respectively, to 236 kN and 178 kN.

Incremental Dynamic Analyses

IDA were also conducted on this frame and the respective results are shown in Table 5.4. Similar results on the structural performance are observed, as in the case of the three-storey frame: flexible joints result in a lower Mean Annual Frequency of exceedance of a certain limit state.

The analyses of frames show that flexible slab-column joints improve the seismic response of flat plate systems, introducing the desired effect through the right combination

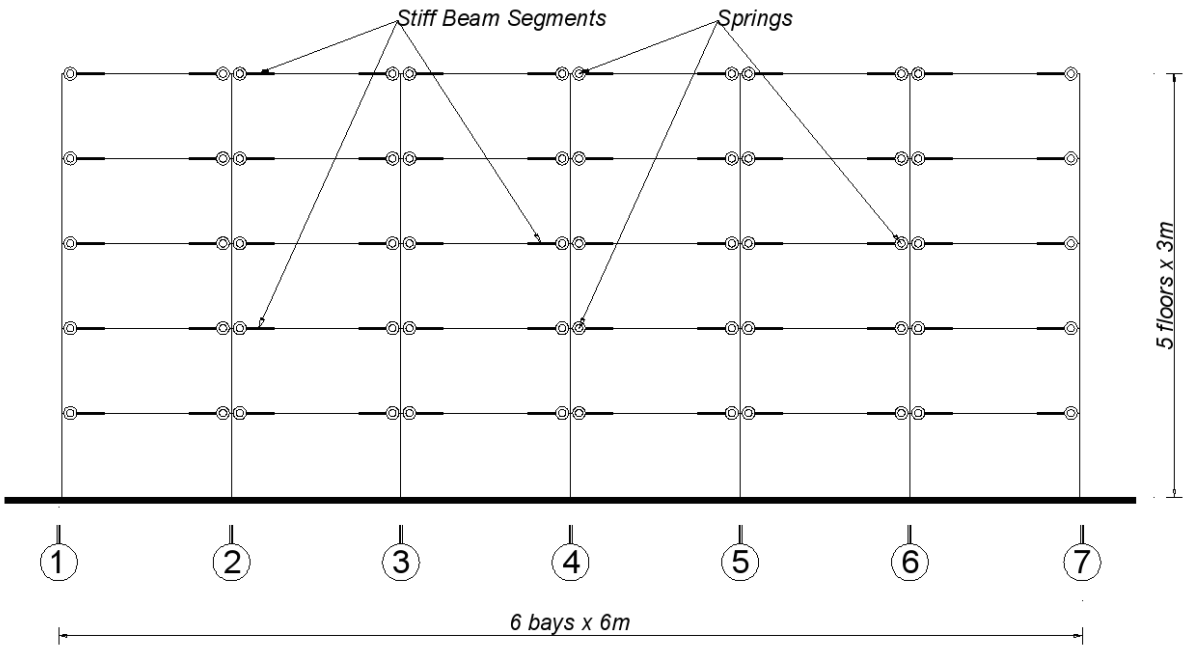

Figure 5.12: Five Storey Frame

Table 5.3: Shear Force Ratio $\frac{R_4}{R_3}$

Floor	Shear Force $R_3(kN)$	Shear Force $R_4(kN)$	Ratio $\frac{R_4}{R_3}$
V	22.6	17.2	0.76
IV	118	132	0.89
III	196	214	0.92
II	247	265	0.94
I	224	234	0.96

of such joints. Other analyses may be conducted similarly with this model to check other parameters, such as:

- Relative joint stiffness to the stiffness of lateral structural elements.
- Effect of the joint response relative to the global stiffness of the building.
- Distribution of forces as a function of various combination of joint responses, alternating along the height and width of the frame.
- Progressive collapse, by removing springs (joints) reaching a certain failure criterion.

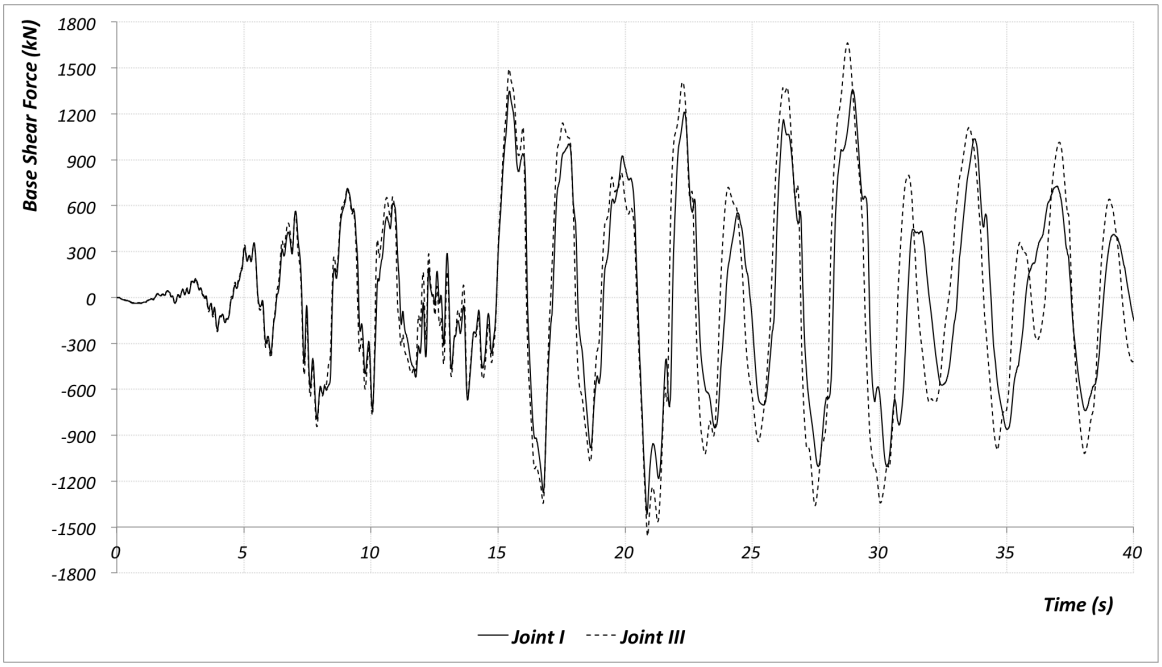

Figure 5.13: Time History (5-storey): Base Shear Force: (18% difference on Peak Load)

This however is beyond the purpose of this research and various available resources applicable to these topics may be considered.

(a) Base Shear V=1500 kN

	Joint I	Joint II	Joint III
MAF of exceedance	0.006874	0.007218	0.008028
return period (years)	145	139	125

(b) Base Shear V=2000 kN

	Joint I	Joint II	Joint III
MAF of exceedance	0.002715	0.002993	0.003915
return period (years)	368	334	255

(c) Base Shear V=2500 kN

	Joint I	Joint II	Joint III
MAF of exceedance	0.000849	0.000908	0.001914
return period (years)	1178	1101	522

Table 5.4: MAF of exceedance and return periods for the three types of springs for the 5-storey frame

Chapter 6

Discussions and Conclusions

This research investigates the performance of reinforced concrete flat-plate systems in seismic areas. A set of six full-scale slab-column connections, shear retrofitted with a new technique and subjected to vertical and lateral cyclic loading, were tested, to check the effect of such reinforcement on the joint strength and ductility. In addition, the effect of this type of shear reinforcement on the punching crack interface response, the lateral slab-column joint behaviour, and globally on flat plate systems was analytically investigated.

6.1 Conclusions from the Experimental Results

The experimental program showed that shear retrofitting existing reinforced concrete flat slabs with anchorage-controlled reinforcement may increase the ductility of slab-column connections without a commensurate increase in lateral strength. This results in a better response of flat-plate systems in seismic areas, as concluded by the analytical investigations.

The four specimens reinforced with a combination of steel bolts and flexible washers experienced strength similar to the unreinforced specimen and deformation capacity similar to the specimen retrofitted with steel bolts only, proving the efficiency of such shear retrofitting technique. All specimens had a similar stiffness up to a lateral drift of

1.5%, which would correspond with a normal response of the flat-plate system subjected to service loading. The response of the connections within this range of lateral drifts is independent of the shear retrofit technique because of the limited opening of cracks which would engage the shear reinforcement. Further increase of lateral deformations is then experienced at a lower lateral force for these four specimens, through a more ductile behaviour of the joint. A difference of 50% on the lateral peak load was observed between the joint reinforced with steel bolts only and the joints reinforced with a combination of steel bolts and flexible washers (Figs. 3.26 to 3.28).

The anchorage-controlled shear reinforcement allowed for larger, but limited opening of punching shear cracks, without hindering the deformability of the connection (the specimens could undergo same lateral drifts). The specimens with anchorage-controlled shear reinforcement allowed for larger opening of cracks than the specimen reinforced with steel bolts only, but did not lead to a sudden increase in crack opening, which was observed in the case of the unreinforced specimen at lateral drifts between 1.5% and 2%.

The achieved lower stiffness results in lower seismic forces attracted by the connection, allowing for a more appropriate distribution of seismic forces into the lateral force resisting elements of the structure (special moment resisting frames or shear walls). Compared to traditionally retrofitted slab-column joints, larger opening of cracks has also resulted in higher plastic deformations, which may be observed as reduced pinching in the joint load-deformation response.

The system presented was designed for the retrofit of existing slab-column connections. However, it can be anticipated that similar concepts can be used in the construction of new slabs in seismic zones.

6.2 Conclusions from the Analytical Results

In parallel with the experimental program, the effect of the flexural shear reinforcement was investigated analytically, from the punching crack interface response, to the lateral joint response, to the global response of flat-plate frames, consisting of assemblages of

these joints. If tested joint responses are available they may be incorporated into the analysis of the flat-plate system. Otherwise, the response obtained from the analysis of such joint may be used.

From the analytical results obtained it may be concluded that:

- Flexible washers introduce a larger, but controlled opening of punching cracks. The response of the crack interface regains a higher stiffness, following the deformation of the flexible washer and the engagement of the stiffer steel bolt, blocking any further significant strength degradation.

- Flexible washers enable the slab-column joint to undergo same lateral drifts at a lower strength, resulting in a connection with a lower stiffness, similar to the response of the tested specimens.

- Stiffer slab-column connections attract higher seismic forces on the respective columns, also increasing the total base shear force of a flat-plate structure as assemblage of such joints. This was shown through comprehensive Incremental Dynamic Analyses, where the exceedance of a certain base shear force had a Mean Annual Frequency higher in the case of the stiffer joints. The higher the limit base shear, the higher the effect of the anchorage-controlled reinforcement.

- Through a combination of different slab-column joints, using different shear reinforcement techniques at each joint, the desired distribution of forces may be achieved. Lateral forces may be transferred from flexible columns to lateral special moment resisting frames or shear walls. This may be concluded from all three types of analyses considered: static pushover, static cyclic displacements, and dynamic nonlinear time history.

- The effect of the flexible washers is higher for larger lateral column drifts, in which case the joints experience the yielding plateau (with a lower stiffness), making this new shear reinforcement technique more advantageous in case of higher seismic forces. This may be concluded from Table 5.2, where for the base shear of 150 kN,

the Mean Annual Frequancy varies from 0.0091 to 0.0120 (13%), while for a higher base shear of 250 kN, the Mean Annual Frequency varies from 0.0012 to 0.0021 (75%). Similar results may be observed from Table 5.4 for the five-storey frame analyses.

The macro-scale nature of these models enables the analysis of slab-column joints and flat plate systems, which would otherwise be computationally expensive if 3D finite elements were to be used. However, this comes at a cost to accuracy, due to the various assumptions accepted in the modelling process. The models are not intended to accurately predict the behaviour of slab-column joints, but may be used successfully for parametric analyses, especially if test results of a similar slab-column specimen are available.

The combination of the experimental and analytical components of this research showed how to achieve the desired characteristics of a flat plate structure subjected to an earthquake - sufficient strength and stiffness to withstand moderate-intensity shaking, and sufficient ductility to act in parallel with a more rigid structural system for strong base motions. Such design of slab-column connections is in agreement with the philosophy of "capacity design", where the designer "tells the structure what it should do in the event of a major earthquake".

6.3 Recommendations For Future Research

The experimental program presented involved a constant direction of loading, which is not the case when a flat-plate structure is subjected to earthquake forces. To better understand the influence of anchorage-controlled reinforcement on the response of shear retrofitted flat slabs, loading should be applied in more than one direction, and possibly changing in time.

Further research is recommended to determine better washer materials, especially with regard to creep and fatigue, properties that are expected to considerably affect the opening of cracks in the long term. The use of washers made of materials that would

significantly creep under sustained stress during serviceability loading would result in larger than expected opening of cracks. Similarly, depending on the washers material, fatigue might result in significant loss of stiffness and strength, affecting the punching crack opening.

The analytical model presented in this research was two-dimensional. To better capture the behaviour of flat plate systems, a 3D model is recommended, especially considering that a slab-beam element does not properly capture the behaviour of a 2D plate.

Improved modelling of the stiffness and strength degradation of the Interface Shear Spring response is also recommended, incorporating the potential degradation of washers strength and stiffness, depending on the material used.

APPENDICES

Appendix A

The Aggregate Interlock Model by Walraven

The Walraven Model [62] is used for modelling the behaviour of the interface-shear spring. It models the shear stress-strain behaviour along the crack faces, using an aggregate interlock model as shown in Fig. 4.1. The following simplifications are made:

- particles are considered as spheres.
- a slice of the volume, with a finite width of Δx, has been considered in order to enable a two-dimensional analysis.
- the cement matrix is considered to be perfectly brittle, with a crushing strength σ_{pu}.

During a shear displacement, particles will penetrate into the matrix. This will cause crushing of the matrix and friction between the matrix and the particles. For the contact area the friction stress can be expressed as $\tau = \mu\sigma_{pu}$, where μ is the coefficient of friction. The equilibrium forces at the contact area can be expressed as following:

$$F_x = \sigma_{pu}(a_y + \mu a_x) \tag{A.1a}$$

$$F_y = \sigma_{pu}(a_x + \mu a_y) \tag{A.1b}$$

where σ_{pu} and μ are material constants and a_x and a_y are the projected contact areas, shown in Fig. 4.1.

The particles crossing the crack are of variable size and embedment depths. To calculate the contact areas for all the particles crossed by the crack the circle diameters are subdivided into 10 classes. The limits of these classes are defined by $i\frac{D_{max}}{10}$, where $i = 1...10$ and D_{max} is the maximum particle diameter. Hence, the average diameter in a class is:

$$D_i = (\frac{i}{10} - 0.05)D_{max} \tag{A.2}$$

The grading curve of the concrete mixture is assumed to be represented by a Fuller curve [20]:

$$p = 100\sqrt{\frac{D}{D_{max}}} \tag{A.3}$$

where p is the percentage by weight passing a sieve aperture with a diameter D.

It has been shown by Walraven that the probability density function for the probability that an arbitrary point in the intersection plane lies in a circle with a diameter D_i is:

$$P_c(D_i) = p_k 0.532 D_i^{-0.5} D_{max}^{-0.5} - 0.213 D_i^3 D_{max}^{-4} - 0.075 D_i^5 D_{max}^{-6} - 0.036 D_i^7 D_{max}^{-8} - 0.025 D_i^9 D_{max}^{-10} \tag{A.4}$$

where p_k is the probability that the point lies in a particle and not in the matrix. The most probable number of circles in the interval between $D_i - 0.05D_{max}$ and $D_i + 0.05D_{max}$ intersected over a length l=1 is:

$$n(D_i) = \frac{p_c(D_i)0.1D_{max}}{\frac{1}{4}\pi D_i} \tag{A.5}$$

Embedment depths t have also been subdivided in 10 classes. $t = 0.1j(D_i/2)$ where j=1...10. It is assumed that these values can occur with the same probability.

This subdivision enables the calculation of the total contact area for all particles, Σa_x and Σa_y, for a given crack size and shear displacement.

Fig. 4.1 shows the case of of a particle with diameter D_i and embedment depth of

$t = 0.1j(\frac{D_i}{2})$ in the cement matrix. The springs represent the reinforcement crossing the crack per unit area. w_0 represents the initial crack opening. The size of the assumed initial crack is an issue which will need to be researched in detail, considering its variability along the slab height as well. In the Walraven model it has been assumed as constant along the height and the crack goes vertically, perpendicular to the beam axis.
An opening of the crack size generates tensile forces in the springs that are equivalent to a compressive stress σ per unit area of the crack plane. σ is calculated from the restraining stiffness of the the spring, which is given as an input parameter depending on the reinforcement properties crossing the crack.

Subsequently, crack faces are subjected to an incremental shear displacement $\Delta\delta$, the crack width $w_0 + \Delta w$ remaining constant. For each shear displacement, the total contact area is calculated numerically, considering all diameters and embedment depths. This calculation is done starting by considering the first aggregate diameter class, D_i. For this diameter, 10 embedment depths $t = 0.1j(\frac{D_i}{2})$ are considered, assumed to occur with the same probability. For the actual displacement status $(w, \delta) = (w_0 + \Delta w, \Delta\delta)$, the contact areas a_x and a_y are calculated geometrically for i=1 and j=1...10. The average contact area for D_i is calculated as:

$$\bar{a}_x(i) = \sum_{j=1}^{10} \frac{a_x(i,j)}{10} \tag{A.6a}$$

$$\bar{a}_y(i) = \sum_{j=1}^{10} \frac{a_y(i,j)}{10} \tag{A.6b}$$

Subsequently the sum of the projected contact areas for all particles is calculated by:

$$\Sigma a_x = \sum_{1=1}^{10} n(i)\bar{a}_x(i) \tag{A.7a}$$

$$\Sigma a_y = \sum_{1=1}^{10} n(i)\bar{a}_y(i) \tag{A.7b}$$

where $n(i)$ is calculated by equation A.5. The internal stresses in the crack area, ac-

cording to A.1 are:

$$\tau(w,\delta) = \tau(w_0 + \Delta w, \Delta\delta) = \sigma_{pu}(\Sigma a_y + \mu\Sigma a_x) \tag{A.8a}$$

$$\sigma(w,\delta) = \sigma(w_0 + \Delta w, \Delta\delta) = \sigma_{pu}(\Sigma a_x + \mu\Sigma a_y) \tag{A.8b}$$

The internal stress σ calculated by A.8 is compared to the external stress applied by the springs for the crack width $(w_0 + \Delta w)$. If the internal stress is smaller than the external stress, the shear displacement δ is not large enough to be in equilibrium. This means that a further shear displacement increment $\Delta\delta$ is necessary and the calculation has to be repeated for the new displacement status $(w_0 + \Delta w, 2\Delta\delta)$. This calculation is repeated until the internal stress is equal to the external stress provided by the springs. This represents an equilibrium point $(\sigma, \tau, w, \delta) = (\sigma, \tau, w_0 + \Delta w, m_1\Delta\delta)$.
A further shear displacement increment would lead to an internal stress larger than the external stress. This stress would further open the crack, extending the springs and consequently loosing the equilibrium. In order to reach another equilibrium point $(\sigma, \tau, w_0 + 2\Delta w, m_2\Delta\delta)$, further shear displacement increments must be applied. Proceeding this way, the whole ascending branch of the $\tau - \delta$ relation is obtained. After the shear stress τ has reached the maximum given shear stress of the loading cycle, unloading will occur. However, no immediate movement of the crack faces will occur because of the friction in the contact areas. A movement in backward direction will occur only when the maximum friction is exceeded. At the moment the backward sliding begins, internal stresses are given by:

$$\tau = \sigma_{pu}(\Sigma a_y - \mu\Sigma a_x) \tag{A.9a}$$

$$\sigma = \sigma_{pu}(\Sigma a_x + \mu\Sigma a_y) \tag{A.9b}$$

The value of δ for which no more contact between the crack faces exists, can be found geometrically. The same procedure is repeated for loading on the opposite direction, which will be symmetric to the $\tau - \delta$ relation previously obtained. The calculation proceeds then with the next loading cycle, which is exactly the same as the first cycle. The only difference is that the crack faces are now damaged and the two parts have to

move further to get in touch. During each cycle, the crack faces are further damaged and the damaged faces are stored in the memory for each cycle.

Appendix B

Degradation of Pinching4 Material

Pinching4 (Fig. 4.15) is a hysteretic material model available in OpenSEES. It is first introduced in Section 3.2.2, and further details related to the degradation model are introduced in this appendix.

Unloading stiffness degradation:

$$k_i = k_0 \cdot (1 - \delta k_i) \tag{B.1}$$

where k_i is the unloading stiffness at time t_i; k_0 is the initial unloading stiffness (for the case of no damage), and δk_i is the value of the stiffness damage index at time t_i.

Reloading stiffness degradation:

$$d_{max,i} = d_{max,0} \cdot (1 + \delta d_i) \tag{B.2}$$

where $d_{max,i}$ is the deformation demand that defines the end of the reload cycle for increasing deformation demand, $d_{max,0}$ is the maximum historic deformation demand (which would be the deformation demand defining the end of the reload cycle if degradation of reloading stiffness is ignored), and δd_i is the value of the reloading stiffness damage index at time t_i.

Strength degradation:

$$f_{max,i} = f_{max,0} \cdot (1 - \delta f_i) \tag{B.3}$$

where $f_{max,i}$ is the current envelope maximum strength at time t_i, $f_{max,0}$ is the initial envelope maximum strength for the case of no damage, and δf_i is the value of strength damage index at time t_i.

The damage indices δk_i, δd_i and δf_i may be defined to be a function of the displacement history only or the displacement history and energy accumulation.
If the damage indices are assumed to be a function of the displacement history and energy accumulation, the unloading stiffness damage index δk_i is computed as following:

$$\delta k_i = gK1 \cdot (\tilde{d}_{max})^{gK3} + gK2 \cdot (\frac{E_i}{E_{monotonic}})^{gK4} \leq gK_{lim} \tag{B.4}$$

where:

$$\tilde{d}_{max} = max(\frac{d_{max,i}}{def_{max}}, \frac{d_{min,i}}{def_{min}}) \tag{B.5}$$

and

$$E_i = \int_{loadhistory} dE \tag{B.6}$$

$$E_{monotonic} = gE \cdot (\int_{monotonicloadhistory} dE) \tag{B.7}$$

$E_{monotonic}$ is equal to the energy required to achieve under monotonic loading the deformation that defines failure;
def_{max} and def_{min} are the positive and negative deformations that define failure.
The other damage indices, δd_i and δf_i are computed similarly, by replacing gK coefficients with gF and gD, accordingly.

If the damage indices are assumed to be a function of the displacement history only, the unloading stiffness damage index δk_i is computed as following:

$$\delta k_i = gK1 \cdot (\tilde{d}_{max})^{gK3} + gK2 \cdot (Cycle)^{gK4} \leq gK_{lim} \tag{B.8}$$

where:

$$\tilde{d}_{max} = max(\frac{d_{max,i}}{def_{max}}, \frac{d_{min,i}}{def_{min}}) \tag{B.9}$$

with *Cycle* equal to the number of cycles accrued in the loading history def_{max} and def_{min} are the positive and negative deformations that define failure.

The other damage indices, δd_i and δf_i are computed similarly, by replacing gK coefficients with gF and gD, accordingly.

References

[1] ACI Committee 318. *Building Code Requirements for Structural Concrete (ACI 318-11) and Commentary (318R-11)*. American Concrete Institute, Farmington Hills, MI, 2011.

[2] B. Adetifa and M. A. Polak. Retrofit of slab column interior connections using shear bolts. *Structural Journal of the American Concrete Institute*, 102(2):268–274, 2005.

[3] H. Anderson, A. Reitzel, E. Muir, and S. Verma. Design of dampening system for earthquake protection. Technical report, University of Waterloo, 2009.

[4] H-P Andrae. Zum tragverhalten von flachdecken mit duebelleistein, bewehrung in auflagerberich. *Beton und Stahlbetonbau*, 75(H 10):239–246, 1981.

[5] E. Bentz. Membrane-2000. <http://www.ecf.utoronto.ca/~bentz/m2k.htm.>, 2015.

[6] W. Bu. *Punching Shear Retrofit Method Using Shear Bolts for Reinforced Concrete Slabs under Seismic Loading*. PhD thesis, University of Waterloo, Waterloo, ON, Canada, 2008.

[7] W. Bu and M. A. Polak. Seismic retrofit of reinforced concrete slab-column connections using shear bolts. *Structural Journal of the American Concrete Institute*, 106(4):514–522, 2009.

[8] F. A. Charney. Unintended consequences of modelling damping in structures. *ASCE Journal of Structural Engineering.*, 134(4):581–592, 2008.

[9] R. DesRoches, J. McCormick, and M. Delemont. Cyclic properties of superelastic shape memory alloy wires and bars. *Journal of Structural Engineering*, 130(1):38–46, 2004.

[10] W. H. Dilger and A. Ghali. Shear reinforcement for concrete slabs. *ASCE Journal of Structural Division*, 107(ST12):2403–2420, 1981.

[11] W. H. Dilger, A. Ghali, and M. Z. El-Masri. Flat plates with special shear reinforcement subjected to static and dynamic moment transfer. *Proceedings, Journal of the ACI*, 75(10):543–549, 1978.

[12] U. Ebead and H. Marzouk. Strengthening of two-way slabs subjected to moment and cyclic loading. *ACI Structural Journal*, 99(4):435–444, 2002.

[13] E. F. El-Salakawy, M. A. Polak, and M. H. Soliman. Reinforced concrete slab-column edge connections with shear studs. *Canadian Journal of Civil Engineering*, 27:338–348, 2000.

[14] E. F. El-Salakawy, M. A. Polak, and K. Soudki. New shear strengthening technique for concrete slab-column connections. *ACI Structural Journal*, 100(3):297–304, 2003.

[15] R. Eligehausen, E. P. Popov, and V. V. Bertero. Eerc report 83/23: Local bond stress-slip relationship of deformed bars under generalized excitations. Technical report, University of California, Berkeley, 1983.

[16] K. J. Elwood. *Shake Table Tests and Analytical Studies on the Gravity Load Collapse of Reinforced Concrete Frames*. PhD thesis, University of California, Berkeley, California, USA, 2002.

[17] J. Feld and K. L. Carper. *Construction Failure*. John Wiley and Sons, New York, New York, 1997.

[18] D. R. Fick. *Experimental Investigation of a Full-Scale Flat-Plate Reinforced Concrete Structure Subjected to Cyclic Lateral Loading in the Inelastic Range of Response*. PhD thesis, Purdue University, West Lafayette, IN, USA, 2008.

[19] D. Fugazza. *Use of Shape-Memory Alloy Devices in Earthquake Engineering: Mechanical Properties, Advanced Constitutive Modelling and Structural Applications*. PhD thesis, Universita degli Studi di Pavia, Pavia, Italy, 2005.

[20] W. Fuller and S. E. Thompson. The laws of proportioning concrete. *Transactions of the American Society of Civil Engineers.*, 59(2):67–143, 1907.

[21] A. Ghali, M. Sargious, and A. Huizer. Vertical prestressing of flat plates around columns. *ACI-SP 42-38, Shear in Reinforced Concrete*, pages 905–920, 1974.

[22] O. Graf. Versuche ueber die widerstandsfaehigkeit von eisenbettonplatten unter konsentrierten last nahe einem auflager. *Deutscher Ausschuss fuer Eisenbeton*, (73):1–16, 1933.

[23] N. M. Hawkins. Shear strength of slabs with shear reinforcement. *ACI SP 42 Shear in Reinforced Concrete*, pages 785–816, 1974.

[24] N. M. Hawkins, I. J. Lin, and F. L Jeang. Local bond strength of concrete for cyclic revearsed loadings. In P. Bartos, editor, *Bond in Concrete*. Applied Science Publishers, London, 1982.

[25] N.M Hawkins and W. G. Corley. Moment transfer to columns in slabs with shearhead reinforcements. *ACI SP 42 Shear in Reinforced Concrete*, pages 847–879, 1974.

[26] N. J. Delatte Jr. *Beyond Failure, Forensic Case Studies for Civil Engineers*. American Society of Civil Engineers, Reston, Virginia, 2009.

[27] T. H.-K. Kang and J. W. Wallace. Punching of reinforced and post-tensioned concrete slab-column connections. *Structural Journal of the American Concrete Institute*, 103(4):531–540, 2006.

[28] T. H.-K. Kang, J. W. Wallace, and K. J. Elwood. Nonlinear modeling of flat-plate systems. *Structural Journal of the American Society of Civil Engineers*, 135(2):147–158, 2009.

[29] Y. Kanoh and S. Yoshizaki. Strength of slab-column connections transferring shear and moment. *Structural Journal of the American Concrete Institute*, 76(3):461–478, 1979.

[30] D. C. Kent and R. Park. Flexural members with confined concrete. *Journal of the Structural Division*, 97(7):1969–1990, 1971.

[31] J. P. Laible, R. N. White, and P. Gergely. Experimental investigation of seismic shear transfer across cracks in concrete nuclear containment vessels. *ACI Special Publication*, 53:203–226, 1977.

[32] H. Langhor, A. Ghali, and W. H. Dilger. Special shear reinforcement for concrete flat plates. *Proceedings, Journal of the ACI*, 73(3):141–146, 1976.

[33] N. Lawler. Punching shear retrofit of concrete slab-column connections with GFRP shear bolts. Master's thesis, University of Waterloo, Waterloo, ON, Canada, 2008.

[34] L. N. Lowes, N. Mitra, and A. Altoontash. A beam-column joint model for simulating the earthquake response of reinforced concrete frames. Technical report, Pacific Earthquake Engineering Research Center, 2004.

[35] J. G. MacGregor and J. K. Wight. *Reinforced Concrete Mechanics and Design*. Pearson Education, Inc., Upper Saddle River, New Jersey, 2005.

[36] H. Marcus. *Die Theorie elastischer Gewebe und ihre Anwendung auf die Berechnung biegsamer Platten*. Springer-Verlag Berlin Heidelberg, Berlin, Germany, 1924.

[37] F.M. Mazzolani and A. Mandara. Modern trends in the use of special metals for the improvement of historical and monumental structures. *Engineering Structures*, 24:843–856, 2002.

[38] F. McKenna. OpenSees (Open System for Earthquake Engineering Simulation). <http://opensees.berkeley.edu.>, 2015.

[39] S. Megally and A. Ghali. Seismic behavior of slab-column connections. *Canadian Journal of Civil Engineering*, 27(1):84–100, 2000.

[40] S. Megally and A. Ghali. Seismic behaviour of slab-column connections. *Canadian Journal of Civil Engineering*, 27(1):84–100, 2000.

[41] R. Meli and M. Rodriguez. Seismic behavior of waffle-flat plate buildings. *Concrete International*, 10(7):33–41, 1988.

[42] A. S. Mokhtar, A. Ghali, and W. Dilger. Stud shear reinforcement for flat concrete plates. *Journal of the American Concrete Institute*, 82(5):676–683, 1985.

[43] A. H. Nilson, D. Darwin, and C. W. Dolan. *Design of Concrete Structures*. McGraw-Hill, New York, New York, 2004.

[44] A. Pan and J. P. Moehle. Lateral displacement ductility of reinforced concrete flat plates. *Structural Journal of the American Concrete Institute*, 86(3):250–258, 1989.

[45] R. Park and W. L.Gamble. *Reinforced Concrete Slabs*. John Wiley and Sons, New York, New York, 2000.

[46] T. Paulay. A simple seismic design strategy based on displacement and ductility compatibility. *Earthquake Engineering and Engineering Seismology*, 1(1):51–67, 1999.

[47] T. Paulay and M. J. N. Priestley. *Seismic Design of Reinforced Concrete and Masonry Buildings*. Wiley-Interscience, New York, New York, 1992.

[48] PEER. <http://peer.berkeley.edu/peer_ground_motion_database.>, 2015.

[49] S. U. Pillai, W. Kirk, and L. Scavuzzo. Shear reinforcement at slab-column connections in a reinforced concrete flat plate structure. *Journal of the American Concrete Institute*, 79(1):36–42, 1982.

[50] A. M. Ramos, V. J. Lucio, and P. E. Regan. Repair and strengthening methods of flat slabs for punching. *Proceedings, International Workshop on Punching Shear Capacity on RC Slabs, Stockholm*, pages 125–130, 2000.

[51] P. E. Regan. Shear combs, reinforcement against punching. *The Structural Engineer*, 63B(4):76–84, 1985.

[52] E. Rosenblueth and R. Meli. The 1985 earthquake: causes and effect in mexico city. *Concrete International*, 8(5):23–34, 1986.

[53] M. Fernandez Ruiz, Y. Mirzaei, and A. Muttoni. Post-punching behaviour of flat slabs. *ACI Structural Journal.*, 110(5):801–812, 2013.

[54] F. Seible, A. Ghali, and W. M. Dilger. Shear reinforcing units, for flat plates. *Journal of The American Concrete Institute*, 77(1):28–35, 1980.

[55] E. Spacone, F. C. Filippou, and F. F. Taucer. Fiber beam-column model for non-linear analysis of r/c frames: Part i. formulation. *Earthquake Engineering and Structural Dynamics*, 25:711–725, 1996.

[56] E. Spacone, F. C. Filippou, and F. F. Taucer. Fiber beam-column model for non-linear analysis of r/c frames: Part ii. applications. *Earthquake Engineering and Structural Dynamics*, 25:727–742, 1996.

[57] Y. Tian, J. O. Jirsa, and O. Bayrak. Strength evaluation of interior slab-column connections. *Structural Journal of the American Concrete Institute*, 105(6):692–700, 2008.

[58] Y. Tian, J. O. Jirsa, and O. Bayrak. Nonlinear modeling of slab-column connections under cyclic loading. *Structural Journal of the American Concrete Institute*, 106(1):30–38, 2009.

[59] Y. Tian, J. O. Jirsa, O. Bayrak, Widianto, and J. F. Argudo. Behavior of slab-column connections of existing flat-plate structures. *Structural Journal of the American Concrete Institute*, 105(5):561–569, 2008.

[60] F. J. Vecchio and M. P. Collins. The modified-compression field theory for reinforced-concrete elements subjected to shear. *Journal of the American Concrete Institute*, 83(2):219–231, 1986.

[61] J. Walraven. Fundamental analysis of aggregate interlock. *Journal of the Structural Division of the American Society of Civil Engineers*, 107(11):2245–2270, 1981.

[62] J. Walraven. Rough cracks subjected to earthquake loading. *Structural Journal of the American Society of Civil Engineers*, 120(5):1510–1524, 1994.

[63] W. H. Wheeler. Thin flat-slab floors prove rigid under test. *Engineering News Record*, 116(2):49–50, 1936.